Last Glacial Maximum to Holocene Arctic sea-ice variability:

Reconstruction from biomarkers

Kumulative Dissertation
zur Erlangung des akademischen Grades eines
Doktors der Naturwissenschaften
– Dr. rer. nat. –
Am Fachbereich Geowissenschaften
Der Universität Bremen
vorgelegt von

Xiaotong Xiao

Bremerhaven, 2014

Gutachter der Dissertation:
Prof. Dr. Ruediger Stein
Prof. Dr. Gesine Mollenhauer

Tag des öffentlichen Kolloquiums:
2nd July 2014

Erklärung

Hiermit versichere ich an Eides statt, die vorliegende Arbeit, abgesehen von der Beratung durch meine akademischen Lehrer, selbständig und ohne Zuhilfenahme fremder als der hier angegebenen Quellen angefertigt zu haben.

Bremerhaven, 25.04. 2014
Xiaotong Xiao

Abstract

Arctic sea-ice extent has been declining rapidly throughout the past decades. To understand the past temporal and spatial sea-ice variability is of significant importance for predicting the future development. Within this thesis, the recently developed sea-ice proxy IP_{25}, exclusively produced by diatoms in sea ice, has given a new insight into the reconstruction of sea ice across major parts of the Arctic Ocean during modern time and the Last Glacial Maximum (LGM).

In the first study, determination of IP_{25}, phytoplankton-derived biomarkers (brassicasterol and dinosterol) and terrigenous biomarkers (campesterol and ß-sitosterol) in surface sediments from the Kara and Laptev seas is used to estimate modern spatial (seasonal) sea-ice variability and organic-matter sources. C_{25}-HBI diene and triene were determined as additional paleoenvironmental proxies in the study area. Furthermore, a combined phytoplankton-IP_{25} biomarker approach (PIP_{25} index) is used to reconstruct the modern sea-ice distribution more quantitatively. Neither IP_{25} nor PIP_{25}, however, show a clear and good correlation with satellite sea-ice distribution due to the complex environmental conditions in our study area. Differences in the diene/IP_{25} and triene/IP_{25} ratios point to different sources of these HBIs and different environmental conditions. The diene/IP_{25} ratio correlates positively with sea-surface temperature, and thus might be used as a potential SST index. Further studies are, however, needed to validate this index.

Furthermore, in the second study, a comprehensive data set of these biomarkers was produced using surface sediment samples from the Central Arctic Ocean proper (>80°N latitude) and the Chukchi Plateau/Basin. In addition, published data from other Arctic and sub-Arctic regions were added to the new data to generate an overview distribution map of IP_{25} across major parts of the Arctic Ocean. The phytoplankton biomarkers brassicasterol and dinosterol were also determined alongside IP_{25} to distinguish between two extreme scenarios, either ice-free or permanent ice conditions. PIP_{25} index values show a positive correlation with satellite-derived spring/summer sea-ice concentration. When calculating and interpreting the PIP_{25} proxy for reconstructions of Arctic sea-ice conditions, the uncertainties of the origin of the sterols need to be considered and thus more than one phytoplankton biomarker should be involved and the resulting PIP_{25} values should be compared.

In the third study, Arctic Ocean sea-ice conditions during the Marine Isotope Stage (MIS) 3–1 were reconstructed by means of IP_{25} and phytoplankton-derived biomarkers data obtained from 7 sediment cores. The summer ice edge remained north of the Barents Sea even during extremely cold (i.e., Last Glacial Maximum (LGM)) as well as during warm periods (i.e., Bølling-Allerød). Spatial sea-ice conditions were reconstructed for the Central Arctic Ocean

and adjacent areas by means of biomarker data from 16 sediment samples covering the LGM time-slice. The western Spitsbergen margin and northern Barents Sea margin were found to be productive regions. In contrast, the LGM high Arctic (>84°N) was covered by thick permanent sea ice throughout the year with rare break up. The spring/summer sea-ice margin significantly extended southwards during LGM in the marginal seas.

Zusammenfassung

Während der letzten Jahrzehnte nahm die Meereisbedeckung im Arktischen Ozean sehr schnell ab. Kenntnisse über die zeitliche und räumliche Veränderung des Meereises sind von enormer Bedeutung für die Vorhersage der zukünftigen globalen Klimaentwicklung. Im Rahmen dieser Dissertation gibt der kürzlich entwickelte Meereisproxy IP_{25}, der ausschließlich von Meereisdiatomeen produziert wird, Aufschluss über die Rekonstruktion der modernen als auch der Paläo-Meereisbedeckung während des Letzten Glazialen Maximums (LGM) für weite Bereiche des Arktischen Ozeans.

In der ersten Studie dient die Bestimmung von IP_{25}, Phytoplanktonbiomarkern (Brassicasterol und Dinosterol) und terrigenen Biomarkern (Campesterol und b-Sitosterol) in Oberflächensedimenten der Kara- und Laptevsee zur Abschätzung der modernen räumlichen (saisonalen) Meereisvariabilität und der Herkunft des organischen Materials. Das C_{25}-HBI Dien und die Triene wurden als zusätzliche Paläoumweltproxies im Untersuchungsgebiet bestimmt. Zusätzlich wird der kombinierte Phytoplankton-IP_{25} Biomarkeransatz (PIP_{25} Index) benutzt, um die moderne Meereisverteilung quantitativ zu rekonstruieren. Aufgrund der komplexen Umweltbedingungen im Untersuchungsgebiet zeigen weder IP_{25} noch PIP_{25} eine eindeutige und gute Korrelation mit der aus Satellitendaten bekannten Meereisverbreitung. Unterschiede in den Dien/IP_{25} und Trien/IP_{25} Verhältnissen weisen auf unterschiedliche Quellen für diese HBIs und unterschiedliche Umweltbedingungen hin. Das Dien/IP_{25} Verhältnis korreliert positiv mit Meeresoberflächentemperaturen und könnte daher als potentieller SST Index genutzt werden. Für die Validierung dieses Indexes sind weitere Studien nötig.

Darüber hinaus wurde für die zweite Studie ein umfangreicher Datensatz dieser Biomarker anhand von Oberflächensedimenten aus dem zentralen Arktischen Ozean (>80°N) und dem Chukchi Plateau/Becken erstellt. Für eine Übersichtskarte der Verteilung von IP_{25} im Arktischen Ozean wurden diese neuen Daten mit bereits publizierten Daten aus anderen arktischen und subarktischen Regionen ergänzt. Zusätzlich zu IP_{25} wurden die Phytoplanktonbiomarker Brassicasterol und Dinosterol bestimmt, um zwischen den zwei Extremsituationen einer entweder eisfreien oder aber permanent mit Meereis bedeckten Meeresoberfläche zu unterscheiden. PIP_{25} Indexwerte zeigen eine positive Korrelation mit Frühlings-/Sommer-Meereiskonzentrationen aus Satellitendaten. Bei der Berechnung und Interpretation des PIP_{25}-Proxies für die Rekonstruktion arktischer Meereisbedingungen müssen Unsicherheiten hinsichtlich des Ursprungs der Sterole berücksichtigt werden. Es sollte daher mehr als ein Phytoplanktonbiomarker benutzt und die resultierenden PIP_{25}-Werte verglichen werden.

In der dritten Studie wurden die Meereisbedingungen im Arktischen Ozean während der Marinen IsotopenStadien (MIS) 3-1 anhand von IP_{25}- und Phytoplanktonbiomarkerdaten aus

7 Sedimentkernen rekonstruiert. Die Sommereisrandlage blieb sowohl während extrem kalter (Letztes Glaziales Maximum; LGM) und auch während warmer Perioden (Bølling-Allerød) nördlich der Barentssee. Die LGM-Meereisbedingungen im zentralen Arktischen Ozean und in den angrenzenden Gebieten wurden anhand der Biomarkerdaten von 16, das LGM umfassenden, Sedimentproben rekonstruiert. Eine höhere Primärproduktion wurde im Bereich des westlichen Kontinentalhangs Spitzbergens und des nördlichen Kontinentalhangs der Barentssee festgestellt. Die zentrale Arktis (>84°N) hingegen war ganzjährig mit einer dicken und permanenten Eisschicht bedeckt, die nur selten aufbrach. Während des LGM dehnte sich die Frühlings-/Sommereisrandlage erheblich bis in die südlichen Randmeere aus.

Acknowledgement

First of all, I would like to express my sincere thanks to my supervisor, Prof. Dr. Ruediger Stein, who gave me the opportunity to study on this topic at the AWI and spent plenty of time to help me solve all the problems during my PhD study. Thanks very much for your patience, inspiring advice and great encouragement over the past four years. I also would like to thank Prof. Dr. Gesine Mollenhauer for taking time to review my thesis.

Great aknoledgement goes to Dr. Kirsten Fahl for introducing me the detailed mechanism of analytical processes and calibration approach of the biomarker. For me, you are more a friend or a mom than a supervisor. Thank you very much for your flowers, your warm smile and your big hug.

I also would like to appreciate Dr. Jens Matthiessen, who is one of my committee members, for the constructive suggestion and helpful discussion in my PhD committee meetings. I also thank you for taking samples for me during RV *Polarstern* expedition ARK XXVI/3 in 2011, in which I could not participate.

I want to express my special thanks to Walter Luttmer, who taught me to handle the lab work at the beginning of my PhD. He not only keeps an eye on my work in the lab but also helps me a lot in the daily life. Susanne Wiebe and Rita Fröhlking are thanked for great help when I measured the TC and TOC.

Many thanks go to my colleagues at Geo department. Juliane Müller spent a lot of time to read and correct my manuscript and answered my questions in patience. Thank Sarah Romahn for occasional small talk to support and encourage each other. All the colleagues are thanked for providing nice work environment. I am grateful to the Chinese community in Bremerhaven with whom I could enjoy the nice homemade dishes.

My deep love goes to my boyfriend, my parents and my grandparents, who care about me and support me a lot during my stay in Germany as well as for my whole life.

Contents

1. Introduction

1.1 The Arctic Ocean and its marginal seas

1.1.1 Modern conditions

The Arctic Ocean is a landlocked sea, comprising of a deep basin surrounded by shallow shelf seas, with one deep gateway, the Fram Strait, connecting the Arctic with the Atlantic Ocean (Figure 1.1; Jakobsson et al., 2008). The deep Arctic Ocean is divided into the Amerasian Basin and the Eurasian Basin by the Lomonosov Ridge. The Amerasian Basin including the Canadian Basin and the Makarov Basin with its surrounding shelf seas refers to western Arctic, while the Eurasia Basin including the Nansen Basin and the Amundsen Basin with its surrounding shelf seas refers the eastern Arctic (Figure 1.1). The continental shelves of the Arctic Ocean make up almost half the total area of the Arctic Ocean (Jakobsson, 2002). The deep Fram Strait (with depth up to 2600 m) provides a major conduit for exchanging warm Atlantic water and cold polar surface water and sea ice between the Arctic Ocean and the Atlantic (Rudels and Friedrich, 2000; Fahrbach et al., 2001). The narrow and shallow Bering Strait, on other hand, only imports Pacific Water into the Arctic Ocean without outflow of polar water into the Pacific (Jones et al. 2003).

The Arctic Ocean is most characterized by its perennial sea-ice cover in the central basin and distinct seasonal and inter-annual sea-ice variability in the marginal seas. By the end of the melt season in September, there is only multi-year ice in the Arctic basin and parts of the Canadian Archipelago and around Greenland, covering about half of the Arctic Ocean (Stroeve et al. 2007; Comiso, 2010). In contrast to the multi-year ice dominated the Central Arctic, the seasonally ice-covered marginal seas are of importance for the growth, melt and deformation processes of sea ice. The growth of sea ice in the Arctic is developed by the congelation of ice, which differs from the frazil growth in the Southern Ocean (Petrich and Eicken, 2010). However, recent reduction in permanent ice cover in the Arctic may trigger the formation of frazil ice (Dieckmann and Hellmer, 2010).

The annual cycle of sea-ice formation and melting processes influences the heat flow (albedo), the gas exchange between the atmosphere and the ocean as well as the deep-water formation (Comiso and Parkinson, 2004; Dieckmann and Hellmer, 2010). A mixing of surface waters results from brine rejection via freezing as the salt is transported away from the interface into the surrounding ocean water, while a freshwater layer is formed during sea-ice melting (Petrich and Eicken, 2010). Sustained freezing of the sea surface waters and rejection of salt trigger a densification and downward convection during sea ice formation, thus causing a stratification of the water column, which restricts the convection to the upper layer

(Dieckman and Hellmer, 2010). The advection of warm water masses advected from Atlantic into the Central Arctic cannot reach the sea ice cover owing to the strong Arctic halocline. After further mixture with the cold water from the continental shelf, these Atlantic Waters are eventually exported from the Arctic Ocean through the Fram Strait as newly formed deep water (Dieckmann and Hellmer, 2010).

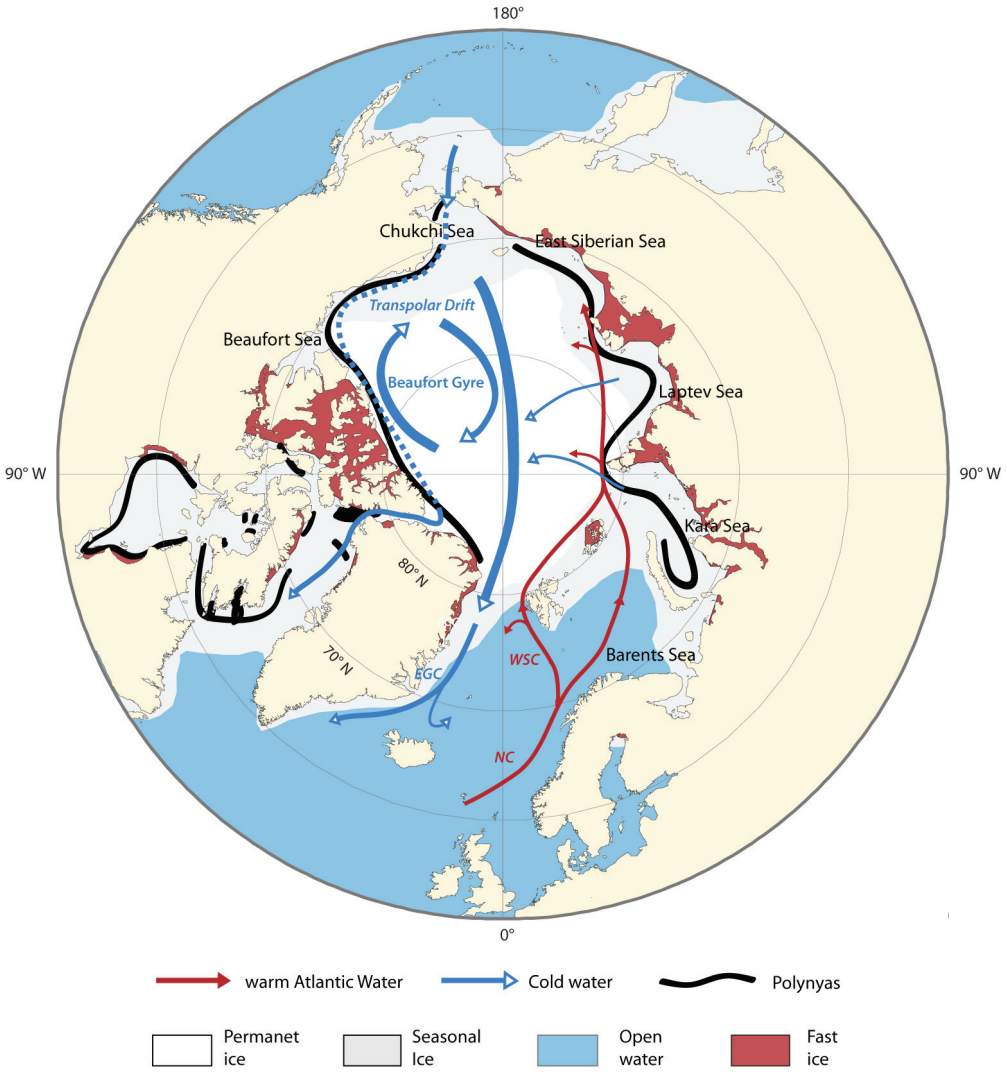

Figure 1.1 Schematic illustration indicating Arctic Ocean sea-ice condition, surface circulation and major riverine freshwater input (after Peterson et al., 2002; Macdonald et al., 2004). The sea-ice coverage represents the average extent of 1979 to 2007 (http://nsidc.org).

Furthermore, as one of the largest biomes on earth with an area covering 7% of the earth's surface in winter (Comiso, 2010 and references therein), sea ice significantly influences the biologic communities, i.e., primary producers in surface water masses, the benthos in the abyss and it is habitat for polar marine mammals and birds (Siegel, et al., 1997; Dieckmann and Hellmer, 2010; Haas, 2010). The occurrence of sea ice triggers an early ice algal spring

bloom, which profoundly contributes to the total primary production in the Arctic (Legendre et al., 1992; Gradinger, 2009). The ice algal assemblage deposits at the sea floor to support the benthos as the ice algal can escape the zooplankton grazers when sinking through the water column due to their earlier bloom than zooplankton (Wassmann and Reigstad, 2011). In the marginal seas, large zones of fast ice occur on the shallow shelf during wintertime connecting with the islands of the Arctic seas, which provides a unique habit for polar microbial assemblage and plays an important role in the ecological system (Arrigo et al., 2010). Along the boundary of the fast ice, there are polynyas and leads, from which the growth of ice algal benefits during early spring (Pesant et al., 1996).

Figure 1.2 Map of the pan-arctic watershed showing average annual discharge of the major Eurasian rivers that contribute water to the Arctic Ocean. Red dots indicate the North Atlantic Deep Water (NADW) source locations. (Figure obtained from Peterson et al., 2002).

Another prominent feature of the Arctic Ocean is the strong freshwater discharge from the Eurasian and Amerasian Arctic rivers, e.g. Yenisei, Ob, Lena and Mackenzie (Figure 1.2; Peterson et al., 2002; Stein and Macdonald, 2004). This supply of freshwater substantially affects the process of freezing, transport, and melting of sea ice and the coastal fast-ice formation (Aagaard and Carmack, 1989; Divine et al, 2004; Bareiss and Görgen, 2005), and is particularly important for ocean circulation and climate (Peterson et al., 2006, 2007). The

global warming and the reduction of the sea-ice cover, consequently, might trigger the increase of river discharge to the Arctic Ocean since the mean annual discharge of fresh water from the six largest Eurasian rivers increased by 7% from 1936 to 1999 (Peterson et al., 2002). As a consequence, the transport of moisture from ocean to atmosphere is supposed to increase and the net high-latitude precipitation also increases, supported by both theoretical arguments and models (Peterson et al., 2002 and reference herein). Increasing river discharge, net precipitation and meltwater from Greenland ice sheet strengthen the freshwater input to the Arctic Ocean, which weaken the North Atlantic Deep Water (NADW) formation (Peterson et al., 2002 and reference herein).

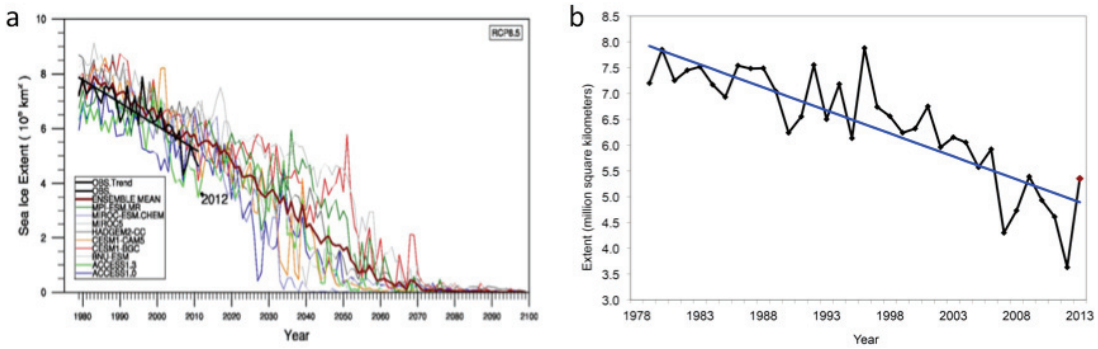

Figure 1.3 (a) Time-series of the simulated (colour lines) September sea ice extent from 1979 to 2100 for the nine selected models under the RCP8.5. The thick black line is the observations, the thick red line is the ensemble mean of the nine models, and the black circle is September sea ice extent in 2012 (figure obtained from Liu et al., 2013). (b) Observed average monthly Arctic sea-ice extent of September 1979-2014 (graph from http://nsidc.org).

A temperature record based on the comparison of proxy and simulation data shows that the Arctic cooling trend was reversed since 20th century and the warmest decades occurred between 1950 and 2000 (Kaufman et al., 2009). The rapid shrinking Arctic sea-ice cover at the end of the melt season over the past decades draws the attention of the entire climate science community (Serreze et al., 2003, 2007; Stroeve et al., 2005, 2007, 2008; Figure 1.3). Following the sea-ice minimum in 2005, Arctic sea ice reached an extreme reduction in September 2007, 23% less than 2005 (Kerr, 2007; Perovich et al., 2008; Wang and Overland, 2009). Recently, the Arctic sea-ice extent fell to a historical minimum with an extent of 3.29 million square kilometers in September 2012 that is 18% less than 2007 and 49% less than 1979 (start of satellite record), respectively (Zhang et al., 2013). The Arctic ice volume had declined by around 40% and the mean ice thickness was thinning from 2007 onward. As a consequence, the thinner ice cover is vulnerable to storms and to melting out in summer (Stroeve et al., 2012; Zhang et al., 2013). According to the observations and simulations, a

hypothesis was proposed that Arctic Ocean might become seasonally ice-free around 2040 (Wang and Overland, 2009; Liu et al., 2013). The observed sea ice extent retreats more rapid than predicted by modeling (Figure 1.3).

1.1.2 Past conditions

According to the geologic records, the onset of Arctic sea ice probably started around 47 Ma (or 44Ma, Figure 1.4) following the Paleocene-Eocene Thermal Maximum when the Arctic Ocean was significantly warmer than today (Backman et al., 2004; Moran et al., 2006; Stickly et al., 2009; Polyak et al., 2010 references therein; Poirier and Hillaire-Marcel, 2011). Almost contemporaneously, the existence of glaciers was documentted by the IRD record in ODP 913 from the Norwegian-Greenland Sea, which provides the first evidence of the existence of some continental ice sheets in the Northern Hemisphere during the Paleogene (Eldrett et al., 2007).

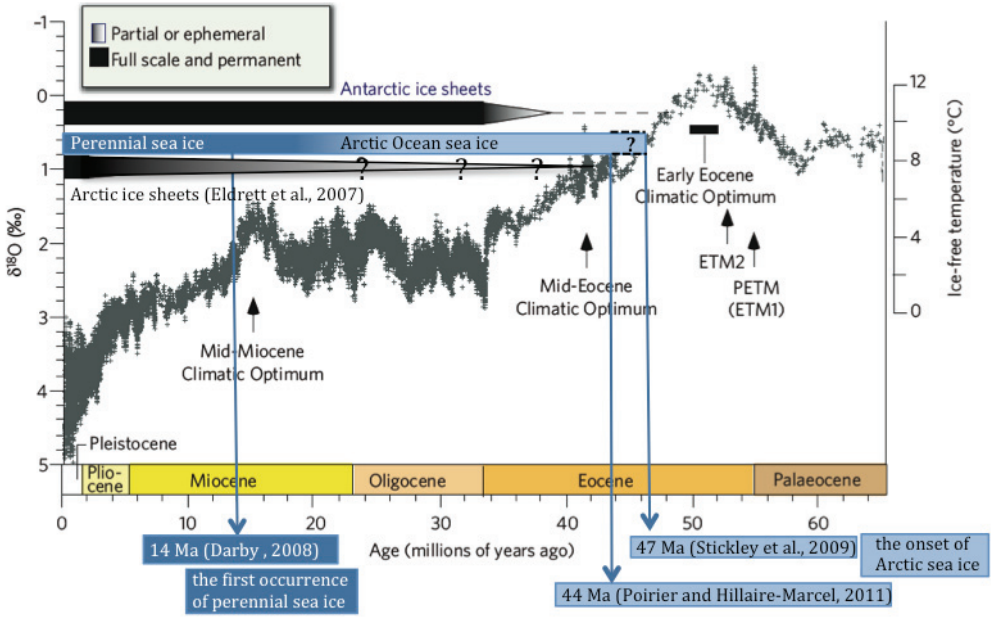

Figure 1.4 Global benthic foraminifer $\delta^{18}O$ curve shows long-term cooling spanning the past 65 million years (modified from Zachos et al., 2008).

The Fram Strait opened during early Miocene at about 17 Ma (Jakobsson et al., 2007). After the opening of the Fram Strait, the modern circulation system established and caused the formation of sea ice around Svalbard, which was transported to the eastern Arctic Ocean and Greenland Sea, and resulted in high numbers of IRD at about 15Ma (Knies and Gaina, 2008). Then, the first perennial sea ice occurred in the Arctic around 14-12Ma (Mid-Miocene), indicated by the mineral provenance and Fe-oxide provenance in IRD from a distal source

requiring more than 1 year to reach the core site by ice drift (Krylov et al., 2008; Darby, 2008).

During most of the Pliocene, the seasonal sea ice prevailed in the Arctic Ocean. The climate was general cooler than in the Miocene but still considerably warmer than in the Pleistocene (Polyak et al., 2010 and references therein) During this period, the Bering Strait opened around probably 3.5 Ma or earlier, which allowed marine organisms to migrate from the Pacific to the Arctic Ocean and deposit in the sediments. The species record showed seasonal ice-free conditions in the Arctic Ocean and perennial ice-free conditions in some regions (Cronin et al., 1993). After 3.0 Ma, cooling conditions in the late Pliocene triggered the initial build-up of the Barents Sea ice sheet, which covered Svalbard, Franz Josef Land and Novaya Zemlya and reached the shelf edge of Northern Barents Sea (Knies et al., 2009). The freshwater input from the ice sheet and the cold-water inflow from the Pacific also enhanced the sea-ice growth in the Arctic (Matthiessen et al., 2009). This cooling climate sustained throughout the Plio-Pleistocene transition, further enhancing the sea ice and ice sheet growth (Jansen et al., 2000). However, the IRD abundance in the Central Arctic considerably reduced during the Mid-Pleistocene between ca 1.5-2 Ma and then varied very slightly until the late Pleistocene, which might result from a stable ice pack limiting the transport of debris incorporated in sea ice from the marginal seas to the Central Arctic rather than reduction of ice sheets (St.John, 2008).

The Quaternary is characterized by the occurrence of alternating warm and cold periods (interglacial and glacial). The Quaternary glacial-interglacial cycles were accompanied by the growth and decay of continental ice sheets and sea-ice cover. During glacial periods, the sedimentation rates were low in the Central Arctic Ocean due to the thick and extensive sea-ice cover (Cronin et al., 2010; Poirier et al., 2012). However, the warm Atlantic water could still reach the northern Norwegian Sea and penetrate through Fram Strait up to northern margin of Svalbard (Hebbeln et al., 1994; Knies, et al., 1999; Cronin et al., 2012). The expanded ice sheets during the glacial (i.e., MIS 3) probably blocked the freshwater input from the Pacific and Arctic rivers, which caused the halocline to deepen thus forcing the warm Atlantic Layer into intermediate depths, which resulted in deep Arctic Ocean warming (Figure 1.5; Cronin et al., 2012). Similar conditions might have occurred earlier during MIS 6, when the Eurasian ice sheet reached its maximum extent (Svendsen et al., 2004). As the exposure of the shallow Arctic continental shelf also limited the freshwater input, the downward displacement of the warm Atlantic water could have also occurred during the LGM (Jakobsson et al., 2013). The closing of the Barents Sea caused by the Svalbard-Barents Sea Ice Sheet and the lower sea level reduced the advection of Atlantic water by ca. 50% (Nørgaard-Pedersen et al., 2003). Consequently, recirculating Atlantic Water may have had a

stronger impact on the surface ocean environment as the limited outflow of low-salinity water in the western Fram due to the reduced riverine input (Nørgaard-Pedersen et al., 2003). In contrast, the interglacial climate conditions were similar to present-day, with higher marine productivity and reduced ice cover (Polyak et al., 2010). For example, seasonal open-water conditions may have occurred in the Central Arctic Ocean during the last interglacial MIS 5a and MIS 5e (Nørgaard-Pedersen et al., 2007), suggesting a much higher temperature at Earth environment than those of present day.

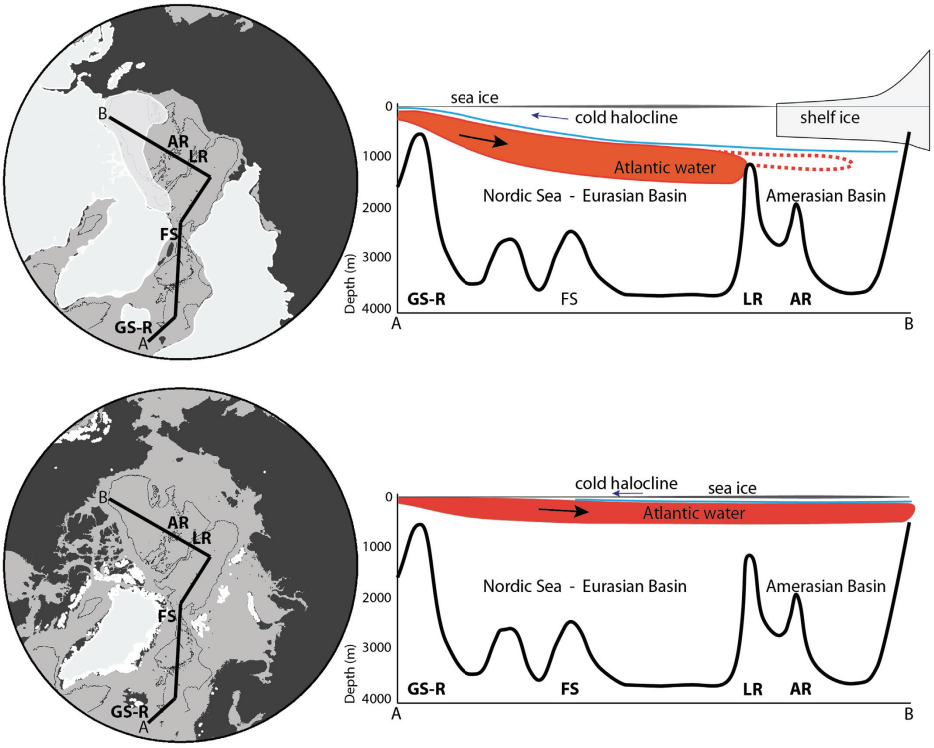

Figure 1.5 Conceptual oceanographic models for the glacial (A) and interglacial (B) Arctic Ocean. AR = Alpha Ridge; LR = Lomonosov Ridge; GS-R = Greenland Scotland Ridge; FS = Fram Strait. (Figure obtained from Jakobsson et al., 2013).

1.1.3 LGM conditions

The LGM is characterized by a maximum extension of the surrounding ice sheets and a perennial ice cover with occasional break up, indicating the peak of the last glacial interval (Stein, 2008; Polyak et al., 2010; Jacobsson et al, 2013 references therein). The extent of sea-ice cover and ice sheets in the glacial Arctic is still debated, relating to the 'floating ice shelf covering the Arctic' hypothesis.

This hypothesis was initially proposed by Mercer (1970) and further supported by Hughes et al. (1977) who suggested that, during the LGM, the entire Arctic Ocean, including the East Siberian and Chukchi seas, was covered with a 1000 m thick ice shelf centered in the Arctic

Ocean (Figure 1.6). The CLIMAP project (CLIMAP, 1976, 1981) also supposed a perennial ice cover in the Arctic Ocean and Nordic Seas and a summer polar front in the North Atlantic reaching as far as 50°N during the LGM. Although the open-water conditions were required to provide moisture for glacial ice sheet build-up (e.g. Hebbel et al., 1994), until recently, some authors still supported the hypothesis that a huge thick LGM ice shelf floating over the entire Arctic Basin connected to the circum-Arctic continental ice sheets, halted the Atlantic water inflow and Polar Drift transport (Grosswald and Hughes, 2002, 2008).

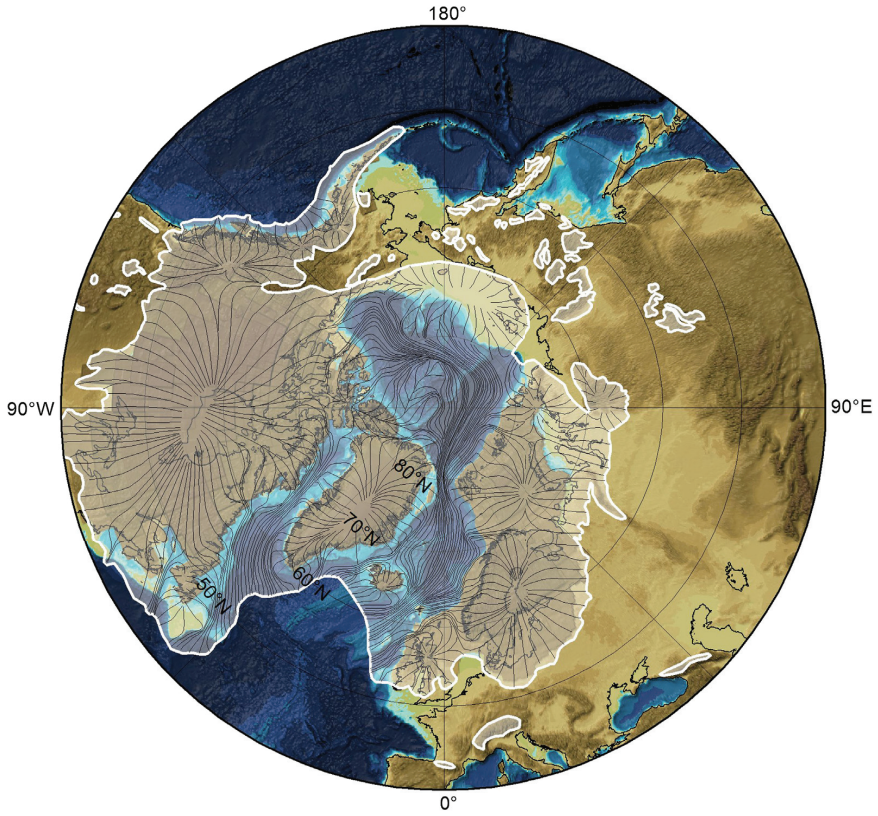

Figure 1.6 The maximum version of the LGM Arctic Ice Sheet by Hughes et al. (1977). All the Arctic Ocean continental shelves are glaciated including that of the East Siberian, and Chukchi seas. (Figure obtained from Jakobsson et al., 2013).

However, the hypothesis of an 'Antarctic style' ice sheet in the Arctic was strongly argued by Sher (1995), who pointed out that contrary to the Western Arctic with extensive geological record, the East Siberian Arctic Shelf Ice Sheet hypothesis was only based on theoretical postulation. The author suggested the existence of extensively exposed shelf land in East Siberia during the late Weichselian and described this area as 'The area, including the present coast and shelf islands, was occupied by dry grassland communities (tundra-steppe) and diverse fauna of grazing mammals' (Figure 1.7). Concerning the sea-ice conditions in the

Nordic Sea, some studies suggested that Atlantic surface water could have penetrated into the Arctic Ocean along the margin of the Svalbard-Barents Sea Ice Sheet and seasonal open water existed on the northern Barents Sea margin due to a coastal polynya caused by offshore katabatic winds during the LGM, which resulted in the high sedimentation rates and relatively high fluxes of planktonic foraminifers and IRD at these sites (Figure 1.8; Knies et al., 1999; Nørgaard-Pedersen et al., 2003). Furthermore, the GLAMAP Group (Pflaumann et al., 2003; Sarnthein et al., 2003a, 2003b) reconstructed the LGM polar front in the north Atlantic, showing polar front retreat to about 73°N with ice-free conditions in eastern Fram Strait during LGM summer. The Svalbard-Barents Sea Ice Sheet was centred over the Barents Sea and the Barents-Kara Ice Sheet extended eastwards as far as Taymyr blocking the drainage of Ob and Yenisei rivers to the Kara shelf (Svendsen et al., 2004; Polyak et al., 2008; Ingólfsson and Landvik, 2013 and references therein). In the Western Arctic, the Laurentide Ice Sheet covered North America and most of the Canadian Archipelago (Dyke et al., 2002). The Innuitian Ice Sheet over Ellesmere Island coalesced with the Laurentide Ice Sheet and the Greenland Ice Sheet, reaching the continental shelf during the LGM (Dyke et al., 2002 and references therein).

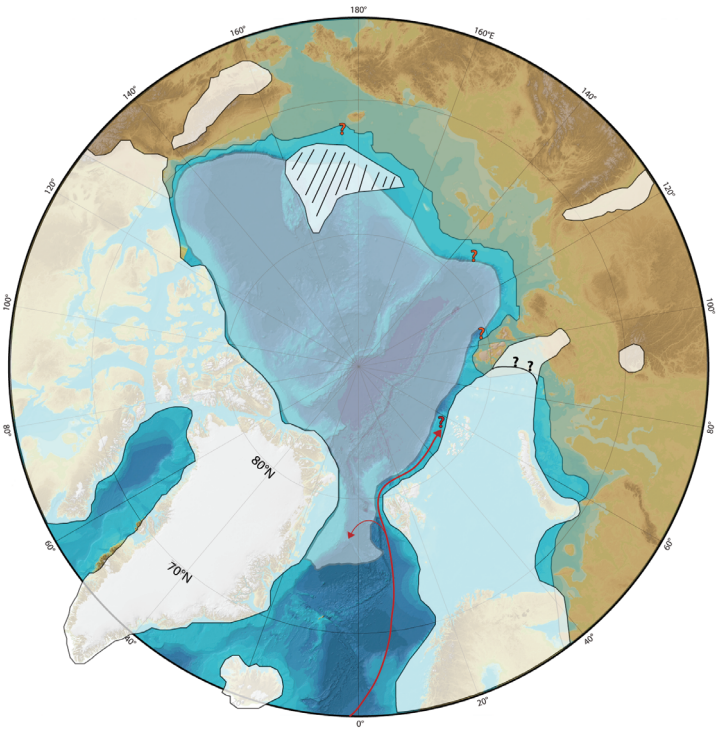

Figure 1.7 Ice-sheet extensions and sea ice cover during the LGM summer. The Eurasian ice sheet is from Svendsen et al. (2004) and the Laurentide-Innuitian-Greenland ice sheet is from Dyke et al. (2002). The summer polar front is based on Sarnthein et al. (2003b). The New results from the cross hatched area of Chukchi Borderland Plateau will likely also lead to future major revisions of ice-sheet extent during the late Quaternary.

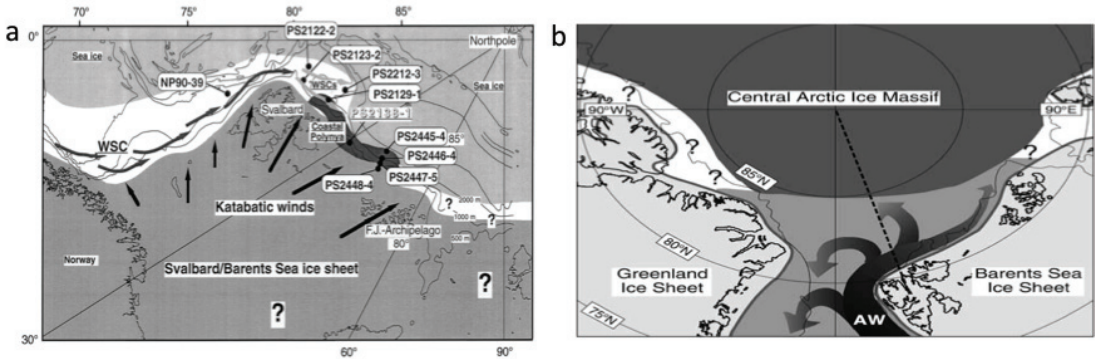

Figure 1.8 (a) Paleoenvironmental model of the SBIS during Last Glacial Maximum (figure obtained from Knies et al., 1999). (b) Simplified model of ice cover character and surface ocean conditions in the Fram Strait-central Arctic Ocean region during the LGM (figure obtained Nørgaard-Pedersen et al., 2003).

Recently Stärz et al. (2012) used a regional North Atlantic-Arctic Ocean circulation model to study LGM conditions. The model studies show an anti-cyclonic rotation in the Canadian Basin, which is shifted compared to the present-day pattern and a Transpolar Drift, which is deflected or not present during LGM (Figure 1.9). The outflowing layer from the Arctic extends down to about 1500 m and that the Atlantic inflow was displaced towards the bottom, which is in agreement with the glacial Arctic Ocean stratification suggested by Cronin et al. (2012), although the Arctic Atlantic Water temperature in the LGM simulation of Stärz et al. (2012) seems to be too cold to match the available Mg/Ca temperature proxies from Arctic Ocean ostracodes reported by Cronin et al. (2012).

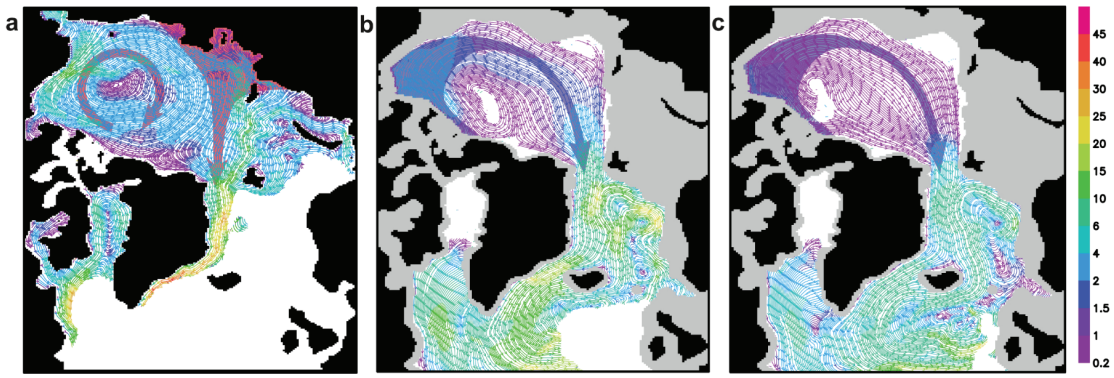

Figure 1.9 Streamlines of 30-yr mean sea-ice drift (cm/s) for modern and glacial conditions. (a) Model study CTRL. (b) LGMG. (c) LGMC. (Figure obtained from Stärz et al., 2012).

1.2 The biomarker approach: ice proxy IP_{25} and phytoplankton biomarkers

Belt et al. (2007) have developed the novel sea-ice biomarker proxy IP_{25}, a mono-unsaturated highly branched isoprenoid (HBI) alkene with 25 carbon atoms biosynthesized specifically by sea-ice diatoms, from their study of Canadian Arctic sediments and sea ice (Figure 1.10). So far, the source diatom species is still uncertain, however, the specific relation of this molecule to sea ice could be deduced from the growth environment of more unsaturated C_{25} HBI alkenes (Belt et al., 2007). C_{25} HBI alkenes (also termed Haslene) with different degrees of unsaturation, produced by certain diatom genera have been determined in different environments, for example, freshwater, seawater, marine sediments, and freshwater and marine species (Volkman et al., 1994; Belt et al., 2000, 2001a; Massé et al., 2004; Grossi et al., 2004). The extent of unsaturation in Haslenes increases with increasing diatom growth temperatures (Belt et al., 2000; Rowland et al., 2001). In the laboratory cultures of *Haslea ostrearia* (Rowland et al., 2001), the authors found that tetraunsaturated haslenes were produced mainly at 25 °C, triunsaturated haslenes were produced at 15 °C, and diunsaturated haslenes were produced at 5 °C. Analogously, monounsaturated haslenes (e.g. IP_{25}) could be biosynthesized by *Haslea* spp. at a lower temperature, for example, in sea ice, as *Haslea* spp. have been identified in both polar regions (Belt et al., 2007 and references therein). IP_{25} is absent in sea ice and surface sediment samples obtained from the Antarctic, probably caused by the different diatom species in the Southern Ocean compared to the Arctic, or the different sea-ice environment controlling the biosynthetic mechanism responsible for IP_{25} production (Massé et al., 2011). Therefore, IP_{25} could be used as a promising indicator only for Arctic sea ice reconstruction. Specific ^{13}C isotope analyses of IP_{25} in sea ice, sediment trap and surface sediment samples from the Arctic further support that this molecule originates from sea ice (Belt et al., 2008). So far, the analytical procedure of the extraction, identification and quantification of IP_{25} have been well established and compared between different laboratories (Belt et al., 2012; 2014).

In the initial study of IP_{25}, the records in the sediment cores from the Canadian Arctic Archipelago went back to around 9 ka BP, which indicated the applicability of IP_{25} in Arctic sediments for sea-ice reconstruction during the Holocene (Belt et al., 2007). Afterwards, IP_{25} has been successfully used for sea-ice reconstruction within the Holocene interval for the Arctic and Sub-Arctic regions, such as Canadian Arctic Archipelago (Vare et al., 2009; Belt et al., 2010), Barents Sea (Vare et al., 2010) and Fram Strait (Müller et al., 2012). In a detailed IP_{25} study performed on a sediment core from the northern North Atlantic, the biomarker sea-ice record was extended back to 30 ka BP (Müller et al., 2009). Recently, Stein and Fahl (2013) and (Stein, personal communication) demonstrated in a pilot study carried out on sediment cores from southern Yermak Plateau that IP_{25} can even be found in marine

sediments as old as 3.6 Ma, i.e., the IP_{25} approach can be used for reconstructions of palaeo sea ice for the entire Late Pliocene to Pleistocene time interval.

As the absence of IP_{25} could refer to either ice-free or permanent sea-ice conditions, Müller et al. (2009) compared IP_{25} data with a biomarker produced by open-water phytoplankton (brassicasterol; Volkman, 2006) to distinguish between two extreme scenarios. The lack of both biomarkers points to perennial ice cover, while the absence of IP_{25} with high phytoplankton biomarker contents reflects ice-free conditions. The occurrence of both biomarkers, on the other hand, suggests stable ice edge conditions or seasonal sea-ice variation. In order to associate the sea-ice proxy IP_{25} with distinct sea-ice conditions, Müller et al. (2011) combined IP_{25} with phytoplankton biomarkers in surface sediments from the continental margins of East Greenland and West Spitsbergen to calculate the phytoplankton-IP_{25} (PIP_{25}) index as a new approach to access the sea-ice conditions more quantitatively:

$$PIP_{25} = IP_{25} / (IP_{25} + \text{phytoplankton biomarker} * C)$$

(C = mean IP_{25} concentration / mean phytoplankton biomarker concentration).

High PIP_{25} values (0.75–1) refer to a permanent sea-ice cover throughout the year, intermediate values between 0.5 and 0.75 reflect seasonal ice cover or a stable ice edge, while low values (0–0.5) indicate less ice or ice-free conditions. The PIP_{25} values of the investigated surface sediments correlate very well with sea-ice concentrations obtained from the satellite observation and modelling simulation, respectively. Furthermore, these authors also pointed out that the individual biomarker concentrations have to be considered using the PIP_{25} index to distinguish different sea-ice scenarios. For instance, the co-occurrence of both low IP_{25} and phytoplankton biomarker contents (referring to permanent ice conditions) might result in high or low PIP_{25} values. Likewise, the co-occurrence of high amounts of both biomarkers (referring to ice edge or seasonal ice conditions) can yield the same results. Further PIP_{25} studies using surface sediments from different areas of the Arctic strengthen the applicability of the PIP_{25} index approach in general (Navarro-Rodriguez et al., 2013; Stoynova et al., 2013; Xiao et al., 2013).

As mentioned above, the diunsaturated C_{25} HBI alkene (C_{25} HBI diene, Figure 1.10) might be produced in a higher temperature environment than IP_{25} (C_{25} HBI monoene). This compound was found in sediment samples from polar areas as well as from more temperate regions (e.g., Volkman et al.; 1983, Vare et al., 2009; Masse et al., 2011). Like for IP_{25}, the stable isotopic composition of the HBI diene also suggests a sea-ice origin (Belt et al., 2008). This was further indicated by the high correlation between HBI diene and IP_{25}, reflecting a common origin between these two compounds (Cabedo-Sanz et al., 2013; Xiao et al., 2013). The diene/IP_{25} ratio, recently termed DIP_{25} index (Cabedo-Sanz et al., 2013) can be used as a

further tool to estimate palaeo sea-ice conditions with relatively high diene/IP_{25} values suggesting warmer SSTs or low sea ice intervals (Fahl and Stein et al., 2012). Furthermore, Cabedo-Sanz et al. (2013) pointed out that the weaker linear correlation between HBI diene and IP_{25} represented a period of unstable sea-ice conditions, which also resulted in variable diene/IP_{25} values. With regard to the spatial variability, the distribution of IP_{25} and the HBI diene in surface sediments from the Kara and Laptev Seas also suggests variable sea-ice conditions, and the diene/IP_{25} ratios seem to correlate positively with SSTs in the study area (Xiao et al., 2013).

For sterol markers, Volkman (1986) pointed out that 'few sterols are sufficiently restricted in distribution to be considered unambiguous markers for specific algal groups, so sterol distributions do not always allow one to distinguish between marine or terrigenous organic matter.' Brassicasterol and dinosterol are universally used as marine phytoplankton biomarkers (Figure 1.10), however, some studies have shown that brassicasterol might have other sources, i.e., fluvial/lacustrine origin (Volkman, 1986; Fahl et al., 2003) or sea-ice origin (Yunker et al., 1995; Belt et al., 2013). On the other hand, campesterol and ß-sitosterol have been acknowledged as terrigenous biomarkers (Huang and Meinschein, 1976; Figure 1.10).

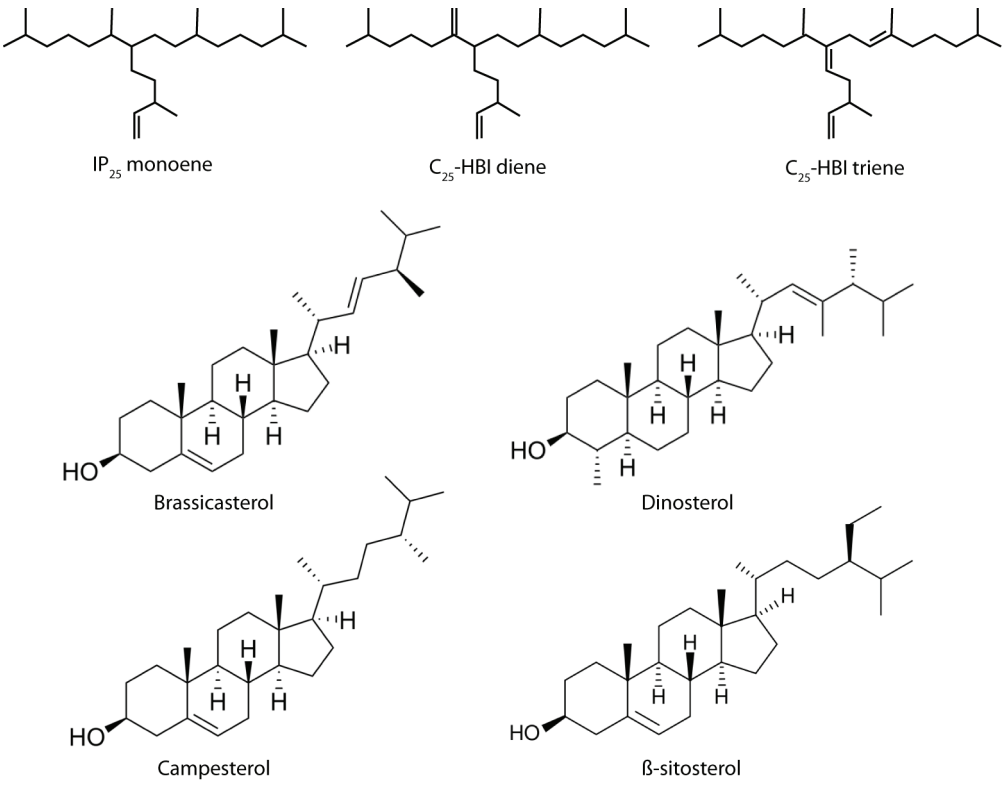

Figure 1.10 Structure of C_{25} highly branched isoprenoid and sterols used within this thesis.

1.3 Outline and objectives of this thesis

The sea-ice cover is one of the most prominent features of the Arctic Ocean and its adjacent marginal seas with strong seasonal and interannual variability, contributing to heat reduction (albedo), deep-water formation and gas exchange between the ocean and the atmosphere. The rapid shrinking Arctic sea-ice cover at the end of the melt season over the past decade draws significant attention from the entire community (details see chapter 1.1). In order to understand the causes of the loss of the multi-year ice, i.e., whether anthropogenic influence and/or natural variability are major controlling processes, it is essential to reconstruct the past variability of sea ice from sedimentary sections, going well beyond the time span of direct measurements of sea-ice distribution and thickness. Therefore, stable and well-preserved biomarker proxies related to sea ice, are required. Here, the recently identified novel sea-ice proxy IP_{25}, a specific, sensitive and stable biomarker proxy seems to be a very promising approach for reconstruction of Arctic palaeo-sea-ice distribution (Belt et al, 2007). Within this thesis, datasets from a broad region covering the Central Arctic Ocean and several marginal seas have been obtained to generate overview distribution maps of biomarkers across the Arctic. The application of IP_{25} in the Arctic Ocean provides a general comparison between the High Arctic and the marginal seas as well as between the modern distribution and palaeo-reconstruction.

In the following Chapter 2 the material and methods used in this thesis are described in detail. Chapters 3-5 consist of three manuscripts that are published, submitted or in preparation, and which provide the main results of this thesis. The conclusion and outlook are presented in Chapter 6, to summarize the current work and future perspective.

The major objects of the three manuscripts that constitute this thesis are:

In Chapter 3, biomarker data determined in the surface sediments from the Kara and Laptev seas are presented and discussed. The following key questions were addressed:

1. What are the main factors controlling organic-carbon accumulation in the study area, i.e., marine productivity or terrigenous input?
2. Does IP_{25} reflect of the complex sea-ice conditions of the study area?
3. Do IP_{25} and phytoplankton-IP_{25} index (PIP_{25}) values correlate with satellite sea-ice concentrations?
4. How does C_{25}-HBI diene and triene correlate with IP_{25}? Do they have a common source?

In Chapter 4, biomarkers determined in surface sediment samples from the Central Arctic

Ocean proper (>80°N latitude) and from the Chukchi Plateau/Basin were presented and discussed for the first time. The published data from other Arctic and sub-Arctic regions were added to generate an overview distribution map of IP_{25} across the Arctic to answer the following questions:

1. Does IP_{25} exist in the high Arctic (>85°N latitude)? Does the signal reflect autochthonous productivity or allochthonous input?
2. How does IP_{25} or PIP_{25} reflect the modern sea-ice conditions within such a comprehensive dataset?
3. How reasonable are the different phytoplankton biomarkers (e.g. brassicasterol and dinosterol) for the calculation of PIP_{25} index?

In Chapter 5, sediment cores and sediments of LGM time-slices across the Arctic Ocean were used to reconstruct the temporal sea-ice variability (MIS 3-1) and the spatial LGM sea-ice variability. Key questions include:

1. How did the IP_{25} record reflect the temporal sea-ice variability in the Central Arctic during MIS 3-1?
2. How did the sea ice and ice sheet respond to the palaeoceanographic changes?
3. Was there any primary productivity during the LGM? How did the productivity relate to the sea-ice conditions?
4. How did the Atlantic Water advection affect the sea ice and ice sheet distribution during the (pre-/post-) LGM?

2. Materials and methods

2.1 Sample materials

The marine sediment materials used for this thesis were recovered during several expeditions of the RV *Polarstern*, RV *Ivan Kireyev*, *Akademik Boris Petrov* and RV *Araon* (for further details see Chapter 4, 5 and 6). Coretop sediments were sampled directly after recovery and stored in brown glass bottles at -30°C. Multicorer sediments were sampled immediately after recovery as whole slices (1 cm) on board, while Kastenlot sediments were stored at -30°C after recovery and sampled at home laboratory.

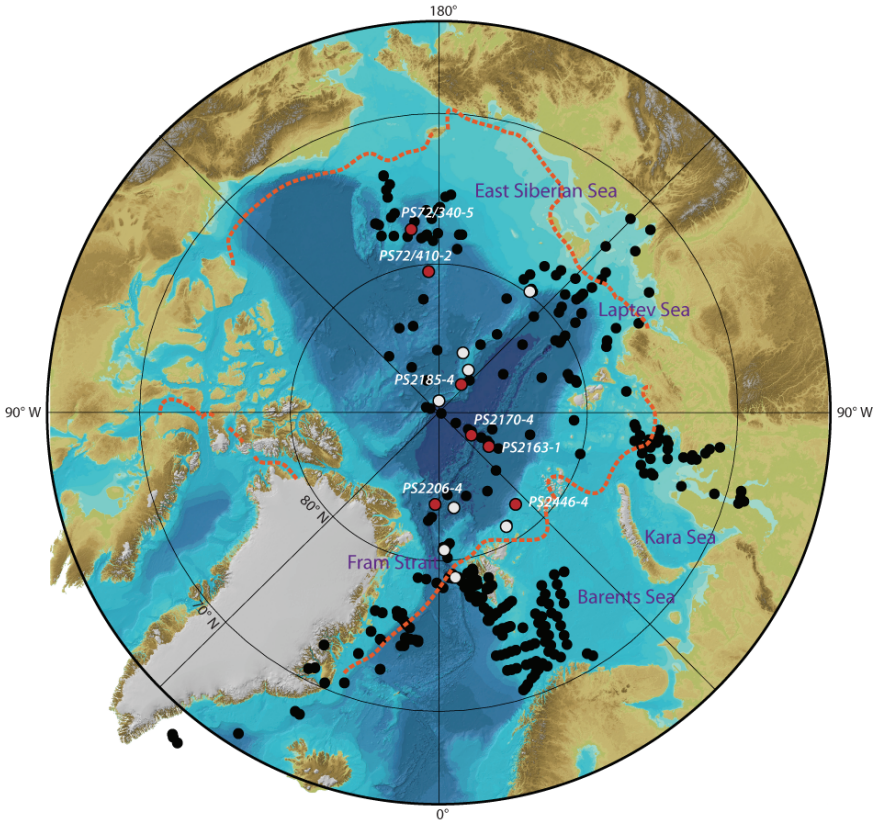

Figure 2.1 Sampling locations of 299 surface sediments (black dots) used for spatial distribution of biomarker study and sediment cores (red and white dots) used for temporal variability. The surface sediment samples include published dataset from previous study (details see Chapter 5). Red dots are sediment cores with continuous sedimentary records and white dots are LGM time-slice of sediment cores. Orange dashed line shows the average of September sea-ice extent of 1988-2007 (http://nsidc.org). International Bathymetric Chart of the Arctic Ocean (Jakobsson et al., 2008).

The coretop sediments were used to study biomarker distributions relevant for modern sea-ice reconstructions in the Central Arctic Ocean (>80°N), adjacent marginal seas and sub-

Arctic (Figure 2.1). In addition to our investigations, biomarker data from previous surface sediment studies from the adjacent marginal seas (Müller et al., 2011; Navarro-Rodriguez et al., 2013; details see Chapter 5) were included. The sediment cores used to reconstruct temporal paleoceanographic variability were taken from different regions of the Arctic Ocean. Sediment Core PS2446-4 was recovered from the northern continental margin of the Barents Sea and contains intercalated debris flow with grayish diamicton (Figure 2.2; Fütterer, 1994; Knies, 1999). This area was characterized by seasonal sea-ice variability, sensitive to the climate changes and Atlantic Water advection. The other cores were taken from the Gakkel Ridge, Amundsen Basin, Lomonosov Ridge and southern Mendeleev Ridge, where the perennial sea-ice cover dominates throughout the year at present-day. The LGM time-slice in 16 sediment cores was used for LGM sea-ice reconstruction. The age determinations for the LGM time-slice and sediment cores are described in Chapter 6.

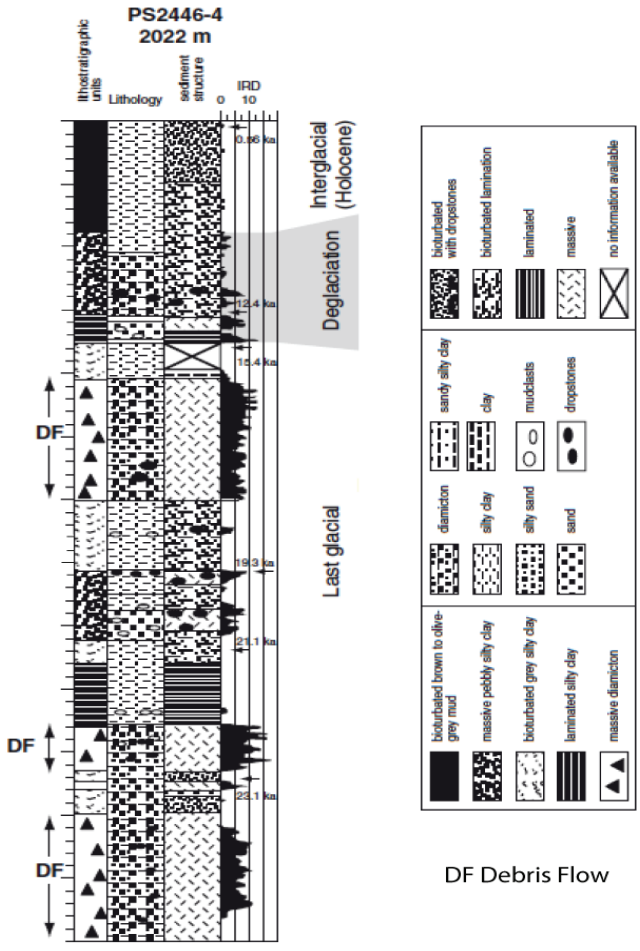

Figure 2.2 Lithostratigraphic units, lithology, sedimentary structure, and IRD content (numbers of detritus >2mm in centimetre core intervals) of sediment cores PS2446-4 (Figure obtained from Stein, 2008).

2.2 Methods

Organic-geochemical proxies (e.g., organic-geochemical bulk parameters, maceral composition and biomarker distributions) may allow to identifying the origin of the organic carbon and its transport and deposition processes and can be used for palaeo-environmental reconstructions in marine sediments. Further information about the analytical procedures of these proxy data and their application in palaeo-environmental reconstructions were described and explained by Romankevich (1984), Tissot and Welte (1984), Schulz and Zabel (2000), Killops and Killops (2005), Stein and Macdonald (2004) and Stein (2008). The analysis and quantification procedure of the organic geochemical bulk parameters and biomarker molecules determined within the framework of this thesis are described below (Figure 2.3).

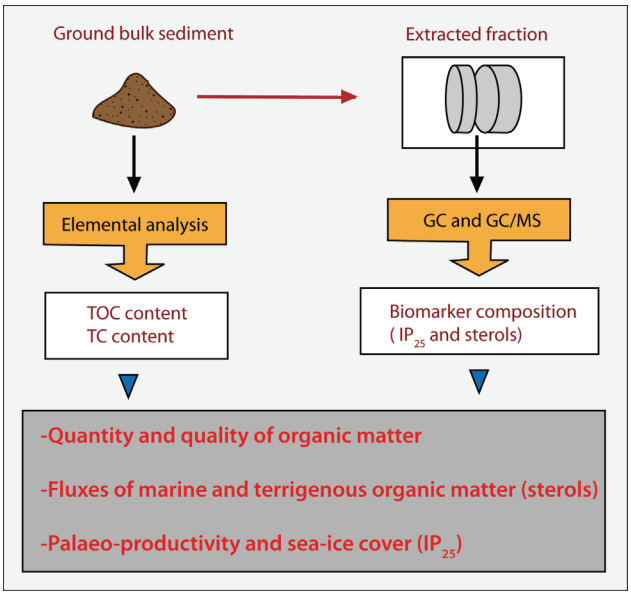

Figure 2.3 A brief schematic diagram of organic geochemical bulk parameters and biomarker molecules determined within this thesis.

2.2.1 Organic-geochemical bulk proxies - TOC and TC measurements

For bulk analysis, samples were freeze-dried and homogenized. TOC contents were determined by a carbon-sulphur analyzer Leco CS-125. Prior to the measurements, 500 ml hydrochloric acid was added to the samples to dissolve carbonates. For calibration of the instrument an external standard was used with the carbon content of 0.90±0.002. Total carbon (TC) contents were measured by a CNS analyzer (Elementar III, Vario) for calculation of carbonate contents. Calcium carbonate ($CaCO_3$) was calculated by means of TOC and TC contents (%) according to $CaCO_3$ (%) = (TC - TOC) x 8.333 (8.333 is a ratio of molecular weight $CaCO_3$ to C) (Stein, 2008 and references therein).

Within this thesis, TOC contents were measured in all the surface sediments and sediment cores. TOC records in sediment cores PS2163-1, PS2170-4, PS2185-4 and PS2206-4 from

Gakkel Ridge, Amundsen Basin and Lomonosov Ridge have been compared to the previous measurements performed on these cores, which show the similar variability patterns and are within the same concentration ranges (Figure 2.4). Furthermore, parallel measurements were carried out in selected layers of the upper part of Core PS72/340-5 to enable the feasibility of the repeated measurements (Figure 2.5; Table 2.1). TC contents were determined in Core PS72/410-2 from the Mendeleev Ridge and then carbonate contents were calculated. The carbonate record was correlated to the record of the neighbouring AMS ^{14}C dated Core PS72/410-1 to get an age model (Figure 2.6).

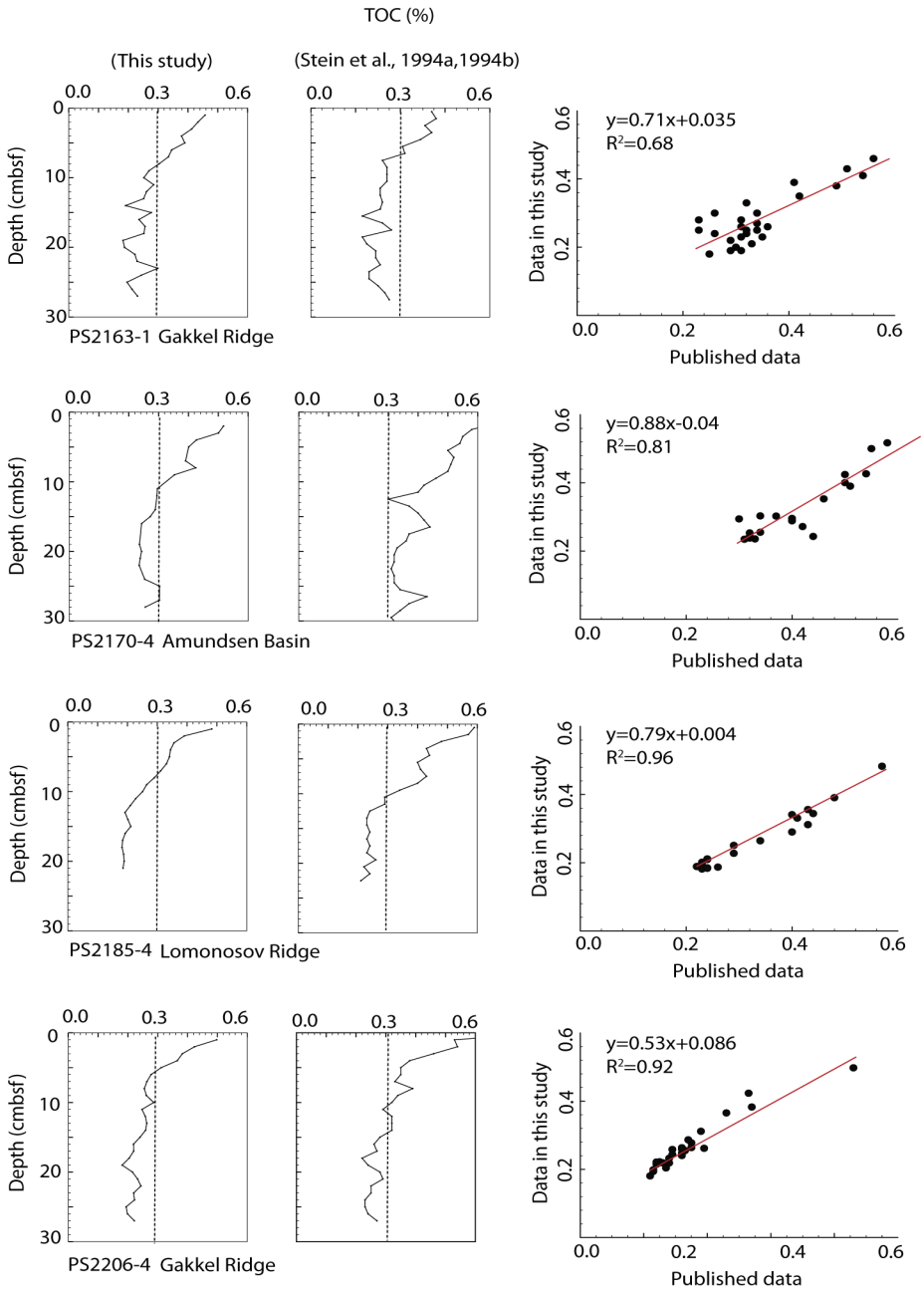

Figure 2.4 TOC records determined in sediment cores within this thesis compared to published data carried out on the same cores.

Table 2.1 TOC values obtained from parallel measurements in Core PS72/340-5.

Depth (cm)		3	5	10	14	19	23	32	42
TOC (%)	Measured on 16.09. 2013	0.54	0.49	0.35	0.31	0.31	0.40	0.49	0.48
	Measured on 14.11.2013	0.54	0.50	0.38	0.33	0.29	0.42	0.52	0.47

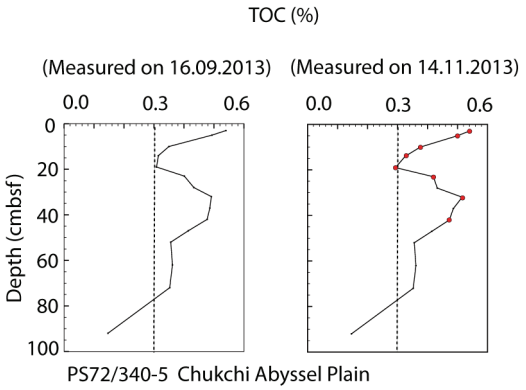

Figure 2.5 TOC contents in Core PS72/340-5. Red dots in the right plot indicate selected depth of sediments measured for parallel experiment

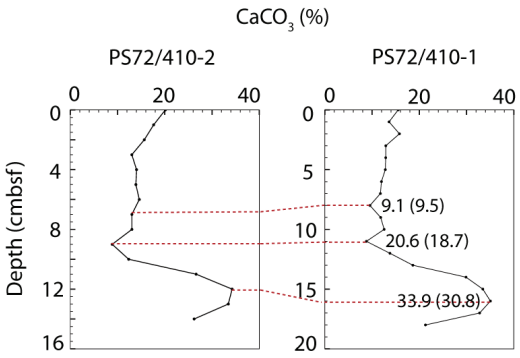

Figure 2.6 $CaCO_3$ contents determined in sediment Core PS72/410-2 and correlated to the neighbouring Core PS72/410-1 for age model.

2.2.2 Biomarkers - sea ice proxy IP_{25} and sterol measurements

For lipid biomarker analyses, we follow the analytical procedure for identification and quantification developed by K. Fahl and J. Müller, which were briefly shown in Figure 2.7.

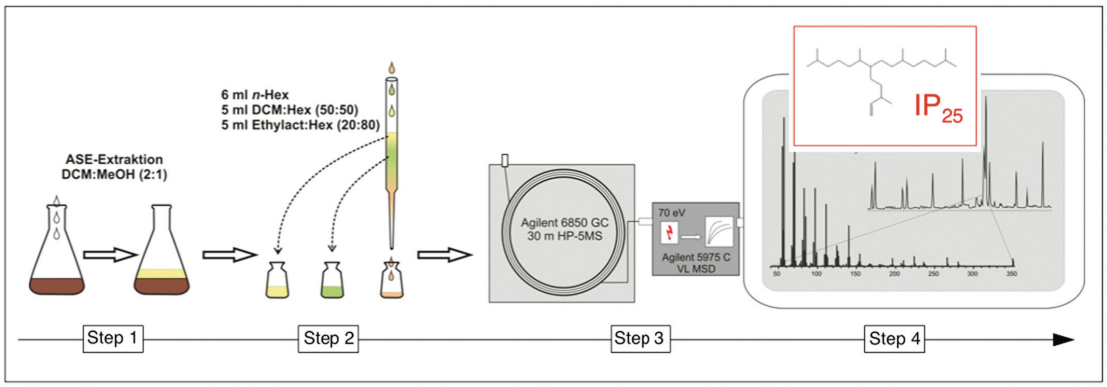

Figure 2.7 Schematic illustration of the AWI analytical procedure for identification and quantification of IP_{25} as well as sterols (Stein et al., 2012).

(1) Extraction and column chromatography: the sediments were freeze-dried and homogenised for further extraction. Prior to the extraction, the internal standards 7-hexylnonadecane (0.076 µg/sample), squalane (2.4 µg/sample) and cholesterol-d_6 (cholest-5-

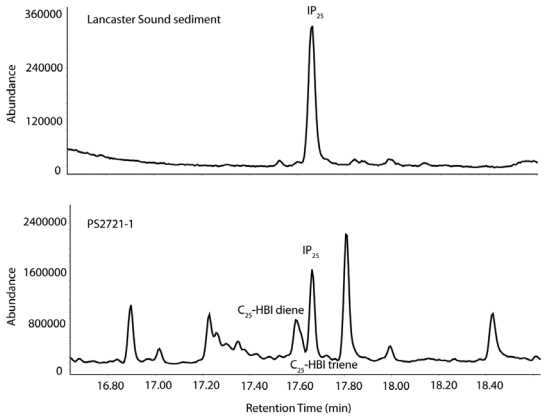

Figure 2.8 Partial total ion current (TIC) chromatograms of GC-MS full scan mode obtained from Lancaster Sound sediment and surface sediment from the Laptev Sea.

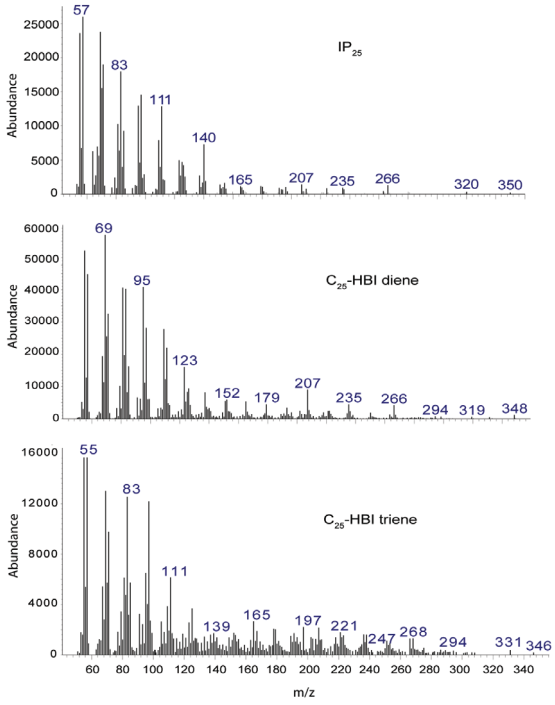

Figure 2.9 Mass spectrums of IP_{25}, C_{25}-HBI diene and triene obtained from PS2721 to show the identification of these compounds.

en-3β-ol-D_6; 20.2 µg/sample) were added to the sediments for quantification. Afterwards the sediments were extracted by an Accelerated Solvent Extractor (DIONEX, ASE 200; 100°C, 5 min, 1000 psi) using dichloromethane:methanol (2:1 v/v) as solvent. Total extracts were esterified with 1 ml 3 N methanolic hydrochloric acid (12 hrs, 50°C) to transfer fatty acids into fatty acid methylesters (FAME) for further separation during the column chromatography. 3 ml *n*-hexane was added to the derivatized extract, and after shaking vigorously and the upper phase was collected and dried by means of Na_2SO_4 (this step has been repeated twice with 2 ml *n*-hexane). Further separation of hydrocarbons, fatty acid and sterols was carried out via open-column chromatography using SiO_2 as stationary phase 5 ml *n*-hexane, 6ml dichloromethane:*n*-hexane (1:1 v/v), and 6 ml ethylacetate:*n*-hexane (20:80 v/v), respectively. Sterols were silylated with 500 µl BSTFA (bis-trimethylsilyl-trifluoroacetamide; 60 °C, 2 h) after elution (Figure 2.7).

(2) Qualification: both IP_{25} and and sterols were analysed by gas chromatography (Agilent 6850 GC; 30 m HP-5MS column, 0.25 mm i.d., 0.25 µm film thickness) coupled to an Agilent 5975 C VL mass selective detector (MSD, 70 eV constant ionization potential, ion source temperature 230 °C) (Figure 2.7). The GC oven was heated from 60°C to 150°C at 15°C min-1, and then at 10°C min-1 to 320°C (held 15 min) for the analysis of hydrocarbons and at 3°C min-1 to 320°C (held 20 min) for sterols, respectively.

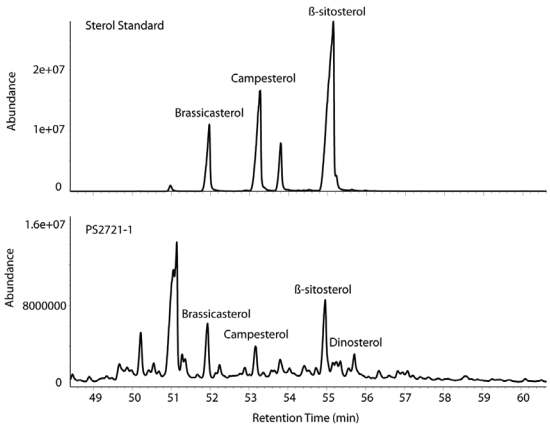

Figure 2.10 Partial total ion current (TIC) chromatograms determined on GC-MS obtained from sterol standard and surface sediment from the Laptev Sea.

Helium was used as carrier gas (1 ml/min constant flow). Hydrocarbons were analyzed in full scan mode as well as in selected ion monitoring (SIM) mode (m/z 350, 348, 346, 266) for detection of the low concentrated IP_{25} (m/z 350) as well as C_{25}-HBI diene (m/z 348) and triene (m/z 346). Fragment ion m/z 266 refers to the internal standard 7-hexylonadecane. Detection limit for the GC-MS system is 10 ng/ml (signal to noise ratio (S/N) > 3).

IP_{25} identification was based on comparisons of its mass spectrum with published data (Belt et al., 2007). A reference sediment from Lancaster Sound with high IP_{25} concentration was used to identify the retention time for samples with low IP_{25} concentration that did not show a clear spectrum (Figure 2.8). The retention time of IP_{25} as well as C_{25}-HBI diene and C_{25}-HBI triene in total ion current chromatograms from one of the surface sediments (PS2721) within this thesis are also shown in Figure 2.8. The spectra used for identification of these compounds in PS2721 are displayed in Figure 2.9 for identification.

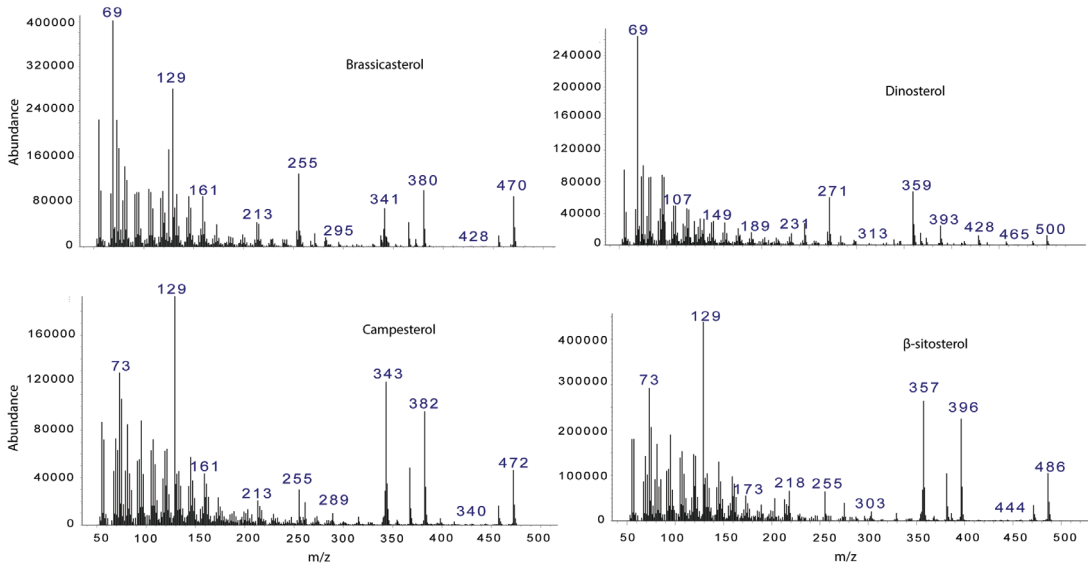

Figure 2.11 Mass spectra of brassicasterol, dinosterol, campesterol and ß-sitosterol obtained from PS2721 to show the identification of these compounds.

Individual sterol identification was based on comparisons of their retention times with that of a sterol standard mixture (containing brassicasterol, campesterol and ß-sitosterol; Figure 2.10) and on comparisons of their mass spectra with published data (Boon et al., 1979; Volkman, 1986; Johns et al., 1999; Figure 2.11).

(3) Quantification: IP_{25} concentrations were calculated on the basis of its GC-MS ion response compared with the internal standard. For the quantification of IP_{25}, the peak area of its molecular ion (m/z 350) was compared to the peak area of the fragment iron (m/z 266) of the internal standard 7-hexylnonadecane by means of the formula below:

$$IP_{25}\ (\mu g/g\ sed) = \text{Calibration factor} \times (IStd\ (\mu g/g) / A_{IStd} \times A_{IP25}) / g\ \text{sediment}$$

where IStd refers to the internal standard added to the sediment and A_{IStd}, A_{IP25} referring to integrated peak areas of the internal standard and IP_{25}, respectively. The calibration factor was used to correct the different percentage of the 350 and 266 ions in the TIC and SIM measurements (Figure 2.12a; Fahl and Stein, 2012). Furthermore, IP_{25} concentrations obtained from MSD and calculated with the calibration factor correlate well with those measured on GC (considered as 'true' values) with the correlation coefficient $R^2 > 0.99$ (Figure 2.12b). The quantification of C_{25}-HBI diene and C_{25}-HBI triene follows the same procedure as performed for IP_{25}.

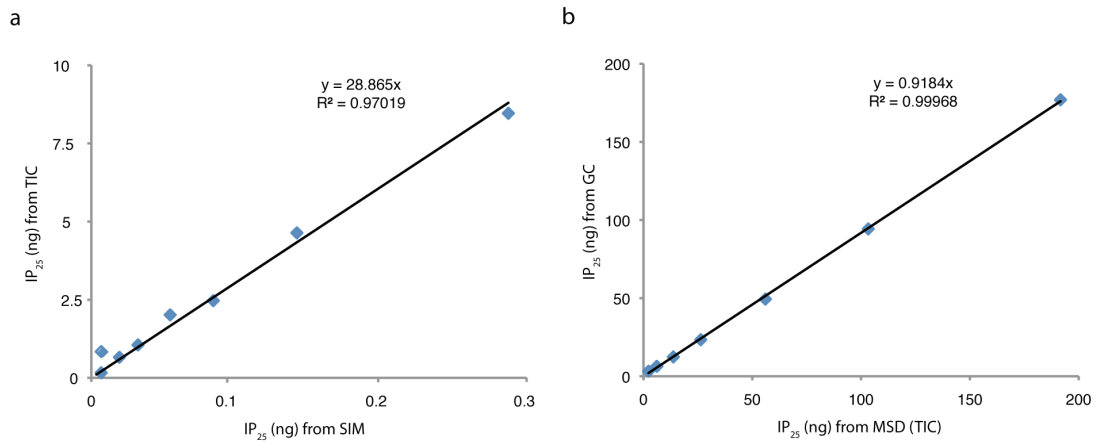

Figure 2.12 Calibration curve (a) of correlation of IP_{25} concentrations obtained from total ion current against corresponding values obtained from selected ion monitoring. The regression line provided the calibration factor for the correction of the different percentage of the 350 and 266 ions in the TIC and SIM measurements. IP_{25} concentrations obtained from MSD and GC (b) show a good correlation.

The sterols were quantified using the molecular ions m/z 470 for brassicasterol (24-methylcholesta-5,22E-dien-3β-ol), m/z 500 for dinosterol (4α,23,24R-trimethyl-5α-cholest-22E-en-3β-ol), m/z 472 for campesterol (24-methylcholest-5-en-3b-ol) and m/z 486 for ß-

sitosterol (24-ethylcholest-5-en-3b-ol) compared with the response of the molecular ion m/z 464 of the internal standard cholesterol-d_6 using the formula below:

$$\text{Sterol (µg/g sed)} = (\text{IStd (µg/g)} / A_{\text{IStd}} \text{ x } A_{\text{Sterol}}) \text{ /g sediment}$$

where IStd refers to the internal standard added to the sediment and A_{IStd}, A_{Sterol} refer to integrated peak areas of the internal standard and individual sterol. Within this thesis, sterols in most of the surface sediment samples were measured on GC, whereas the measurement of sterols in the sediment cores were carried out on MSD as the spectra were needed to permit a proper identification of the weakly concentrated sterols, which, in addition, might have been affected by co-elutants. Therefore, we compared the concentrations of brassicasterol and campesterol (marine and terrigenous biomarkers, respectively) obtained from MSD to those from GC, which show a very well correlation (Figure 2.13). The GC detection threshold for samples is about 10ng/g.

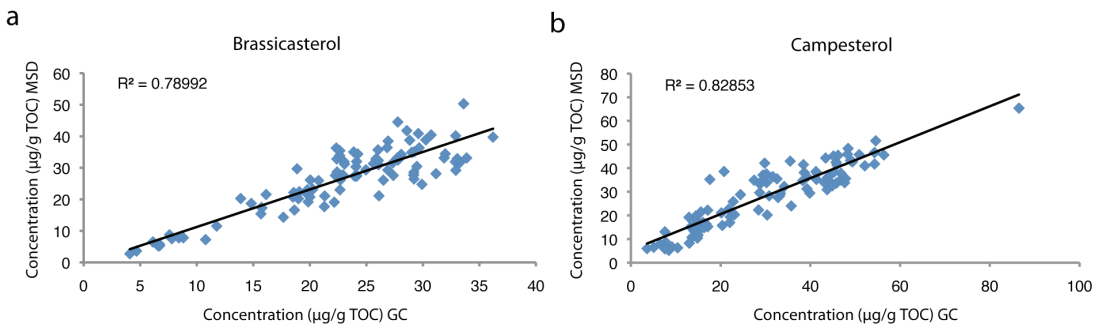

Figure 2.13 Correlation of sterol concentrations obtained from MSD and GC for brassicasterol (a) and campesterol (b).

The biomarker concentrations were corrected to the amount of extracted sediment. The absolute biomarker concentrations have been normalised to the TOC content to account for the different sedimentation rates in our study area, which might have led to an overestimation or underestimation of the biomarker concentrations.

(4) Instrument accuracy: in order to evaluate the accuracy of the measurements on the instruments, we performed multiple measurements on the GC-MSD and GC, respectively. We measured HBIs (e.g. IP_{25}) 10 times on the MSD and sterols (e.g. brassicasterol) 10 times on the GC, as IP_{25} measurement and identification are always performed on the MSD, while sterol measurements for surface sediment samples within this thesis were carried out on the GC. First of all, the values of the multiple measurements basically distribute very close to the mean values with low deviations (Figure 2.14), which indicate the high accuracy and low variation of the measurements on both instruments. Secondly, as known, if a dataset

distribution is approximately normal ('normal' refers to 'close to the mean value') then about 68% of the data values are within one standard deviation of the mean (μ ± σ), about 95% are within two standard deviations (μ ± 2σ), and about 99.7% are within three standard deviations (μ ± 3σ). The normal distribution curves based on our multiple measurements show that 100% data lie within three standard deviations (μ ± 3σ) (Figure 2.14), further indicating the good reproducibility on both the MSD and GC.

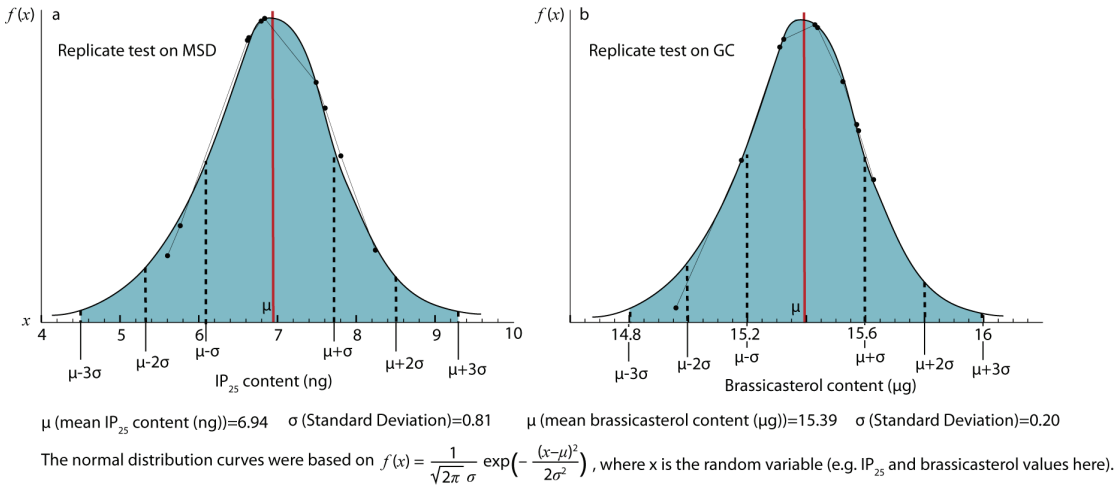

Figure 2.14 Normal distribution curves based on the multiple measurements of IP_{25} and brassicasterol on the MSD (a) and GC (b), respectively.

(5) Influence of ASE extraction method on C_{25}-HBIs: for the C_{25}-HBI diene and C_{25}-HBI triene it has to be pointed out that the results produced by ASE extraction have to be considered with caution (Belt et al., 2014). IP_{25} concentrations based on 7-HND as an internal standard showed excellent agreement between the ASE and sonication extraction methods, whereas recoveries of some more unsaturated HBIs were lower with the ASE procedure, possibly due to partial degradation of these compounds caused by higher temperatures used in this method. A small depletion of HBI diene was found relative to IP_{25}. However, this deleption was more noticeable for HBI triene (for further details see Belt et al., 2014). The distinct depletion of HBI triene resulted by ASE procedure was noticed after the paper included in this thesis (Chapter 3) had been published. For future measurements, the ASE method for extraction of HBI diene and HBI triene need to be developed, for example, by means of additional internal standard employed.

3. Biomarker distributions in surface sediments from the Kara and Laptev Seas (Arctic Ocean): Indicators for organic-carbon sources and sea-ice coverage

Xiaotong Xiao*, Kirsten Fahl, Ruediger Stein

Alfred Wegener Institute, Helmholtz Center for Polar and Marine Research, Am Alten Hafen 26, 27568 Bremerhaven, Germany

Published in Quaternary Science Review (November, 2013)

Abstract

Studies of spatial and temporal changes in modern and past sea-ice occurrence may help to understand the processes controlling the recent decrease in Arctic sea-ice cover. Here, we determined concentrations of IP_{25}, a novel biomarker proxy for sea ice developed in recent years, phytoplankton-derived biomarkers (brassicasterol and dinosterol) and terrigenous biomarkers (campesterol and ß-sitosterol) in the surface sediments from the Kara and Laptev seas to estimate modern spatial (seasonal) sea-ice variability and organic-matter sources. C_{25}-HBI dienes and trienes were determined as additional palaeoenvironmental proxies in the study area. Furthermore, a combined phytoplankton-IP_{25} biomarker approach (PIP_{25} index) is used to reconstruct the modern sea-ice distribution more quantitatively. The terrigenous biomarkers reach maximum concentrations in the coastal zones and estuaries, reflecting the huge discharge by the major rivers Ob, Yenisei and Lena. Maxima in phytoplankton biomarkers indicating increased primary productivity were found in the seasonally ice-free central part of the Kara and Laptev seas. Neither IP_{25} nor PIP_{25}, however, shows a clear and simple correlation with satellite sea-ice distribution in our study area due to the complex environmental conditions in our study area and the transportation process of sea-ice diatom in the water column. Differences in the diene/IP_{25} and triene/IP_{25} ratios point to different sources of these HBIs and different environmental conditions. The diene/IP_{25} ratio seems to correlate positively with sea-surface temperature, while negatively with salinity distributions.

3.1 Introduction

The polar sea ice is a fundamental component of Earth's climate system, contributing to heat reduction (albedo), deep-water formation and gas exchange between the ocean and the atmosphere. The annual cycle of sea-ice formation and melting processes plays an important role in determining the global climate, furthermore it influences the primary productivity of

surface water masses, the benthos in the abyss and the habitat for polar marine mammals and birds (Siegel, et al., 1997; Stein, 2008; Dieckmann and Hellmer, 2010). In this context the rapid shrinking sea ice, especially in the Arctic Ocean, is of major interest for the entire community (Johannessen et al, 1995; Francis et al., 2005; Stroeve et al., 2005, 2007, 2008; Thomas and Dieckmann, 2010). In order to understand processes controlling the recent dramatic reduction in Arctic sea-ice cover, it is essential to determine spatial and temporal changes in sea-ice occurrence and its natural variability in the present and past.

The recent Arctic sea-ice conditions have been determined by microwave satellite remote sensing observation (Johannessen et al, 1995, 1999; Comiso and Parkinson, 2004; Stroeve et al., 2005, 2007, 2008) as well as from the dataset based on cruise reports, aerial observation and digitization of the sea-ice charts for the early 20th century (Rothrock, 1999; Walsh et al, 2001; Rayner et al, 2003), while the reconstruction of the palaeo-latitudinal extent of sea ice is mainly derived from geological data, including sedimentological, geochemical and micropalaeotological parameters of surface sediments and sediment cores (Fahl and Stein, 1999, 2007; Cremer, 1999; Knies et al., 2001; Polyakova and Stein, 2004; Armand and Leventer, 2010). However, the use of some of these parameters, e.g. siliceous frustules and calcareous microfossils as indicators of sea ice, has been limited due to the restricted preservation of diatoms and foraminifera in Arctic Ocean sediments (Wollenburg et al., 2001, 2004; Armand and Leventer, 2010). Therefore, stable and well-preserved biomarker proxies derived from sea ice, have been developed recently. The novel sea-ice biomarker IP_{25}, a mono-unsaturated highly branched isoprenoid (HBI) alkene with 25 carbon atoms biosynthesized specifically by sea-ice algae, has been used to reconstruct the sea-ice distribution (Belt et al, 2007). These authors also showed that this biomarker is stable in marine sediments due to its resistance to degradation in the water column and to other diagenetic processes in the sediment. IP_{25} data were compared with historical sea-ice records and other proxy data (e.g. isotopic composition, foraminifera and particle size) in further studies (Massé et al., 2008; Vare et al., 2009), which provided evidence for the stable preservation of this new proxy in marine sediments. The occurrence of this monoene in sediment cores from the North Icelandic Shelf, the central Canadian Arctic Archipelago, the central Arctic Ocean and the northern Fram Strait, consistent with other palaeoclimatic parameters, has demonstrated that IP_{25} is a reliable proxy to reconstruct past sea-ice distribution (Massé et al., 2008; Müller et al., 2009; Vare et al., 2009; Belt et al., 2010, Fahl and Stein, 2012; Stein et al., 2012). Stein and Fahl (2012) could show that IP_{25} is even preserved in sediments as old as 2.2 Ma. The absence of IP_{25} illustrates ice-free or permanent ice conditions, whereas the presence of IP_{25} indicating spring sea-ice occurrence (Belt et al., 2007; Müller et al., 2009). Recently, the combination of brassicasterol derived from open-

water phytoplankton with IP_{25} enables the reconstruction of various sea-ice conditions (Müller et al., 2009, 2011). The absence of both biomarkers demonstrates a permanent ice cover, whereas the absence of IP_{25} with elevated brassicasterol suggests ice-free conditions. On the other hand, the occurrence of both biomarkers reflects the seasonal ice margin. Müller et al. (2011) have reconstructed modern sea-ice distribution using a combined phytoplankton marker – IP_{25} approach ("PIP_{25} index"), which may provide a more quantitative evaluation of paleo sea-ice conditions to be incorporated into models for forecasting further climate change.

3.2 Study area

In this study, we analysed surface sediments from the Kara and Laptev seas, fringing the northeastern rim of the Eurasian continent and covering large part of the Siberian shelf area. Both seas are of essential importance for water-mass and sea-ice transport into the Arctic Ocean (Lisitsyn and Vinogradov, 1995). The hydrography of this area is influenced by the inflow of warm Atlantic Water and supply of freshwater from major rivers (Jones, 2001; Peterson et al, 2002) (Figure 3.1).

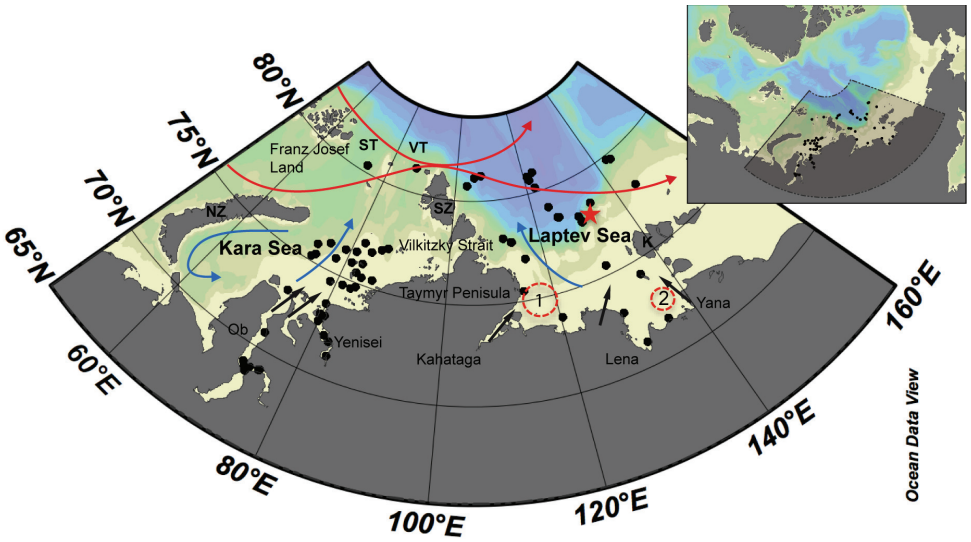

Figure 3.1 Map of sampling location (black dots) and oceanographic setting (Jones, 2001). Red arrows show the flow of warm Atlantic Water and the blue arrows represent the water entering the Arctic Ocean from Kara and Laptev seas. Straight arrows indicate river discharges (Peterson et al, 2002). SZ: Severnaya Zemlya; NZ: Novaya Zemlya; K: Kotelnyy; ST: St. Anna Through; VT: Voronin Through. The location of Core PS2458 is shown as red star. Dashed circles indicate (1) Taymyr ice massif and (2) Yana ice massif.

Relatively warm, dense water from the Atlantic Ocean enters the Arctic Ocean through Fram

Strait between Greenland and Svalbard and through the Barents Sea. This water transport occurs through two branches, the Fram Strait Branch and the Barents Sea Branch (Figure 3.1). The Barents Sea Branch crosses the Barents Sea and enters the Kara Sea via the St. Anna Trough. The Fram Strait Branch flows eastward along the continental slope north of the Barents Sea after entering the Eurasian Basin. Here, north of the Kara Sea, part of the Fram Strait Branch returns in the vicinity of the Nansen-Gakkel Ridge, and part joins the Barents Sea Branch to continue to cross the boundary of the Kara and Laptev seas (Schauer et al, 1997; Jones, 2001). The cold freshwater from the Kara and Laptev seas joins the Transpolar Drift, flowing from the Siberian Coast towards the Fram Strait.

River inflow into the Kara and Laptev seas is dominantly contributed by three of the largest rivers on Earth: Yenisei, Ob and Lena, which drain about 60% of Eurasian Arctic landmass and transport myriads of organic matter into the Kara and Laptev seas (Peterson et al, 2002; Fahl et al., 2003; Stein et al., 2004; Stein and Fahl, 2004a, 2004b). This supply of freshwater substantially affects the process of freezing, transport, and melting of sea ice (Aagaard and Carmack, 1989), and is particularly important for coastal fast ice processes (Divine et al, 2004; Bareiss and Görgen, 2005).

The ice realm of the Kara and Laptev seas is characterized by strong seasonal and interannual variability, comprising a variety of sea-ice conditions such as drift ice, fast ice, ice massifs and coastal polynyas (Parkinson et al., 1999; Bareiss and Görgen, 2005, Figure 3.2a-c). Corresponding to the sea-ice conditions, the sea-surface temperature (SST) also shows a distinct seasonal variability in this area and increases gradually from north to south in summer (Figure 3.2d). The sea-ice cover reaches its maximum in March and then starts to retreat northward (Figure 3.2a). The sea-ice extent reaches its minimum in September with major parts becoming ice-free (Figure 3.2b). With respect to sea-ice conditions, the Kara and Laptev seas present a complex system. First, the sea-ice cover of these areas is characterized by large zones of fast ice (motionless ice along the shore line) during winter (Pfirman et al., 1995; Polyakov et al., 2003; Divine et al., 2004; Bareiss and Görgen, 2005; Figure 3.2c) and the winter polynyas (long and narrow zones of open water) occur along the boundary of the fast ice on the continental shelf (Martin and Cavalieri, 1989; Dethleff et al., 1998; Bareiss and Görgen, 2005; Kern, 2008; Figure 3.2c). Second, during summer sea ice is transported into the Kara and Laptev seas from the Arctic Basin, whereas during winter sea ice is exported towards the Arctic Basin (Mironov et al., 2007a). Furthermore, sea ice from the Kara and Laptev seas is exported by the Transpolar Drift throughout the Arctic Ocean to the Greenland Sea and North Atlantic (Meese et al., 1997; Mironov et al., 2007b). Third, the strong fluvial input influences the formation and melting of sea ice (Fahl et al., 2003; Stein et al., 2004; Rivera et al., 2006), especially the fast-ice processes. This region also includes several

archipelagos on the shelf, which are glaciated at present: Novaya Zemlya, Severnaya Zemlya, and Kotelnyy.

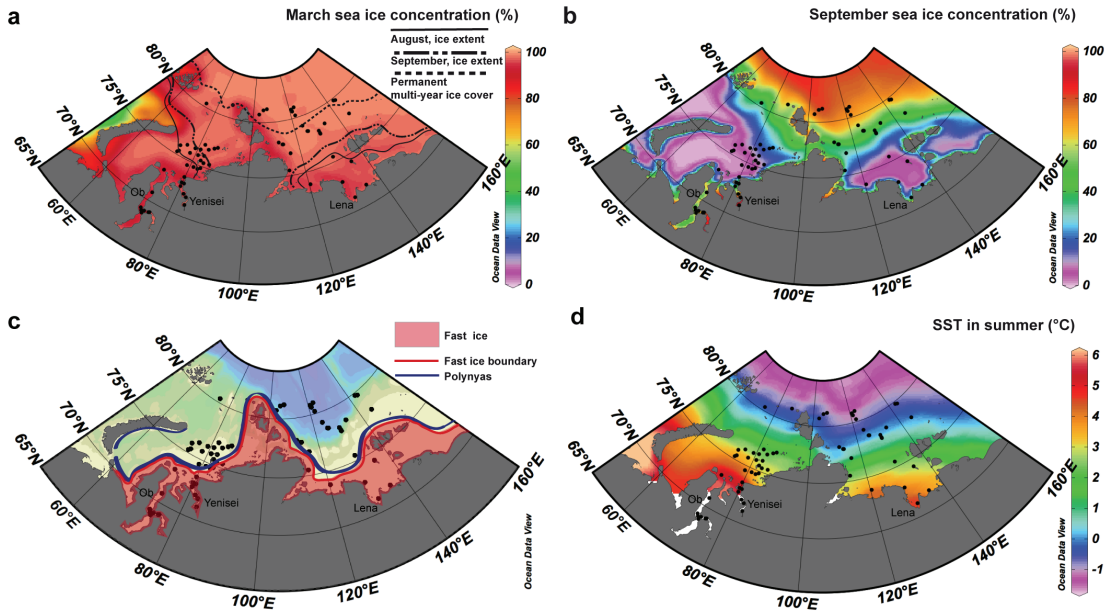

Figure 3.2. Average sea-ice concentration in (a) March and (b) September from 1978 to 2007 (http://nsidc.org). Location of fast ice and polynyas and sea-surface temperature (SST) (http://odv.awi.de/en/data/ocean/world_ocean_atlas_2009/) are shown in (c) and (d), respectively. Dashed line indicates southern boundary of permanent sea-ice cover (>60% throughout the year). August and September boundaries of sea-ice cover represent the 30% isoline for the specific months.

3.3 Materials and methods

3.3.1 Sediment sampling

The surface sediment samples from the Laptev Sea shelf and slope were taken in 1993 during the RV *Polarstern* expedition ARK IX/4 (Fütterer, 1994) and the Transdrift I expedition with RV *Ivan Kireyev* (Kassens and Karpiy, 1994), and during RV *Polarstern* expedition ARK XXVI/3 in 2011 (TransArc, Schauer, 2012). The surface sediment samples from the Ob and Yenisei transects and the inner and central Kara Sea shelf were taken during the *Akademik Boris Petrov* expeditions in 2000, 2001and 2002 (Stein and Stepanets, 2001, 2002; Schoster and Levitan, 2003). The sampling was carried out with a giant boxcorer and a multicorer. Whereas total organic carbon was measured in all samples (cf., Stein and Fahl, 2004a, 2004b), the biomarker parameters were determined on selected samples (see Appendix 1).

3.3.2 Biomarker analyses

For biomarker analyses, the freeze-dried surface sediments were extracted by an Accelerated Solvent Extractor (DIONEX, ASE 200; 100°C, 5 min, 1000 psi) using dichloromethane:methanol (2:1 v/v). For quantification the internal standards 7-hexylnonadecane, squalane and cholesterol-d_6 (cholest-5-en-3β-ol-D_6) were added before any analytical treatment. Further separation of hydrocarbons and sterols was carried out via open-column chromatography using SiO_2 as stationary phase. Hydrocarbons were eluted with *n*-hexane (5 ml) and sterols with ethylacetate:*n*-hexane (20:80 v/v; 6 ml). The latter were silylated with 500 µl BSTFA (60 °C, 2 hrs). Compound analyses of both fractions were carried out on an Agilent 6850 GC (30 m HP-5MS column, 0.25 mm i.d., 0.25 µm film thickness) coupled to an Agilent 5975 C VL mass selective detector. The GC oven was heated from 60 °C to 150 °C at 15 °C min^{-1}, and then at 10 °C min^{-1} to 320 °C (held 15 min) for the analysis of hydrocarbons and at 3 °C min^{-1} to 320 °C (held 20 min) for sterols, respectively. Mass spectrometer conditions were 70 eV and 230 °C (ion source). Helium was used as carrier gas. Individual compound identification was based on comparisons of their retention times with that of reference compounds and on comparisons of their mass spectra with published data (Belt et al., 2007; Boon et al., 1979; Johns et al., 1999; Volkman, 1986). Biomarker concentrations were calculated on the basis of their individual GC–MS ion responses compared with those of respective internal standards. For further details concerning the C_{25}-HBI alkenes (IP_{25}, C_{25}-HBI diene, and C_{25}-HBI triene) quantification see Müller et al. (2011) and Fahl and Stein (2012). Brassicasterol (24-methylcholesta-5,22E-dien-3β-ol), dinosterol (4α,23,24R-trimethyl-5α-cholest-22E-en-3β-ol), campesterol (24-methylcholest-5-en-3b-ol) and ß-sitosterol (24-ethylcholest-5-en-3b-ol) were quantified as trimethylsilyl ethers using gas chromatography (for details see Fahl and Stein, 1999). The biomarker concentrations were corrected to the amount of extracted sediment.

3.3.3 Calculation of "PIP_{25} index"

In order to assess more quantitative reconstructions of sea-ice distributions, Müller et al. (2011) have calculated a phytoplankton-IP_{25} index (PIP_{25}), which provided new insights into the evaluation of the sea-ice distribution in the northern North Atlantic (Fram Strait). In our study, we calculated P_BIP_{25} (using brassicasterol) and P_DIP_{25} (using dinosterol), using the following formulae (for details see Müller et al., 2011):

(1) $P_BIP_{25} = IP_{25} / (IP_{25} + \text{brassicasterol}*c)$

(2) $P_DIP_{25} = IP_{25} / (IP_{25} + \text{dinosterol}*c)$

With c = mean IP_{25} concentration / mean (1) brassicasterol or (2) dinosterol concentrations

of all surface sediments.

3.3.4 Data presentation and storage

Maps of sea-ice distribution, sea-surface temperature, total organic carbon, and biomarker distributions were generated using the Ocean Data View program (Schlitzer, 2012).

All data are available on PANGAEA (http://dx.doi.org/10.1594/PANGAEA.803232).

3.4 Results

3.4.1 Total organic carbon (TOC)

The TOC values are about 0.2–3% and 0.5–2.5% in Kara Sea and Laptev Sea, respectively (Figure 3.3; Fernandes and Sicre, 2000; Fahl et al., 2001; Stein et al., 2003; Stein and Fahl, 2004a, 2004b). In the Kara Sea, maximum TOC values of 1.5–2.5% occur in the estuaries and the St. Anna Through, separated by relatively low TOC values (<1%) in the central Kara Sea. The TOC distribution pattern of the Laptev Sea is similar to that of Kara Sea. Maximum values of up to 2% occur in the vicinity of Lena Delta.

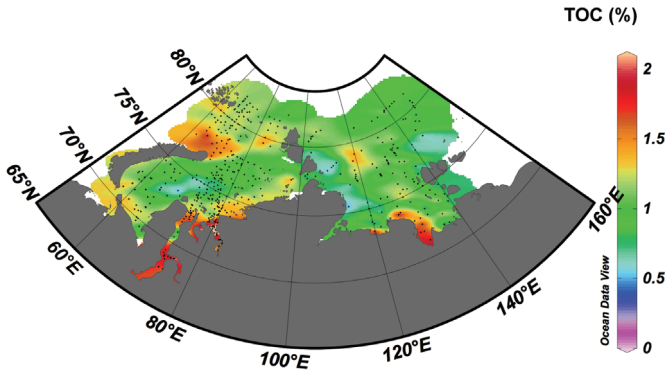

Figure 3.3 Distribution map of TOC (Total Organic Carbon) in surface sediments from the Kara and Laptev seas (Stein and Fahl. 2004a. 2004b).

3.4.2 Sterols

The concentrations of phytoplankton biomarkers (brassicasterol and dinosterol) and terrigenous biomarkers (campesterol and ß-sitosterol) in surface sediments are shown in distribution maps (Figure 3.4). The distribution patterns of both brassicasterol and dinosterol are very similar. The highest brassicasterol (62–180 µg/g TOC) and dinosterol (48–94 µg/g TOC) contents occur in the Central Kara Sea and along the continental slope of Laptev Sea, and they decrease towards the deep sea and river mouths, respectively. Low concentrations were detected for brassicasterol (17–88 µg/g TOC) and dinosterol (10–38 µg/g TOC) in the Ob and Yenisei rivers. In contrast, the maximum values of the terrigenous biomarkers

(campesterol, 141–667 µg/g TOC; ß-sitosterol, 233–525 µg/g TOC) are localized in the rivers and estuaries and correlate with elevated TOC contents (Figure 3.3). The campesterol and ß-sitosterol concentrations decrease gradually northward and reach the minimum values (12-21 µg/g TOC and 53-104 µg/g TOC, respectively) along the continental slope to the north of Kara and Laptev seas.

3.4.3 C_{25} highly branched isoprenoid (HBI) alkenes and Phytoplankton-IP_{25} index

The mono-unsaturated C_{25}-HBIs (IP_{25}, Figure 3.5a, Appendix 2) show highest contents (3–11µg/g TOC) in the Central Kara Sea and then decrease gradually from the central area to the rivers, reaching low concentrations (0.2–0.7 µg/g TOC) in the vicinity of estuaries. Directly in the Ob and Yenisei rivers IP_{25} is completely absent. In the Laptev Sea, minimum concentrations of IP_{25} (1.5–2.3 µg/g TOC) are found in sediments from the continental margin. In contrast, maximum IP_{25} values (4–11 µg/g TOC) occur along the outer shelf and continental slope. From here, IP_{25} values slightly decrease southward but obviously increase in the east of Taymyr Peninsula (8–9 µg/g TOC) and southwest of Kotelnyy (5–8 µg/g TOC). Low IP_{25} values were detected near the Lena River mouth.

In general, the P_BIP_{25} and the P_DIP_{25} index (Figure 3.5b-c) display a distribution quite similar to the IP_{25} data. Maxima occur in the central Kara Sea as well as east of Taymyr Peninsula and around Kotelnyy Island.

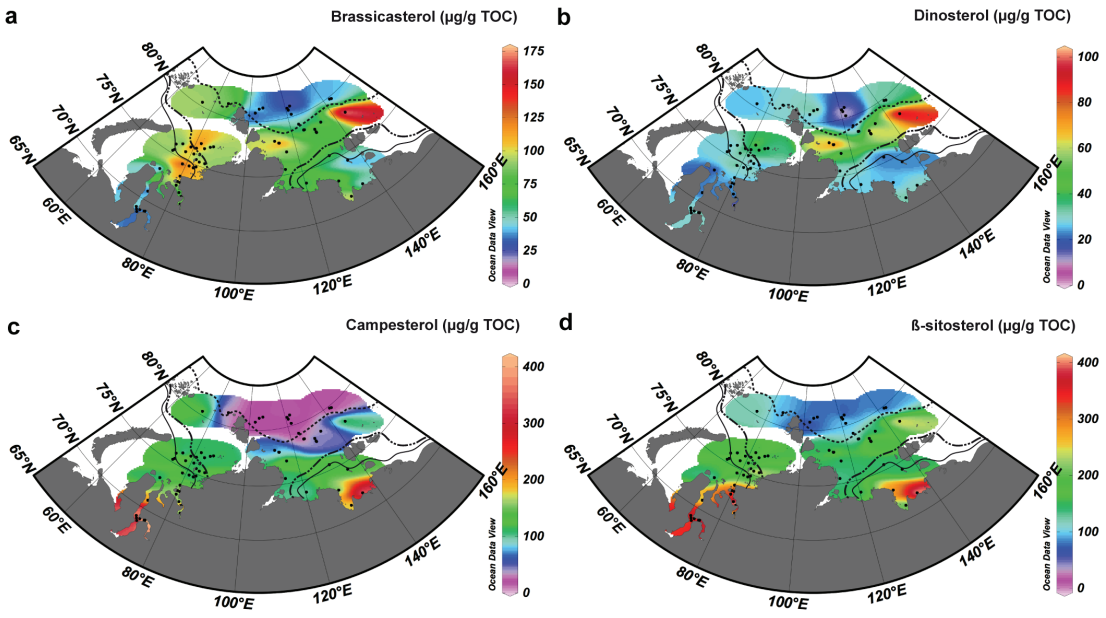

Figure 3.4 Concentrations (µg/g TOC) of open-water phytoplankton biomarkers (brassicasterol (a) and dinosterol (b)) and terrigenous biomarkers (campesterol (c) and ß-sitosterol (d)) in surface sediments from the Kara and Laptev seas. For explanation of dashed and solid lines see Figure 3.2.

High C_{25}-HBI diene values (Figure 3.6a) occur in the central Kara Sea (6–14 µg/g TOC), east of Taymyr Peninsula (8–20 µg/g TOC) and southwest of Kotelnyy (5–8 µg/g TOC), while decreasing values were determined in the rivers and adjacent continental margin. C_{25}-HBI trienes (Figure 3.6b) occur in relatively high concentrations (0.31–0.67 µg/g TOC) in the western Laptev Sea, along the east coast of Taymyr Peninsula; they are completely absent in the rivers and deep-sea environment. The diene/IP_{25} ratio as well as the triene/IP_{25} ratio (Figure 3.6c-d; Appendix 2) generally increase from the deep sea towards the river. Their correlations are shown in Figure 3.9.

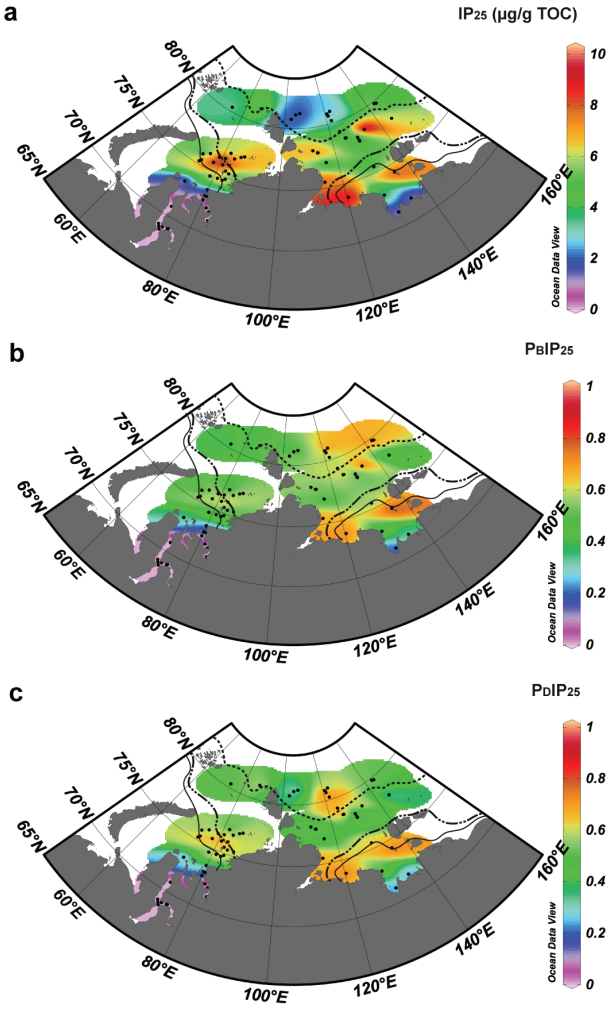

Figure 3.5 Concentrations (µg/g TOC) of IP_{25} (a) in surface sediments from the Kara and Laptev seas and values of P_BIP_{25} index (b). For explanation of dashed and solid lines see Figure 3.2.

3.5 Discussion

Strong seasonal and regional variability in the Kara and Laptev sea-ice extent are reflected in changes in organic-carbon sources, i.e. phytoplankton and sea-ice algae production as well as terrigenous input. Thus, we determined concentrations of C_{25}-HBI alkenes (IP_{25}, diene and triene), open-water phytoplankton-derived biomarkers (brassicasterol and dinosterol) and terrigenous biomarkers (campesterol and ß-sitosterol) to reconstruct recent surface-water characteristics with special emphasis on sea-ice conditions in these areas. The interpretation of our biomarker data is illustrated in a schematic diagram (Figure 3.7), showing the general sea-ice formation and melting processes in the Siberian marginal seas. Additionally, it reveals the variable terrigenous input and productivity of ice algae and phytoplankton during different seasons.

3.5.1 Organic carbon source and terrigenous biomarker distributions

The TOC preserved in surface sediments is predominantly originated either from primary production or terrigenous input. In the rivers and estuaries of the Kara and Laptev seas, the organic matter is almost entirely of terrigenous origin (Stein and Fahl, 2004a, b), which is well reflected by the organic geochemical bulk parameters. High C/N ratios > 10, low HI (hydrogen index) < 100 mgHC/gOC and light $\delta^{13}C_{org}$ values of about -28.7‰ (Ob), -27‰ (Yenisei) and -27.1‰ (Lena) reflect the predominantly terrigenous origin of TOC (Fahl and Stein, 1997; Rachold and Hubberten, 1999; Fernandes and Sicre, 2000; Krishnamurthy et al., 2001; Fahl et al., 2003). North of the Ob and Yenisei estuaries, for example, the proportion of terrigenous organic carbon ranges between 66 and 89% of the TOC (Fernades and Sicre, 2000). Nearly the same conditions were recorded in the Laptev Sea off the Lena River (Stein and Fahl, 2004b). Furthermore, TOC values are influenced by freshwater diatom productivities to some degree (Cremer, 1999; Polyakova, 2003). In contrast, the relatively low TOC values in the central part of Kara and Laptev seas are attributed to the decreasing terrigenous organic-carbon input towards the north. This northward decrease in terrigenous input is also reflected in a characteristic decrease of the biomarkers campesterol and ß-sitosterol (Figure 3.4c-d), synthesized by higher plants (Huang and Meinschein, 1976; Volkman, 1986).

Highest concentrations of campesterol and ß-sitosterol in the rivers and estuaries agree with observations of Fahl and Stein (1997), Fernandes and Sicre (2000) and Gaye et al. (2007), who detected light $\delta^{13}C$ and $\delta^{15}N$ values, and high concentrations of long-chain *n*-alkanes ($C_{27}+C_{29}+C_{31}$) of about 350–410 µg/g TOC in the estuaries of the Kara Sea rivers and about 600 to > 1000 µg/g TOC off the Laptev Sea rivers, especially off the Lena Delta. This can be interpreted as a result of strong riverine input and the "marginal filter" effect near the river mouths, where most of the organic matter accumulates in the surface sediments (Lisitzin, 1995). Furthermore, high concentrations of campesterol and ß-sitosterol (Figure 3.4c-d), TOC (Figure 3.3), and long-chain *n*-alkanes (Fahl et al., 2001) were determined north of the estuaries (>72°N), following the submarine channels. Moreover, sediment organic matter can be incorporated into the sea ice during ice formation on the shallow shelf and then transported to the open ocean via sea-ice export to the Arctic Basin, reflecting seasonal ice variability, inducing the sea-ice exchange between marginal seas and the Arctic Ocean (Nürnberg et al., 1994; Eicken et al., 1997; Pfirman, 1997).

3.5.2 Marine biomarker distributions and sea-ice conditions

Minimum concentrations of IP_{25} (Figure 3.5a) and phytoplankton biomarkers (Figure 3.4a-b)

occur in surface sediments from the adjacent continental margin (>80°N, northeast of Severnaya Zemlya), interpreted as all-season permanent sea-ice cover in this area. This is also supported by the combined phytoplankton-IP_{25} biomarker approach. High P_BIP_{25} values (0.65–0.79, Figure 3.5b), based on both low contents of IP_{25} and brassicasterol, point to permanent sea-ice conditions north of the Laptev Sea continental margin. The sea ice along the northern continental slope survives the spring and summer melting and remains at the end of melting period in September. Thus, this sea-ice cover causes a restricted marine primary productivity due to the extremely limited light penetration (Cremer, 1999; Belchansky and Douglas, 2002).

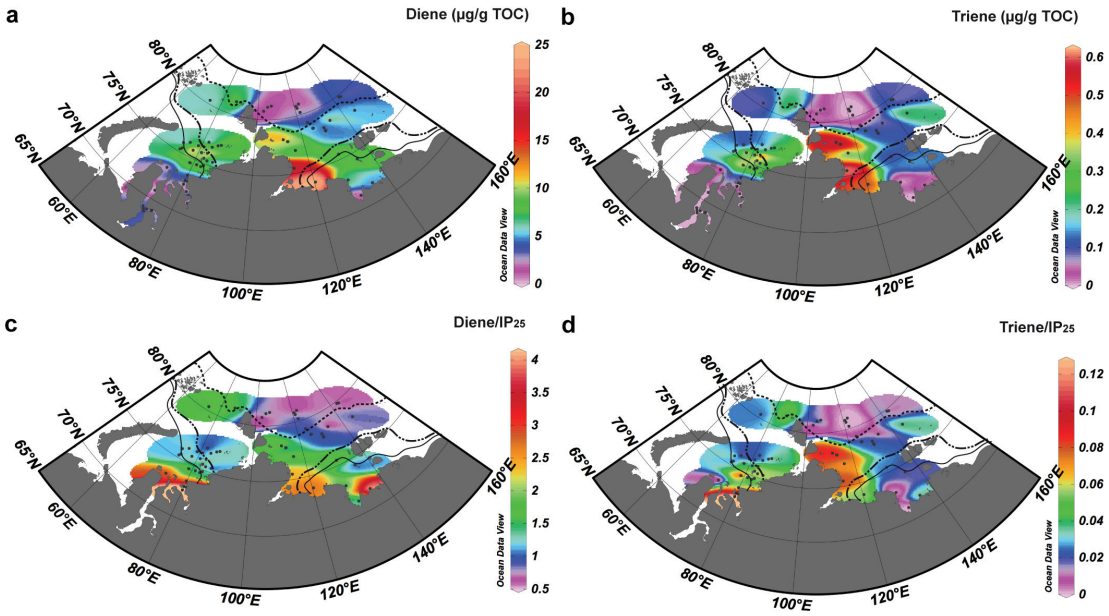

Figure 3.6 Concentrations (µg/g TOC) of C_{25} HBIs diene (a) and C_{25} HBIs triene (b) in surface sediments from the Kara and Laptev seas and values of diene/ IP_{25} (c) and triene/ IP_{25} ratios (d). For explanation of dashed and solid lines see Figure 3.2.

In contrast, the co-occurrence of increased IP_{25} values and open-water phytoplankton biomarkers from Franz Josef Land to southwest of Severnaya Zemlya (>75°N; including the central part of Kara Sea) and from Vilkitzky Strait to the north of Kotelnyy, along the southern continental slope, lead to the assumption of an existing sea-ice edge during summer (Figures 3.2b and 3.7) resulting in favourable living conditions for both ice algae and open-water phytoplankton (cf., Müller et al., 2011). At these sites, the sea-ice cover along the outer shelf becomes thinner in the summer and thus light penetration allows algae growth. This

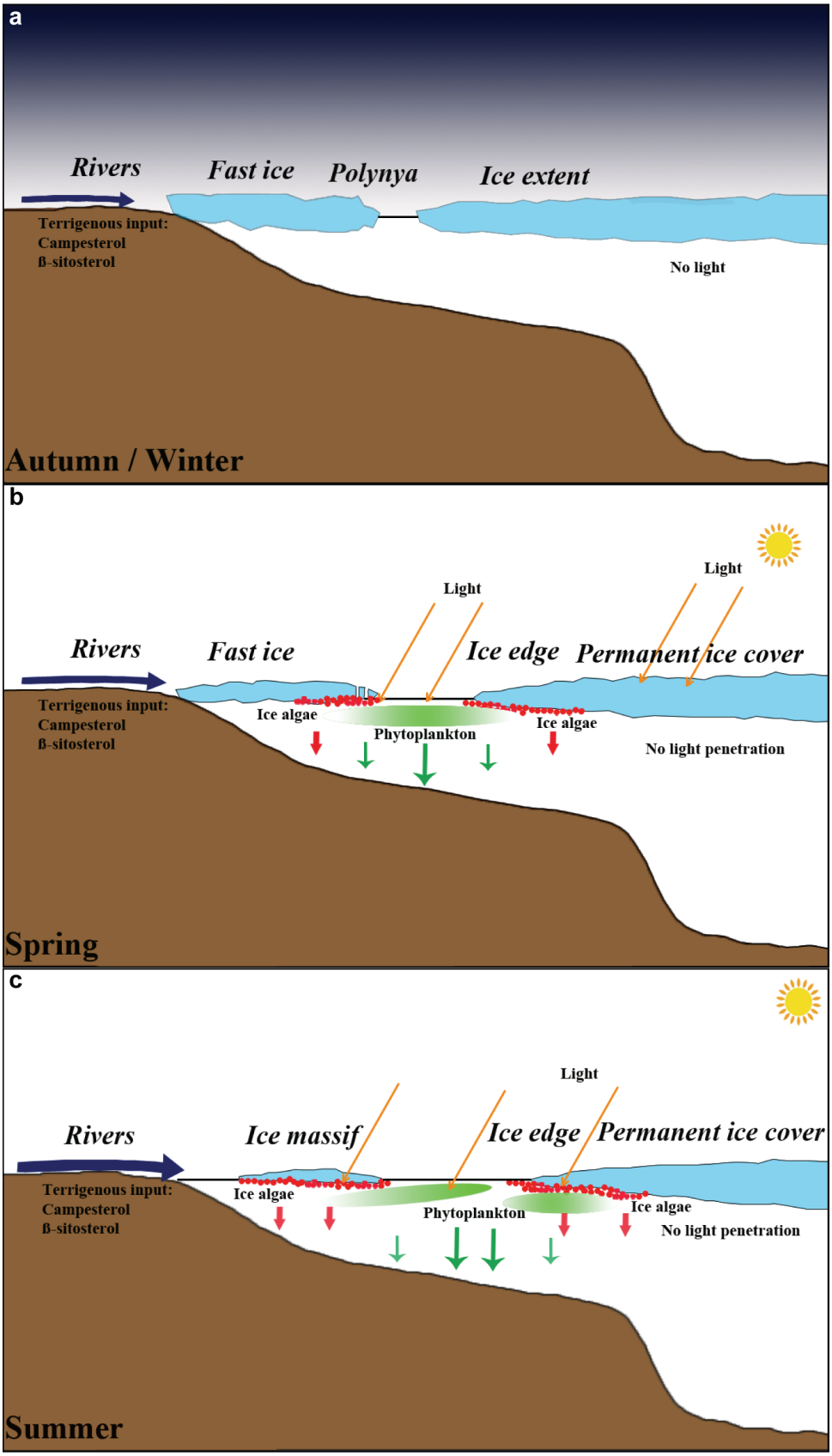

Figure 3.7 A schematic illustration showing the primary production (ice algae and open-water phytoplankton), riverine input and sea-ice distribution during winter (a), spring (b) and summer (c).

interpretation is in agreement with the enriched marine fatty acids observed near the sea-ice edge of the Laptev Sea, where the melting processes induce phytoplankton blooms (Fahl et al., 2001). Furthermore, winter polynyas occur where a summer sea-ice edge exists, resulting in an early bloom of primary productivity in April and May (for locations of polynyas see Mironov et al., 2007b; Figure 3.2c). High concentrations of marine biomarkers in the central Kara Sea result from spring blooms of both sea-ice algae and phytoplankton in the Central Kara polynya (Gaye et al., 2007; Kern, 2008). These findings agree with the investigations of Polyakova (2003), who described the interrelation between the distribution of sea-ice diatoms and sea-ice cover during spring and summer and, in this context, extremely high abundance of these algae at the location of the winter polynya. Regarding the polynyas in the Laptev Sea, high IP_{25}, brassicasterol and dinosterol values east of the Vilkitzky Strait and north of Kotelnyy (Figures 3.4a-b and 3.5a) are probably caused by an enhanced primary productivity near the Northeastern Taymyrskaya and North Novosibirskaya polynyas during spring (Dethleff et al., 1998; Karklin et al., 2007). Similar results were published by Cremer (1999), reporting a dominance of a sea-ice diatom assemblage in sediments from the central and northwestern Laptev Sea shelf and low abundances of these diatoms in the deep sea. All samples with high abundance of sea-ice diatoms occur north of the polynyas (Cremer, 1999). In addition, elevated P_BIP_{25} and P_DIP_{25} values occur in the areas along the northern shelf of the Kara and Laptev seas and the central part of both marginal seas (Figure 3.5b-c), suggesting favourable living conditions for sea-ice algae and phytoplankton produced by a relatively stable sea-ice edge in summer.

IP_{25} values gradually decline southward from the central part of the Kara Sea, reflecting a reduced sea-ice cover from the north to the south. Different from the distribution trend of IP_{25} in Kara Sea, IP_{25} values decrease less gradually towards south in Laptev Sea (Figure 3.5a). Maximum IP_{25} values are found in the sediments east of Taymyr Peninsula and southwest of Kotelnyy in the southern Laptev Sea. In general, sea-ice conditions in these areas reflect a clear seasonal variability with sea ice melting during the summer. In accordance with these observations the $\delta^{18}O$ and $\delta^{13}C$ composition of benthic foraminiferal calcite in the Laptev Sea reflects ice-free conditions during summer and sea-ice cover during winter (Bauch et al., 2004). However, two stationary ice fields occasionally remain during summer: the Taymyr ice massif east of Taymyr Peninsula and Severnaya Zemlya and the Yana ice massif in the south-eastern Laptev Sea (Karklin et al., 2007; for locations see Figure 3.1), which probably provide favourable conditions for sea ice-diatom growth during summer (Figure 3.7c). Barreiss and Görgen (2005) noted these two ice massifs on the satellite-derived sea-ice concentration chart of Laptev Sea from August 1984. Maximum P_BIP_{25} (0.67–0.80) due to high IP_{25} concentrations, are probably related to the occurrence of these ice massifs surviving

into the summer in areas characterized by seasonal sea-ice variability. Reduced concentrations of both brassicasterol and dinosterol near the Yana ice massif are probably caused by unsuitable environmental conditions, while the higher values of both sterols near the Taymyr ice massif east of Taymyr Peninsula can be related to the occurrence of the Eastern Taymyrskaya and Anabaro-Lenskaya polynyas (Martin and Cavalieri, 1989; Karklin et al., 2007).

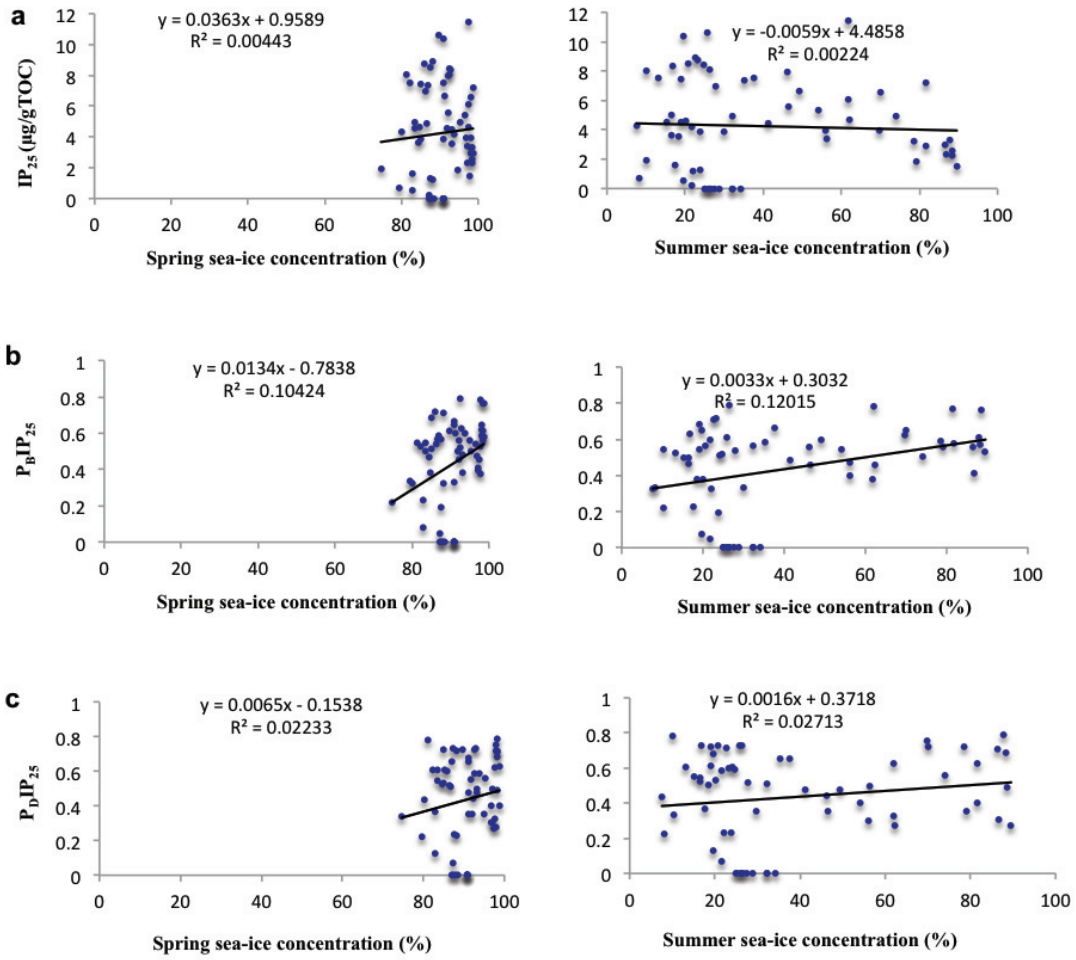

Figure 3.8 Correlation of IP_{25} (a), P_BIP_{25} (b) and P_DIP_{25} (c) with average spring and summer sea-ice concentrations from 1978-2007. Zero values of both IP_{25} and PIP_{25} are found in Ob and Yenisei.

Both IP_{25} and phytoplankton biomarker concentrations diminish towards the river mouths (Figure 3.4a, b and 3.5a), indicating less sea-ice occurrence. In these areas, the seasonal sea-ice cover starts melting in spring and summer. The P_BIP_{25} index also diminishes towards the rivers and reaches low values (P_BIP_{25}, 0.22–0.33) in the vicinity of the estuaries (Figure 3.5b), which points to ice-free conditions during summer. Increasing brassicasterol (Figure 3.4a) concentrations indicate the growth of open-water phytoplankton, coinciding with the retreat

of sea ice in summer. Furthermore, the absence of IP_{25} in the rivers confirms that this proxy exclusively is produced by marine sea-ice algae, for example, *Haslea* spp. including *Haslea vitrea* and *Haslea crucigeroides* (Round et al., 1990; Witkowski et al., 2000; Belt et al., 2007). P_BIP_{25} values of 0 are found directly in the Ob and Yenisei rivers caused by the absence of IP_{25}, with the occurrence of relatively low concentrations of phytoplankton biomarkers, reflecting the riverine environment. These data show that the absence of IP_{25} coinciding with zero (very low) phytoplankton biomarker concentrations may not only be caused by a permanent sea-ice cover (cf., Müller et al., 2009, 2011).

In contrast to the good correlation between IP_{25} and PIP_{25} with sea-ice concentration derived from satellite data described for the Fram Strait area (Müller et al., 2011), our data set does not show this correlation (Figure 3.8). This may be explained by the more complex environmental situation in our study area, influenced by sea ice and fast-ice formation, occurrence of ice massifs and river discharge (see schematic illustration Figure 3.7). The abundance of IP_{25} preserved in sediments controlled by variable factors, for example, transportation of ice algae in the water column, sediment deposition rates and sediment grain size. In our study area, the strong riverine discharge transports plenty of suspended matter to the inner estuaries and outer estuaries (Fahl et al., 2003; Stein et al., 2004; Rivera et al., 2006), which influences the transportation process, sedimentation rates and the formation and melting of sea ice. Furthermore, the occasional occurrence of ice massifs may provide favourable living conditions for sea-ice diatoms during summer, but is not shown in average sea-ice satellite distribution map.

3.5.3. C_{25}-HBI monoene, diene and triene concentrations

C_{25} highly branched isoprenoid (HBI) alkenes with different degrees of unsaturation, produced by diatom genera (e.g. *Haslea ostrearia, Rhizosolenia setigera, Pleurosigma intermedium and Navicula sclesvicensis*), have been determined in freshwater, seawater, marine sediments, and freshwater and marine species (Volkman et al., 1994; Belt et al., 2000, 2001a; Massé et al., 2004; Grossi et al., 2004). The extent of unsaturation in HBIs depends on the growth conditions and culture temperatures (Belt et al., 2000; Rowland et al., 2000). As mentioned above, the C_{25}-HBI monoene (IP_{25}) has been used as novel promising ice proxy. In contrast, the C_{25}-HBI diene and triene are found in marine sediments and diatoms from both polar areas and temperate regions (Gearing et al., 1976; Barrick et al., 1980; Volkman et al., 1983; Nichols et al., 1988; Wraige et al., 1997; Johns et al., 1999; Belt et al., 2007; Barbara et al, 2010; Denis et al, 2010; Massé et al., 2011). However, the C_{25}-HBI diene occurred in Antarctic sea ice, while the C_{25}-HBI triene are found in Antarctic phytoplankton samples (Johns et al., 1999; Massé et al., 2011). Previous studies have commonly reported that the

C_{25}-HBI triene may become the predominant hydrocarbon fraction in coastal sediments and particulate matter from nutrient-rich environment, e.g. the Gulf of Mexico shelf, Florida, USA (Gearing et al., 1976), Puget Sound (Barrick et al., 1980) and upwelling zones off Peru (Volkman et al., 1983). In order to investigate the different sources of these compounds and their relation to environmental conditions, we herein compared the three HBIs alkenes with different extents of unsaturation by means of diene/IP_{25} and triene/IP_{25} ratios (Figure 3.6c, d).

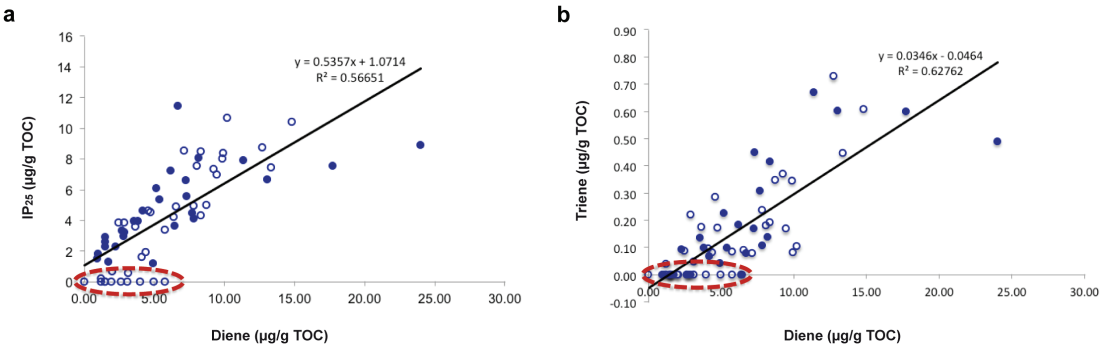

Figure 3.9 Correlations of diene concentrations (µg/g TOC) with IP_{25} concentrations (µg/g TOC) (a) and triene concentrations (µg/g TOC) (b). Zero contents of IP_{25}, located in Ob and Yenisei, are highlighted by a red dashed circle in (a). Zero values of triene are allocated in Ob, Yenisei, estuary of Lena and along the continental slope of Laptev sea and highlighted by a red dashed circle in (b). Open circles: samples from the Kara Sea; solid circles: samples from the Laptev Sea.

In our study area a good correlation between diene and IP_{25} concentrations is obvious (Figure 3.9a), except for the samples in Ob and Yenisei rivers. Based on the similarity in the distributions of IP_{25} and diene (excluding samples in Ob and Yenisei rivers) (Figures 3.5a and 3.6a), these two HBI alkenes probably originate from a common source, e.g. *H. ostrearia*, which has been identified as a major source of C_{25} HBIs in recent studies (Volkman et al., 1994; Wraige et al., 1998; Belt et al., 2000; Rowland et al., 2000; Massé et al., 2004). The distribution of the diene/IP_{25} ratio increasing from north to south, especially in the Laptev Sea, reveals that the enrichment of IP_{25} is stronger than that of the diene in the north and decreases gradually towards the south (Figure 3.6c; see also Vare et al., 2009). The increase in the diene/IP_{25} ratio from north to south seems to be in line with an increase of measured sea-surface temperature (Figure 3.2d), as also reflected in the correlation plot of Figure 3.10a. This observation supports the study by Rowland et al. (2000) who described an increase in unsaturation of HBIs with increasing sea-surface temperature. Furthermore, Fahl and Stein (2012) found distinctly increased diene/IP_{25} ratios during Bølling–Allerød warm intervals, followed by a decrease in diene/IP_{25} ratios coinciding with the Holocene cooling trend, in a

biomarker study of core PS2458 (See Figure 3.1 for location). Based on these preliminary data, they propose that the diene/IP_{25} ratio might be used as proxy for reconstruction of sea-surface temperature in Arctic low-temperature environments, a hypothesis, however, that has to be approved by further data. Furthermore, the diene/IP_{25} ratios show a negative correlation with the salinity distribution in our study area (Figure 3.10b), suggesting that the increasing salinity may result in decreasing unsaturation to a certain extent. Wraige et al. (1998) reported the influence of salinity on the distribution of C_{25} HBI alkenes in *H. ostrearia*. They concluded that the HBI concentrations (the only HBI observed was triene, which is consistent with the study of the effects of temperature on unsaturation in C_{25} HBI alkenes of *H. ostrearia*) were slightly higher at salinities of 25–35 than those at salinities of 15 and 40 at 14–15°C, however, the salinity is not as important as other factors in controlling the productions of C_{25} HBI alkenes. Rowland et al. (2001) found that increased salinity from 15 to 35 at 18°C decreased haslene production, and unsaturation in haslenes was not changed by increased salinity. The study of influence of salinity on the C_{25} HBI alkenes at low temperature is still limited.

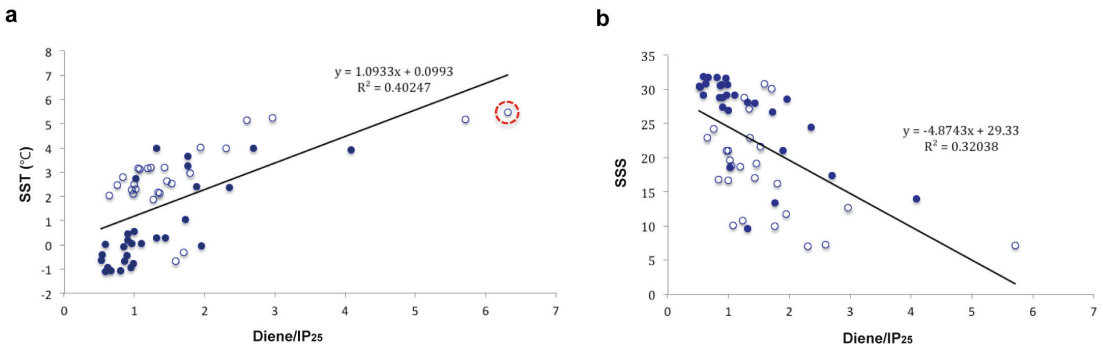

Figure 3.10 Correlations of diene/IP_{25} ratios with SST (sea surface temperature) (a) and SSS (sea surface salinity) (b). Open circles: samples from the Kara Sea; solid circles: samples from the Laptev Sea. The open circle highlighted by a red dashed circle (a) is located in the Yenisei estuary, where the salinity data is not available (b).

The triene concentrations correlate less clearly with IP_{25} concentrations (Figure 3.11), but show a better correlation with diene concentrations (Figure 3.9b), suggesting that the triene probably originates from a different (non-sea ice) source as the IP_{25} but has a common source with the diene. Considering the good correlation between diene and IP_{25}, we suggest that the diene might be produced by a mixed diatom community, as also observed in Antarctic sea ice (Johns et al., 1999). Johns et al. (1999) and Massé et al. (2011) have found C_{25}-HBIs triene in Antarctic phytoplankton, while in our study, the triene concentrations show poor correlations with phytoplankton biomarkers concentrations (both brassicasterol and dinosterol) (Figure

3.11), suggesting that the triene is probably not derived from open-water phytoplankton in this area. Due to the generally low contents of trienes (Figure 3.6b), the triene/IP_{25} ratios are relatively low (Figure 3.6d). High triene/IP_{25} ratios, however, occur in the estuaries of Ob and Yenisei rivers and along the east coast of Taymyr Peninsula, where relatively high concentrations of trienes were found, supporting that the formation of triene is enhanced along coastal area. Furthermore, the triene/IP_{25} is not consistent with the SST distribution (see supplementary material) due to the unsuitable living conditions for the triene production (Rowland et al., 2000). We propose that the triene probably may also originate from the diatom species, *Pleurosigma intermedium and Navicula slesvicensis*, which have been observed in costal sediments and Arctic regions (Belt et al., 2000, 2001b; von Quillfeldt, 2000; Grossi, 2004).

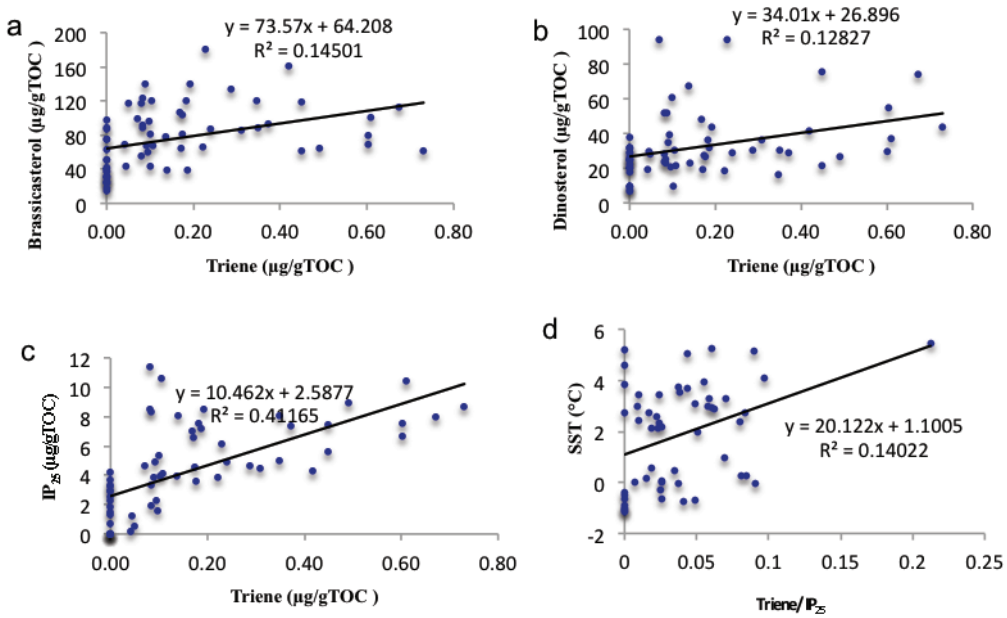

Figure 3.11 Correlation of triene concentration with concentrations of both brassicasterol (a) and dinosterol (b) are poor. Correlation of triene with IP_{25} and triene/IP_{25} with SST are shown in c and d, respectively. Zero values of IP_{25} are found in Ob and Yenisei, whereas zero values of triene are allocated in Ob, Yenisei, estuary of Lena and along the continental slope of Laptev Sea.

3.6 Conclusions

Based on the concentration of IP_{25} and open-water phytoplankton biomarkers, we can conclude that a quite stable marginal ice zone exists along the continental shelf/slope of the Kara and Laptev seas during summer/early fall. Further to the north, lower IP_{25} and phytoplankton biomarker concentrations point to a more closed sea-ice cover situation. There are no IP_{25} and very low brassicasterol and dinosterol concentrations in the river mouths but

high terrigenous biomarker (campesterol and ß-sitosterol) concentrations due to the freshwater inflow transporting terrigenous matter to estuaries. In our study, IP_{25} and PIP_{25} do not show any clear and simple correlations with satellite sea-ice data due to the complex environmental situation characterized by sea ice, fast ice, polynyas and the occasional occurrence of ice massifs, and the influence of river discharge on transportation of sea-ice diatom and formation of sea ice.

The distribution patterns of C_{25}-HBI diene and IP_{25} are very similar suggesting a common (sea-ice) origin of both compounds. The diene/IP_{25} ratio increases southwards correlating with an increase in sea-surface temperature and showing a negative correlation with salinity. The C_{25}-HBI triene, on the other hand, has a less clear correlation with IP_{25} but correlates well with diene concentrations, suggesting that the diene probably originates from mixed diatom sources including a non-sea ice source, by which triene is produced.

Acknowledgement

We thank the Alfred Wegener Institute (Bremerhaven) and China Scholarship Council for the financial support. We are grateful to Xuezhu Wang (AWI, Bremerhaven) for offering the sea-ice satellite data. We thank two anonymous reviewers for numerous constructive suggestions for improving the manuscript.

4. Spatial variability of modern Arctic sea-ice distribution: New biomarker records from Central Arctic Ocean surface sediments

Xiaotong Xiao, Ruediger Stein, Kirsten Fahl, Juliane Müller

Alfred Wegener Institute, Helmholtz Center for Polar and Marine Research, Am Alten Hafen 26, 27568 Bremerhaven, Germany

Submitted to Geochimica et Cosmochimica Acta (Since May 2014)

Abstract

Records of the spatial and temporal variability of Arctic Ocean sea ice are of significance for understanding the causes of the dramatic decrease in Arctic sea-ice cover of recent years. In this context, the newly developed sea-ice proxy IP_{25}, a mono-unsaturated highly branched isoprenoid alkene with 25 carbon atoms biosynthesized specifically by sea-ice associated diatoms and only found in Arctic and sub-Arctic marine sediments, has been used to reconstruct the sea-ice distributions. Within our study, for the first time a comprehensive data set of these biomarkers was produced using fresh and deep-frozen surface sediment samples from the Central Arctic Ocean proper (>80°N latitude) characterized by a permanent ice cover today and recently recovered surface sediment samples from the Chukchi Plateau/Basin partly covered by perennial sea ice. In addition, published and new data from other Arctic and sub-Arctic regions were added to generate an overview distribution map of IP_{25} across major parts of the Arctic Ocean. The phytoplankton biomarkers 24S-brassicasterol and dinosterol were also determined alongside IP_{25} to distinguish between two extreme scenarios, i.e., either ice-free or permanent ice conditions, and to estimate the sea-ice conditions more accurately by means of the phytoplankton-IP_{25} index (PIP_{25}). PIP_{25} index values calculated by combination of IP_{25} and phytoplankton biomarkers reflect modern sea-ice conditions quite well and show a positive correlation with spring/summer sea ice.

When interpreting and calculating PIP_{25} index as a (semi-quantitative) proxy for reconstructions of present and past Arctic sea-ice conditions from different Arctic/sub-Arctic areas, information of the source of phytoplankton biomarkers and the possible presence of allochthonous biomarkers is needed.

4.1 Introduction

Sea ice, prevailing in the polar region and characterized by distinct seasonal and interannual variability, plays a pivotal role in the climate system. For instance, the variability of sea ice affects the interplay between the atmosphere and the ocean by means of changing the heat flow (albedo) and gas exchange (Haas, 2010), as well as the deep-water formation related to the salinity variation caused by brine rejection/absorption during sea-ice formation/retreat (Petrich and Eicken, 2010). Furthermore, sea ice is also one of the largest biomes on earth with an area covering 7% of the earth's surface in winter (Comiso, 2010 and references therein), influencing the ecological system including the primary production, the microbiological and macrobiological communities, and even the top predators of the food web, polar marine mammals and birds (Legendre et al., 1992; Thomas and Dieckmann, 2010).

By the end of the melt season in September, there is only multi-year ice in the Arctic basin and parts of the Canadian Archipelago and around Greenland (Comiso, 2010). In the marginal seas, large zones of fast ice occur on the shallow shelf during wintertime, connected with the islands of the Arctic seas. Along the boundary of the fast ice, there are polynyas and leads. Both fast ice and polynyas influence the dynamics and thermodynamics of the ocean circulation as well as the climate system (Ólason and Harms, 2010; Polyakov et al., 2003). Additionally, the occurrence of fast ice and polynyas plays an important role in the ecological system. The presence of fast ice in spring limits the light penetration, and thus the primary production. The polynyas, on the other hand, provide favourable living conditions for phytoplankton, resulting in significantly increased productivity (Pesant et al., 1996).

One of the characteristics of the Arctic Ocean is that it is a landlocked sea, comprising shallow shelf seas with one deep gateway, the Fram Strait, connecting the Arctic with the Atlantic Ocean (Figure 4.1). Therefore, the sea ice in the Arctic is strongly subjected to freshwater discharge from the Eurasian and Amerasian Arctic rivers, e.g. Yenisei, Ob, Lena and Mackenzie (Figure 4.1; Peterson et al., 2002; Stein and Macdonald, 2004). The supply of freshwater is essential to the process of formation, transport and decay of sea ice; conversely, changes in sea-ice cover may affect the freshwater input, contributing to the Arctic current circulation (Aagaard and Carmack, 1989; Holland et al., 2006, 2009).

Observation of seasonal and interannual sea-ice variability by means of satellites shows the rapid shrinking of sea-ice cover at the end of the melt season during the last decades (Comiso and Parkinson, 2004; Johannessen et al., 1995; Perovich et al., 2008; Serreze et al., 2003, 2007; Stroeve et al., 2005, 2007). Following the extreme sea-ice reduction in summer of 2007 (Kerr, 2007; Perovich et al., 2008; Wang and Overland, 2009), the Arctic sea ice reached a minimum with an extent of 3.29 million square kilometers in September 2012 that is 18% less

than in 2007 and 49% less than in 1979, respectively (Boetius et al., 2013). However, the loss of multi-year ice in recent years is still unexplained.

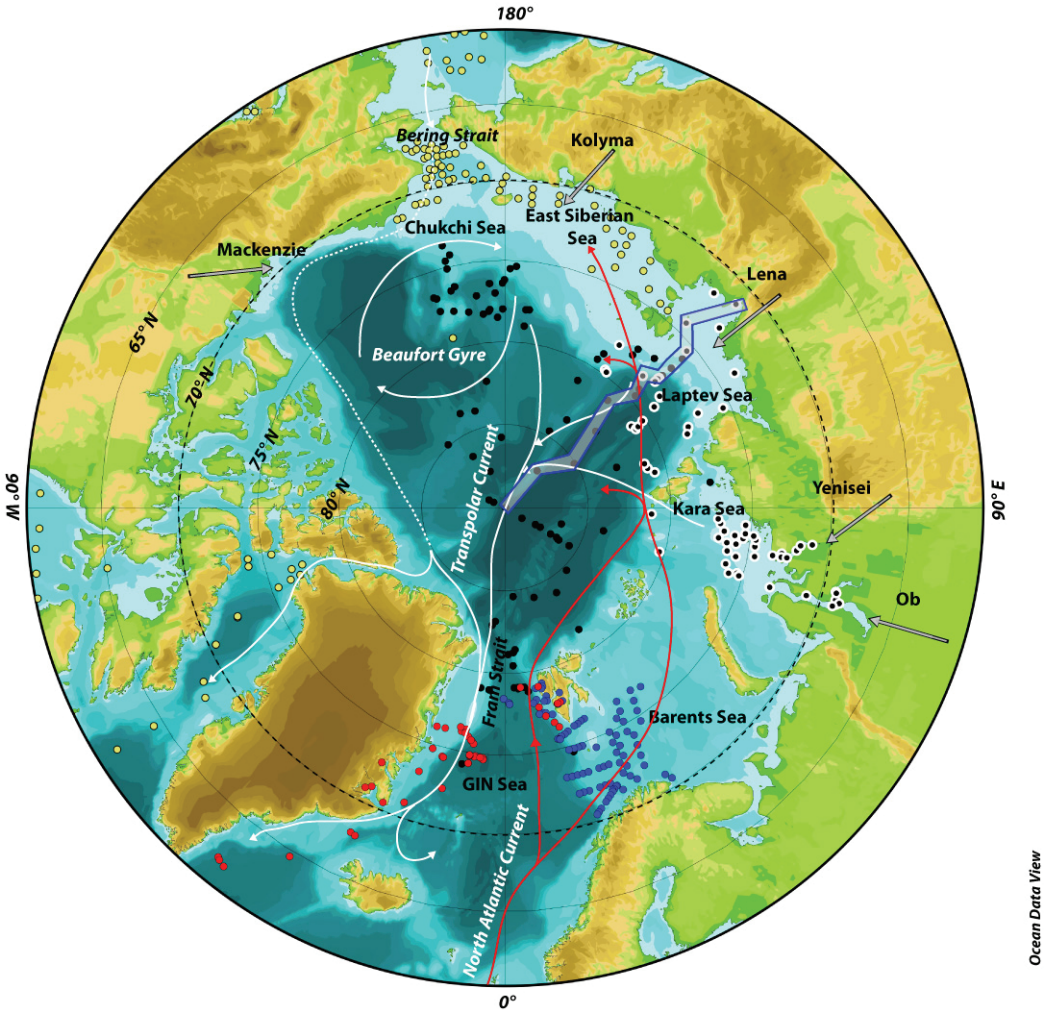

Figure 4.1 Locations of surface sediments used for IP_{25} study in the Arctic Ocean. Dots with different colors reflect the samples from different studies: black dots (this study); red dots (Müller et al., 2011); blue dots (Navarro-Rodriguez et al., 2013); yellow dots (Stoynova et al., 2013); black dots with white circle (Xiao et al., 2013). A transect from North Pole to Laptev Sea along Lomonosov Ridge with sea-ice and biomarker distributions discussed in more detailed and illustrated in Figure 4.8, is indicated by semi-transparent grey bars. Red arrows show the warm and salty surface water from the Atlantic enters the Arctic Ocean, while white arrows show the process of the cold and less salty water (Jones, 2001). Straight arrows indicate rivers draining into the Arctic Ocean.

In order to understand the causes of sea-ice loss, i.e., whether anthropogenic influence and/or natural variability are major controlling processes, it is essential to reconstruct the past variability of sea ice from sedimentary sections, going well beyond the time span of direct measurements of sea-ice distribution and thickness. Besides microfossil sea-ice proxies such

as, for example, dinoflagellate cysts (de Vernal et al., 2005), especially the newly developed sea-ice proxy IP_{25} (Ice Proxy with 25 carbon atoms), which is a mono-unsaturated highly-branched isoprenoid (HBI) alkene biosynthesized specifically by Arctic sea-ice diatoms (Belt et al., 2007; Belt et al., 2013; Brown et al., 2011), may give a unique opportunity to get this type of data.

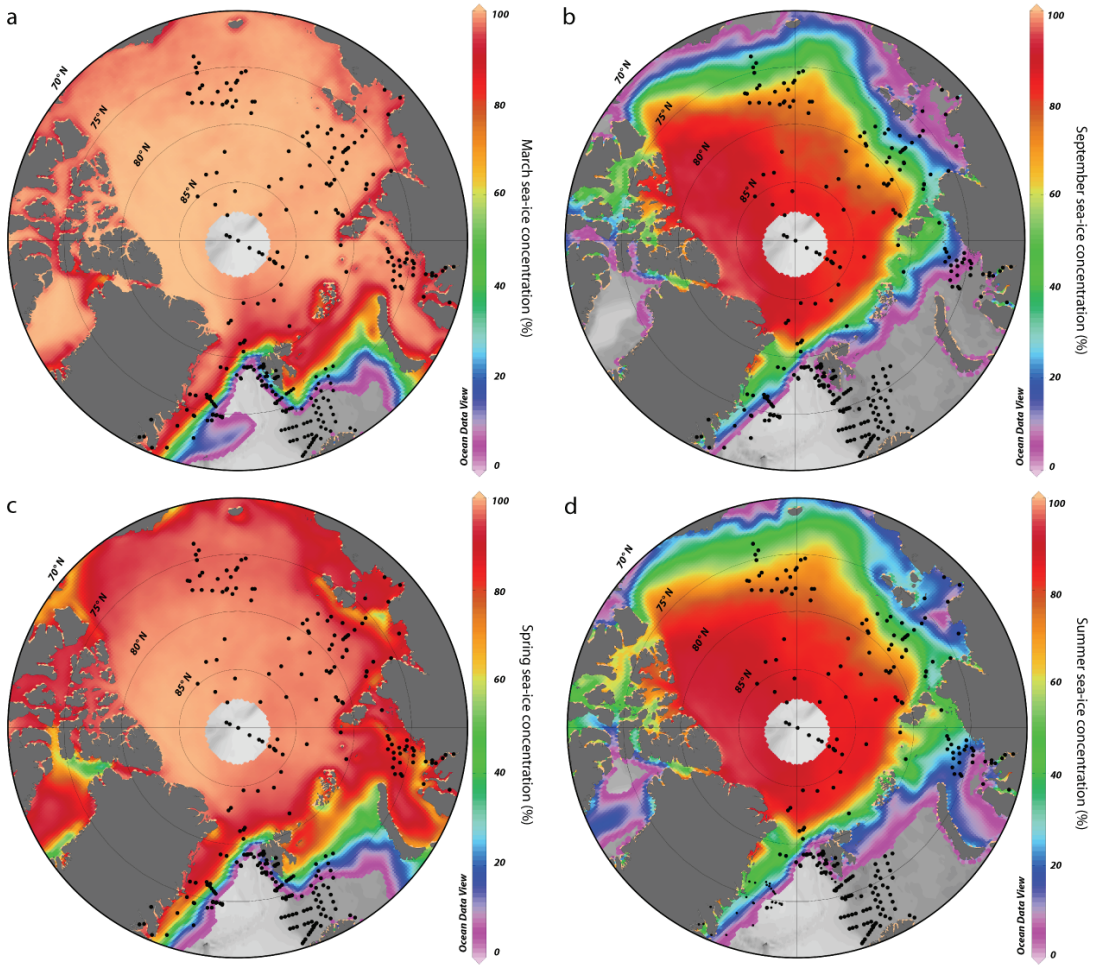

Figure 4.2 Average of sea-ice concentrations in (a) March, (b) September, (c) spring (April, May and June) and (d) summer (July, August and September) from 1988 to 2007 (http://nsidc.org). Black dots are surface sediment samples included in this study.

Since the absence of IP_{25} can refer to either ice–free or permanent ice conditions, however, Müller et al. (2009) proposed to use IP_{25} together with a phytoplankton biomarker to distinguish these two extreme scenarios. That means the lack of both biomarkers points to perennial ice cover, while the absence of IP_{25} with elevated phytoplankton biomarker contents reflects more ice-free conditions. The occurrence of both biomarkers, on the other hand, suggests stable ice-edge or seasonal sea-ice situations. In order to interpret sea-ice conditions more quantitatively, the PIP_{25} index based on the combination of the sea-ice diatom

biomarker (IP_{25}) and phytoplankton biomarkers (e.g., brassicasterol and dinosterol) was developed by Müller et al. (2011) in their study of surface sediments from the Norwegian-Greenland Sea and Fram Strait area (calculation formulas see the following chapter). Following Müller et al. (2011), high PIP_{25} values (0.75–1) refer to a permanent sea-ice cover throughout the year, intermediate values between 0.5 and 0.75 reflect seasonal ice cover or a stable ice edge, while low values (0–0.5) indicate less ice or ice-free conditions.

Meanwhile, several studies using the IP_{25}/PIP_{25} biomarker approach have been carried out to study modern sea-ice conditions to validate the application of IP_{25} proxies in surface sediments in the Arctic marginal seas and sub-Arctic areas (Figure 4.1), and to reconstruct late Quaternary sea-ice conditions in sediment cores in the Arctic realm (see recent reviews by Stein et al., 2012 and Belt and Müller, 2013). Furthermore, IP_{25}/PIP_{25} can be even used for sea-ice reconstruction in sedimentary records going back in time to the early/mid Pliocene (Stein and Fahl, 2013; Stein et al., 2014).

4.2 Materials and methods

The surface sediment samples (0-1cm; n=97) were collected during various expeditions to the Arctic Ocean from 1995 to 2012 using a giant box corer or a multicorer. All samples were stored at -30°C until further treatment. In addition to our investigations, biomarker data from previous studies obtained from surface samples from the adjacent marginal seas and adjacent areas (Müller et al., 2011; Navarro-Rodriguez et al., 2013; Xiao et al., 2013) were included.

The sediments were freeze-dried and homogenised before any further treatment. Prior to the biomarker analyses, the internal standards 7-hexylnonadecane (0.076 µg/sample), squalane (2.4 µg/sample) and cholesterol-d_6 (cholest-5-en-3β-ol-D_6; 20.2 µg/sample) were added to the sediments for quantification. Afterwards the sediments were extracted by an Accelerated Solvent Extractor (DIONEX, ASE 200; 100°C, 5 min, 1000 psi) using dichloromethane:methanol (2:1 v/v) as solvent. Further separation of hydrocarbons, fatty acid and sterols was carried out via open-column chromatography using SiO_2 as stationary phase using 5 ml *n*-hexane, 6ml dichloromethane:*n*-hexane (1:1 v/v) 6 ml ethylacetate:*n*-hexane (20:80 v/v), respectively. Sterols were silylated with 500 µl BSTFA (bis-trimethylsilyl-trifluoroacetamide; 60 °C, 2 h) after elution. Both C_{25}-HBIs (IP_{25} and C_{25}-HBI diene) and sterols were analysed by gas chromatography (Agilent 6850 GC; 30 m HP-5MS column, 0.25 mm i.d., 0.25 µm film thickness) coupled to an Agilent 5975 C VL mass selective detector (MSD, 70 eV constant ionization potential, ion source temperature 230 °C). For further details concerning the instrumental method see Müller et al. (2011) and Fahl and Stein (2012). Individual compound identification was based on comparisons of their retention times with that of reference compounds and on comparisons of their mass spectra with published

data (Belt et al., 2007; Boon et al., 1979; Johns et al., 1999; Volkman, 1986). For further details concerning the C_{25}-HBIs quantification, the reader is referred to Müller et al. (2011) and Fahl and Stein (2012). The identification and quantification of 24S-brassicasterol (24-methylcholesta-5,22E-dien-3β-ol), dinosterol (4α,23,24R-trimethyl-5α-cholest-22E-en-3β-ol), 24R-campesterol (24-methylcholest-5-en-3β-ol), and 24R-ß-sitosterol (24-ethylcholest-5-en-3β-ol) were described in Fahl and Stein (1999). The biomarker concentrations were corrected to the amount of extracted sediment. The absolute biomarker concentrations have been normalised to the TOC content to compensate the different sedimentation rates in our study area, which might cause an overestimation or underestimation of the biomarker concentrations.

In order to associate the sea-ice proxy IP_{25} with distinct sea-ice conditions, we followed the new approach described by Müller et al. (2011) who combined IP_{25} with phytoplankton-derived biomarkers (24S-brassicasterol or dinosterol) to calculate the phytoplankton-IP_{25} (PIP_{25}) index:

$$PIP_{25} = [IP_{25}] / ([IP_{25}] + [\text{phytoplankton biomarker}]*C)$$

(C = mean IP_{25} concentration / mean phytoplankton biomarker concentration).

For this study, we calculated the P_BIP_{25} (B=24S-brassicasterol) and P_DIP_{25} (D=dinosterol) values using all the data and a uniform C factor of 0.023 and 0.11, respectively. In addition, we also calculated the PIP_{25} values for different areas separately, using regional C factors (Table 4.1, (2)–(7)) to compare these PIP_{25} values with those obtained by one uniform C factor and their correlations with satellite sea-ice data.

Table 4.1 Uniform C factor for the study area (1) and regional C factors (2)–(7) used for calculation of PIP_{25}. '–' denotes that this C factors has been not used in this area before and is obtained from our new dataset. n.d.: no data.

	C factors for P_BIP_{25}		C factors for P_DIP_{25}	
	This study	Published	This study	Published
(1)Uniform C factors	0.023	–	0.11	–
(2)$C_{\text{Central Arctic}}$	0.071	–	0.35	–
(3)$C_{\text{Chukchi Plateau/Basin}}$	0.12	–	0.28	–
(4)$C_{\text{Kara Sea}}$	0.045	0.056[a)]	0.12	0.13[a)]
(5)$C_{\text{Laptev Sea}}$	0.055	0.056[a)]	0.13	0.13[a)]
(6)$C_{\text{East Greenland and Fram Strait}}$	0.014	0.014[b)]	0.071	0.067[b)]
(7)$C_{\text{Barents Sea and West Spitzbergen}}$	0.0018	0.0018[c)]	n.d.	n.d.

[a)] Xiao et al. (2013) [b)] Müller et al. (2011) [c)] Navarro-Rodriguez et al. (2013)

All IP_{25}, C_{25}-HBI diene, phytoplankton biomarker (24S-brassicasterol and dinosterol) and terrigenous biomarker (24R-campesterol and 24R-ß-sitosterol) data used in this study are available on www.pangaea.de. The distribution maps of the biomarker concentrations and PIP_{25} indices were generated by means of the Ocean Data View software (Schlitzer, 2013).

Satellite sea-ice concentration data in this paper were derived from Nimbus-7 SMMR and DMSP SSM/I-SSMIS passive microwave data (Cavalieri et al., 1996) from the National Snow and Ice Data Center (NSIDC) and obtained for the interval 1988–2007 to generate average sea-ice distributions for March, September, spring (April, May and June) and summer (July, August and September) (Figure 4.2a–d). Maps of sea-ice distribution were produced using the Ocean Data View software (Schlitzer, 2013).

4.3 Results

Both IP_{25} (0–2.31 µg/g TOC) and phytoplankton biomarkers (0–31.6 µg/g TOC for brassicasterol and 0–7.42 µg/g TOC for dinosterol, respectively) show low values in the High Arctic proper >85°N (Figure 4.3a–c). Low IP_{25} concentrations expand southwards from the Central Arctic Ocean to the Barents Sea, while the brassicasterol values increase from the Central Arctic Ocean towards the Barents Sea and Fram Strait. In general, high IP_{25} values occur along the southern part of the continental shelf of Kara Sea, Laptev Sea and East Siberian Sea, and east of Greenland, varying between 2.59 µg/g TOC and 11.4 µg/g TOC. In these areas, also high concentrations of brassicasterol and dinosterol were found in the range of 55.8–271 µg/g TOC, and 29.7–83.8 µg/g TOC, respectively. In the Chukchi Plateau and Basin area, we determined increased IP_{25} contents and relatively low brassicasterol and dinosterol contents in most of the samples. In addition to IP_{25}, the C_{25}-HBI diene was determined. There is a similar distribution pattern and a positive correlation between both biomarkers, supporting a sea-ice origin of the diene (Figure 4.4; cf., Vare et al., 2009; Massé et al., 2011; Fahl and Stein, 2012; Xiao et al., 2013).

High P_BIP_{25} and P_DIP_{25} values calculated with a uniform C factor were detected in the Central Arctic Ocean, the Chukchi Plateau and Basin, and the Laptev Sea with the exception of moderate values northwest of Kotelnyy (Figure 4.5a–b). In the Central Kara Sea, the PIP_{25} values decrease gradually southwards (the absence of IP_{25} results in $PIP_{25} = 0$ in the rivers). From the Central Arctic Ocean to the Fram Strait, both P_BIP_{25} and P_DIP_{25} values generally decrease reaching the minimum values in the Barents Sea and West of Svalbard (No P_DIP_{25} data available in the Barents Sea). East of Greenland, some higher PIP_{25} values occur. The PIP_{25} values calculated with individual C factors (Figure 4.6) differ from the PIP_{25} values determined by using a uniform C factor (see discussion below).

4.4 Discussion

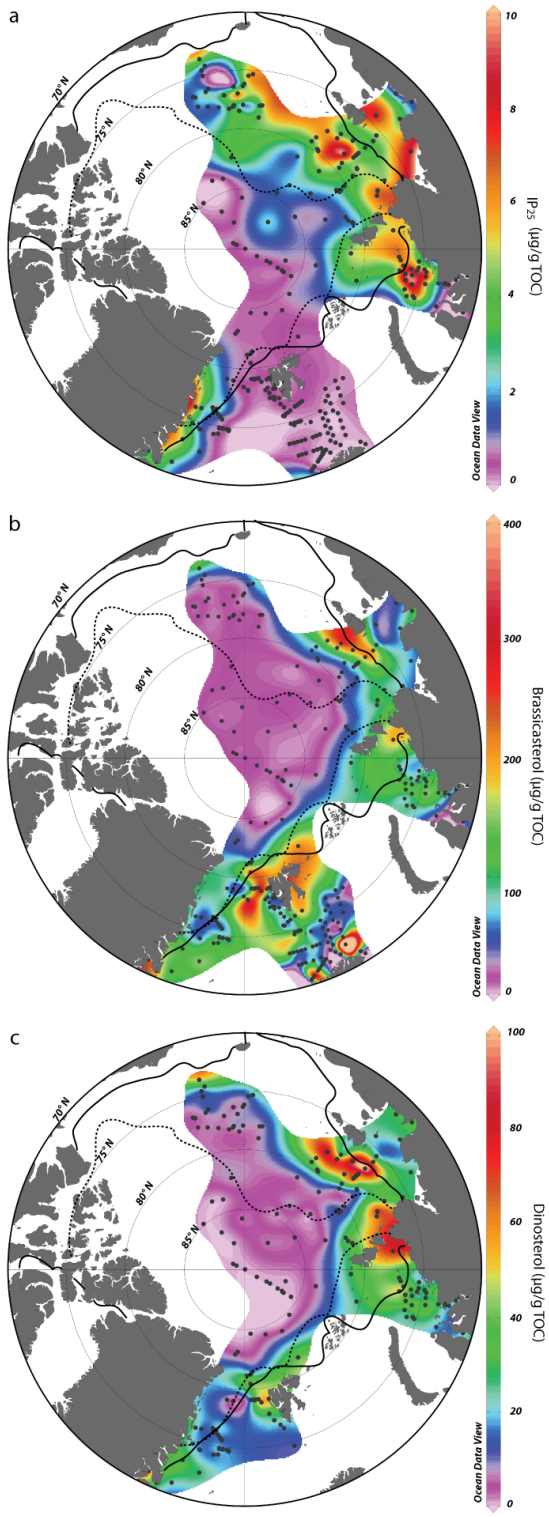

In our study, for the first time numerous surface sediment samples from the Central Arctic Ocean have been used to determine IP_{25} and phytoplankton biomarker distributions under permanent sea-ice cover (80–100% during spring and summer), i.e., an environmental situation that limits the light penetration and, thus, the growth of both sea-ice algae and marine phytoplankton. These records extend ground truth data of IP_{25} and PIP_{25} that are important for the palaeo-sea-ice reconstruction in the Central Arctic Ocean. Thus, the dataset of this study spans a broad region combining the Central Arctic Ocean and several marginal seas. It includes new data as well as published data from the Fram Strait area (Müller et al., 2011), the area west of Svalbard and the Barents Sea (Navarro-Rodriguez et al., 2013) and the Kara-Laptev seas (Xiao et al., 2013), as all these studies used the same analytical procedure and identification and quantification approach (cf., Belt et al., 2014). In contrast, we have not included IP_{25} data from sub-polar North Atlantic and Pacific surface sediments published by Stoynova et al. (2013) in our main IP_{25}/PIP_{25} distribution maps (Figures 4.3a and 4.5a–b) as they used a different analytical approach (Figure 4.7). Their IP_{25} data as well as data from the North Pacific

Figure 4.3 Concentrations (µg/g TOC) of IP_{25} (a), open-water phytoplankton biomarkers brassicasterol (b) and dinosterol (c) in surface sediments from the Central Arctic Ocean and its marginal seas. Black line indicates average of September sea-ice extent of 1988–2007 and dotted line indicates September sea-ice extent of 2007. Note: For the Barents Sea area, dinosterol data are not available.

(Meheust et al., 2013), however, have been included in a IP_{25} distribution map presented in the appendix material (Figure 4.7). IP_{25} concentrations from the Bering Strait determined by Stoynova et al. (2013), for example, are about 3 times higher than those in our study from regions with similar sea-ice conditions, such as the continental shelves of the Kara Sea, Laptev Sea and East Greenland. The IP_{25} concentrations in sediments from the Baffin Bay and Hudson Bay where we do not have own data, are even far beyond the range of our measurement. Whether these discrepancies are related to different ice conditions in this area, polynyas in winter and sea-ice extent in summer, or whether they are just caused by the different analytical and quantification methods in the different laboratories, we cannot decide yet. For this, we need further determinations performed on same samples in different laboratories. For the latter aspect, we refer to Belt et al. (2014) who recently carried out an inter-laboratory calibration of identification and quantification of IP_{25} in marine sediments and found great variation between laboratories.

4.4.1 General aspects on using PIP_{25} as (semi-quantitative) sea-ice proxy

Following Müller et al. (2011), further PIP_{25} studies using surface sediments from different areas of the Arctic strengthen the applicability of the PIP_{25} index approach in general (Navarro-Rodriguez et al., 2013; Stoynova et al., 2013; Xiao et al., 2013). In these studies, partly different phytoplankton biomarkers have been used for PIP_{25} calculation. Müller et al. (2011) using 24S-brassicasterol, dinosterol and short-chain *n*-alkanes as phytoplankton biomarkers for PIP_{25} calculation, yielded similar results and pronounced correlations with satellite sea-ice concentration in Fram Strait. As the 24S-brassicasterol-based PIP_{25} shows the best correlation with the sea-ice concentration, these authors used the 'P_BIP_{25} index' for their final discussion. Stoynova et al. (2013) who used the PIP_{25} approach for sea-ice reconstruction in the North Pacific, North Atlantic and Fram Strait, on the other hand, indicated that PIP_{25} values based on dinosterol correlate slightly better with satellite sea-ice concentrations than those calculated with 24S-brassicasterol. As these sterols may have different sources, i.e., a marine, terrestrial or even sea-ice origin, some further information and discussion is useful before using this approach.

4.4.1.1 The origin of phytoplankton biomarkers- 24S-brassicasterol and dinosterol

In general, Volkman (1986) pointed out that only few sterols are restricted to be considered as unambiguous indicators for specific algal groups and the source of sterols should be supported by other lipids. According to Volkman (1986), 24S-brassicasterol, e.g. might have a marine or a fluvial/lacustrine algae (diatom) origin. Recently, Belt et al. (2013) found abundant sterols in sea-ice samples collected from the Canadian Arctic Archipelago and

pointed out that 24S-brassicasterol is produced by the majority of sea-ice diatoms. Likewise, 24S-brassicasterol was found in sediment trap and subjacent surface sediment samples from the ice-covered Mackenzie shelf (Yunker et al., 1995). Whereas these authors interpreted these data as indicative for a sea-ice algae origin of 24S-brassicasterol, a riverine/terrestrial source cannot be excluded. In the Kara Sea estuaries, for example, 24S-brassicasterol mainly has a fluvial/lacustrine origin (cf., Volkman, 1986), then incorporated into sea ice and transported to the open ocean (Fahl et al., 2003). On the other hand, dinosterol is considered to be mainly produced by dinoflagellates, despite a minor proportion was found in other algae (Volkman, 2003; Giner and Wikfors, 2011). Dinoflagellates occur in surface waters as a dominant group while in sea ice they only occur as a minor group compared to diatoms; they can be abundant, however, in the water column prior to sea ice formation (e.g. Niemi et al., 2011). This is in line with the more or less absence of dinosterol in sea-ice samples showed by Belt et al. (2013). Taken together these observations, dinosterol is probably a quite reliable biomarker for marine phytoplankton.

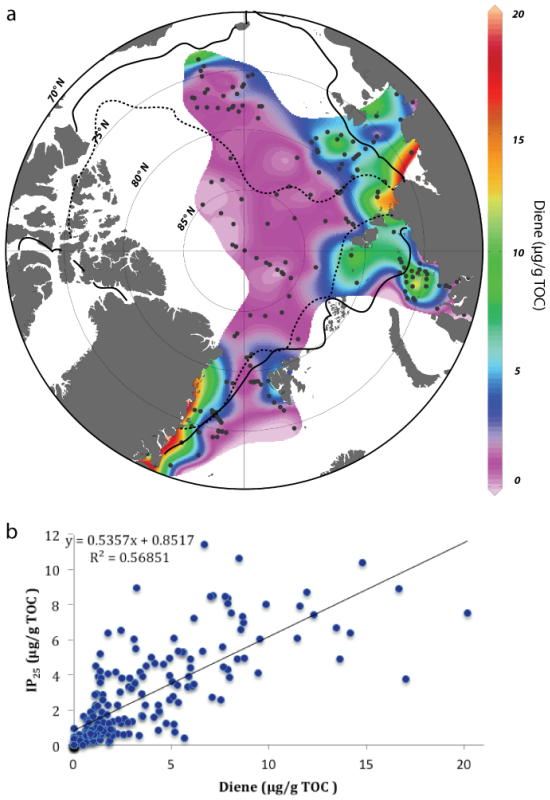

Figure 4.4 Concentration (µg/g TOC) of C_{25}-HBI diene (a) and correlation between diene and IP_{25} (b). For explanation of black and dotted lines, see Figure 4.3.

In our study, we used both 24S-brassicasterol and dinosterol. As both biomarkers show basically similar distribution patterns (Figure 4.3b–c), we assume that the predominant source of 24S-brassicasterol in these surface sediments is also of phytoplankton origin. For example, in the open Kara and Laptev seas, the distribution patterns of 24S-brassicasterol and dinosterol increasing from the river to the ice edge and then decreasing to the Central Arctic Ocean, suggest that the majority of both sterols are also produced by marine phytoplankton (Figure 4.3b–c; Xiao et al., 2013). Compared to the sea-ice diatom-derived biomarker IP_{25} dominating at the ice edge (Figure 4.3a) and the terrigenous biomarkers 24R-campesterol and 24R-ß-sitosterol prevailing in the river estuaries (Figure 4.8a–b), relatively high concentrations of both 24S-brassicasterol and dinosterol were found in the seasonally ice-covered areas between the ice edge and river mouths. This further supports that the main

source of both sterols is probably open-water phytoplankton rather than ice algae or higher plants. Thus, P_BIP_{25} and P_DIP_{25} basically show similar distribution trends (Figure 4.5a–b). To further support the different origin of sterols, compound-specific carbon stable isotopes may be used (cf., Belt et al., 2008) as planned in further research of our samples.

In order to compare and interpret the sea-ice and phytoplankton proxy data more comprehensively, a transect along the Lomonosov Ridge from the North Pole to the inner Laptev Sea is schematically illustrated together with sea-ice conditions and corresponding concentrations of biomarkers and diatom assemblages in the underlying sediments (Figure 4.9). Generally, concentrations of both IP_{25} and phytoplankton biomarkers increase from the Central Arctic southwards to the continental slope along this transect. Further south, the biomarker distributions are variable in these areas corresponding to the complex sea-ice situations (details see Xiao et al., 2013). High IP_{25} concentrations were found near the stable ice margin (north of winter polynya) as well as on the continental shelf where occasional ice massifs occur in summer. Dinosterol shows maximun concentrations at sites between the ice edge and seasonal sea-ice conditions and has a general decrease southwards. 24S-brassicasterol concentrations show a strong maximum at the winter polynya position where sea ice starts melting early in spring resulting in high primary productivity of phytoplankton, and then decrease towards the continental shelf due to the occasional occurrence of summer ice massif, followed by increased concentrations (intermediate values) towards the river mouth along the transect (Figure 4.9). These increased 24S-brassicasterol concentrations in the vicinity of estuaries may suggest a freshwater diatom source (cf. Fahl et al., 2003), which is also supported by the freshwater diatom abundances determined in the surface sediments from the southern Laptev Sea (Cremer, 1999; Figure 4.9). The freshwater diatom abundances significantly increase off the inner shelf of the Lena Delta, while abundance of the marine diatom and sea-ice diatom decrease to near-zero values here (Figure 4.9). Therefore, freshwater diatoms might be the main source of 24S-brassicasterol in this environment, i.e., river and estuary settings. Likewise, the occurrence of intermediate values of 24S-brassicasterol together with abundant freshwater diatom assemblages in the Yenisei Estuary also supports our interpretation (Polyakova, 2003). On the continental shelf of the Laptev Sea, the co-occurrence of sea-ice diatoms and marine planktic diatoms points to seasonal ice cover and ice-edge conditions resulting in ice-algal growth and spring phytoplankton bloom (Cremer, 1999), consistent with variable IP_{25} and 24S-brassicasterol contents on the Laptev Sea shelf (Figure 4.9).

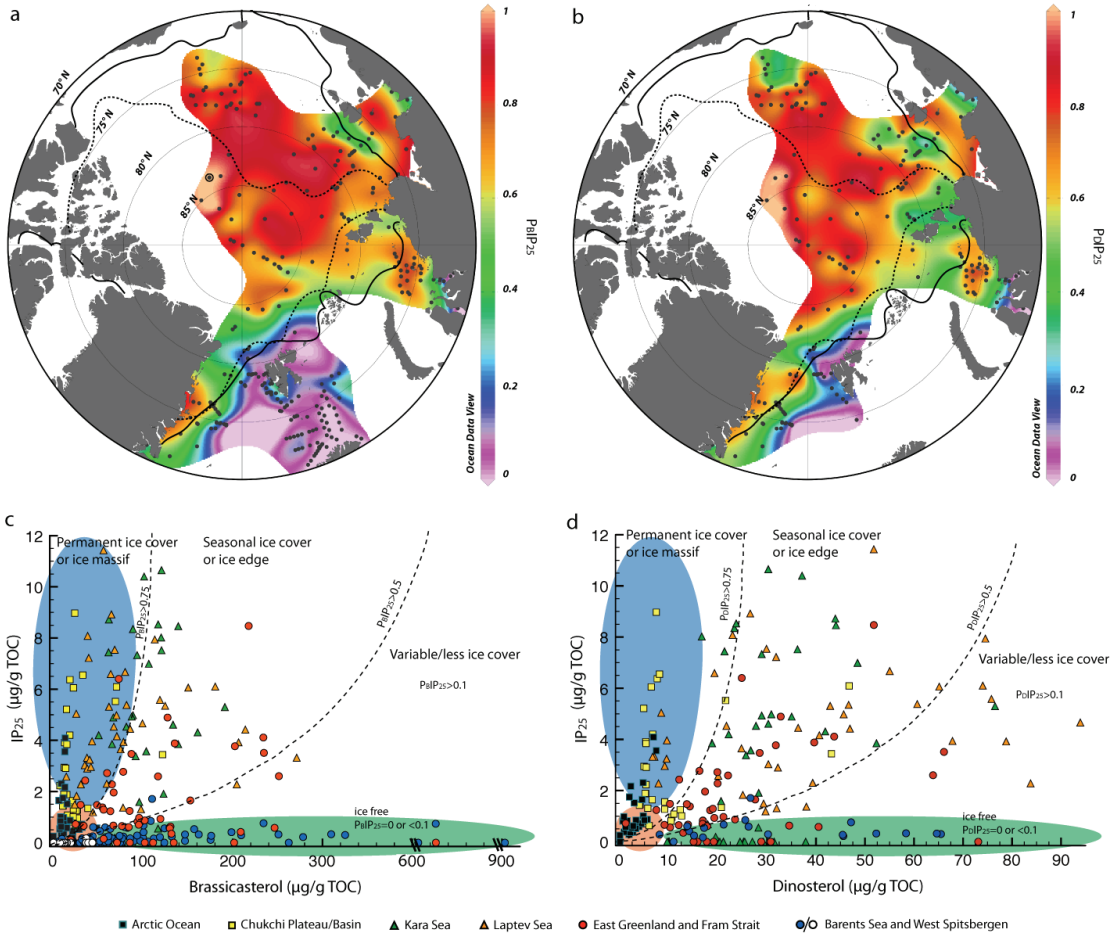

Figure 4.5 Values of PIP_{25} index calculated using brassicasterol (P_BIP_{25}, a) and using dinosterol (P_DIP_{25}, b), respectively. The dot with black circle (a) indicates one data point not considered when producing the distribution map because of zero value of IP_{25} and very low concentration of brassicasterol. Correlations of IP_{25} versus brassicasterol (c) and dinosterol (d) to denote different zones of sea-ice conditions. Data area close to the origin was considered as a threshold of 'permanent ice cover'. For explanation of black and dotted lines (a and b), see Figure 4.3.

4.4.1.2 The phytoplankton vs. IP_{25} plot

Müller et al. (2011) already pointed out that the individual biomarker concentrations have to be considered when using the PIP_{25} index to distinguish different sea-ice scenarios. For example, the co-occurrence of both low IP_{25} and phytoplankton biomarker contents (referring to permanent ice conditions) might result in high or low PIP_{25} values. Likewise, the co-occurrence of high amounts of both biomarkers (referring to ice edge or seasonal ice conditions) can yield the same results. Here, the correlation diagram of IP_{25} versus the phytoplankton biomarker is most helpful to interpret and to denote different zones of sea-ice conditions (Figure 4.5c–d). The extremely low to zero concentrations of IP_{25} and 24S-brassicasterol in sediments from the high Central Arctic can result in high PIP_{25} values (0.77–

1.0) as well as intermediate PIP_{25} values (0.40–0.70), even 0 values. Most of the data points from the Central Arctic, however, are located in the area close to the origin in the correlation diagrams of IP_{25} versus 24S-brassicasterol and IP_{25} versus dinosterol (Figure 4.5c–d), pointing to permanent ice conditions. In contrast, the zero or near-zero IP_{25} concentration and low brassicasterol concentration (marked as white dots in Figure 4.5c, located in 'permanent ice cover' data area) found in sediments from the northern coast of Norway result in low PIP_{25}, characterized by ice-free conditions in this area. Navarro-Rodriguez et al. (2013) suggested that the reduced 24S-brassicasterol concentrations here are probably caused by other factors than increased sea ice. If this is correct, of course, this also has impact on the interpretation of combined biomarker indices such as the PIP_{25} index. More details about the influence on the fate and post-production of the biomarkers by the environmental factors, such as ice thickness, snow cover, irradiance, nutrient, etc., are discussed by Belt and Müller (2013).

4.4.1.3 PIP_{25} calculation using different balance factors

In order to test the robustness of calculation of PIP_{25} values, our data based of a uniform balance factor C for the entire study area was compared with PIP_{25} values calculated with different C values for different areas (Table 4.1; $PIP_{25.D}$, Figure 4.6). The P_BIP_{25} and P_DIP_{25} values calculated with different regional C factors differ from PIP_{25} values calculated with one uniform C factor, especially in the Barents Sea, where $P_BIP_{25.D}$ shows significantly higher values south of Svalbard (No P_DIP_{25} data available at these sites).

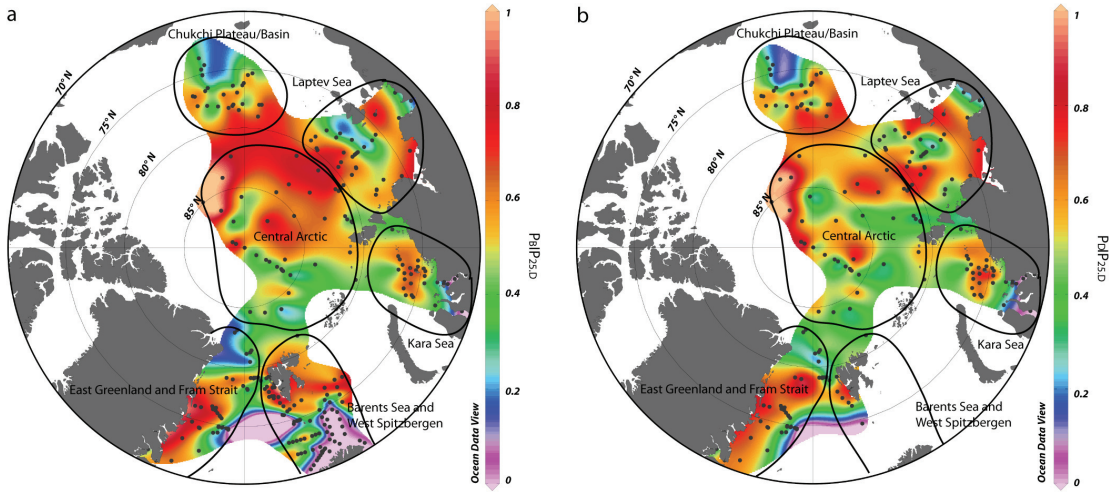

Figure 4.6 Values of PIP_{25} index with different regional c factors (Table 4.1) calculated using brassicasterol (P_BIP_{25}, a) and using dinosterol (P_DIP_{25}, b), respectively. The definition of the regional boundaries is indicated by black lines.

$PIP_{25.D}$ and PIP_{25} show similar distribution pattern in the Central Arctic, Kara and Laptev Seas, and Chukchi Plateau and Basin with $PIP_{25.D}$ values lower than PIP_{25} values due to an increase in C factors (Table 4.1). Along the East Greenland margin with a lower C factor (Table 4.1; for P_BIP_{25}: C= 0.014; for P_DIP_{25}: C = 0.071), on the other hand, the $PIP_{25.D}$ values are higher than PIP_{25}. The most obvious difference between $PIP_{25.D}$ and PIP_{25} distributions occurs in the Barents Sea (due to the lack of dinosterol data only P_BIP_{25} values are available for this area), where the $P_BIP_{25.D}$ values apparently overestimate the sea-ice concentrations (i.e. $P_BIP_{25.D}$ values indicate a spring sea ice cover in the northern Barents Sea although sea ice does not extend as far as north of Norway). Thus, we conclude that the P_BIP_{25} values with one uniform C factor reflect the sea-ice situation more reasonable than $P_BIP_{25.D}$ with the regional C factor ($C_{Barents\ Sea}$ = 0.0018).

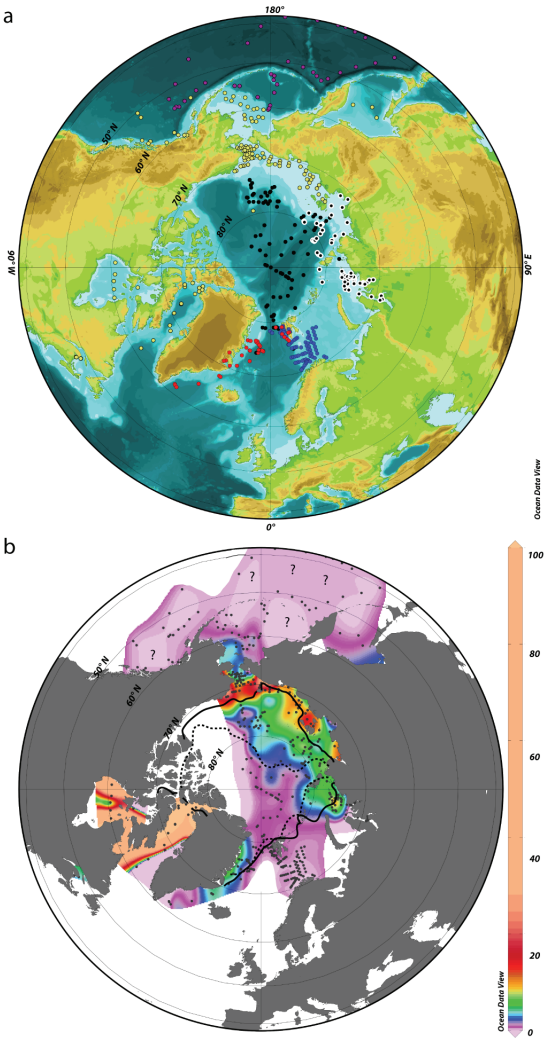

Figure 4.7 Sampling station including all IP_{25} study in surface sediments from the Arctic and sub-Arctic (a) and concentrations (µg/g TOC) of IP_{25} (b) with supplementary data to Figure 4.3 from sub-polar North Atlantic and Pacific (Meheust et al., 2013; Stoynova et al., 2013). The magenta dots are samples from the study by Meheust et al. (2013). For explanation of the rest colour dots see Figure 1. For explanation of black and dotted lines, see Figure 4.3.

It seems that the uniform C factor derived from the combined datasets may improve the PIP_{25}-sea-ice correlation (Figure 4.10) when the regional datasets included anomalous biomarker concentrations as mentioned above for the Barents Sea, where the samples were largely located in the ice-free area and the heterogeneity of the samples caused low C factor value ($C_{Barents\ Sea}$ = 0.0018). This results in high P_BIP_{25} values even in the less-ice conditions (Figure 4.6a), which probably can be corrected by the larger biomarker datasets (Figure 4.5a). The PIP_{25} values with different regional C factors, therefore, show poor correlations with both spring and summer satellite sea-ice concentrations (Figure 4.11).

4.4.2 Biomarker distributions and sea-ice conditions

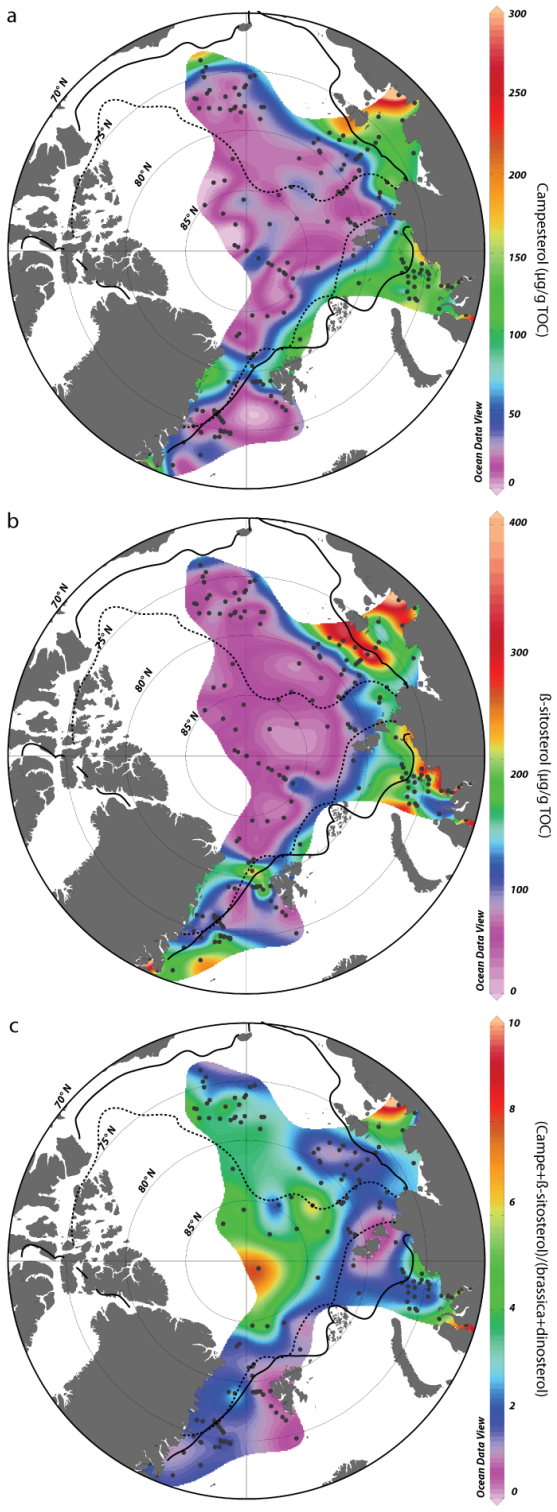

Figure 4.8 Concentrations (µg/g TOC) of terrigenous biomarkers campesterol (a) and ß-sitosterol (b) and values of (campe+ß-sitosterol)/(brassica+dinosterol) (c). For explanation of black and dotted lines, see Figure 4.3.

The occurrence of minimum IP_{25} concentrations in the high Central Arctic (>85°N) and the Barents Sea may refer to either permanent sea-ice or ice-free conditions (Figure 4.3a). Considering the minimum and elevated 24S-brassicasterol concentrations found in the surface sediments from these two areas (Figure 4.3a–b), however, permits a clear discrimination between sea-ice situations. The high PIP_{25} values ranging from 0.8 to 1.0 in the Central Arctic reflect 80–100% sea-ice concentration during spring/summer, whereas close to zero PIP_{25} values in most of the samples from the Barents Sea indicate open-ocean conditions related to the influence of warm Atlantic Water (Figure 4.5a). Around Svalbard, the inflow of the warm Atlantic water limits ice algae growth thus IP_{25} concentrations, while provides favorable living conditions for phytoplankton growth (Figure 4.3), also reflected in increased TOC values in surface sediments from the Eastern Fram Strait (Birgel et al., 2004; Hebbeln and Berner, 1993). For further detailed discussion of the IP_{25} data from the Barents Sea we refer to Navarro-Rodriguez et al (2013).

In the Central Arctic, the light limitation and nutrient stress due to the multi-year ice persisting throughout the year limit both the under-ice production and ice-algal

production within the sea ice (Walsh, 1989; Gosselin e al., 1997). That means, in comparison to low to mid-latitude oceans the deep Arctic Ocean productivity is quite low, limit numbers of about 10g C. $m^{-2}y^{-1}$ are reached, with about 40% related to phytoplankton productivity and 60% related to sea-ice algae productivity (Sakshaug, 2004). 24R-campesterol and 24R-ß-sitosterol, commonly related to terrigenous input (Huang and Meinschein, 1979; Volkman, 1986), also show minimum contents in the Central Arctic Ocean due to the long-distance transport and low sea-ice melting rates (Figure 4.8a–b). Due to the very low primary production, the terrigenous sterols dominate over the phytoplankton sterols (Figure 4.8c). This dominance of terrigenous organic matter in the Central Arctic is also supported by organic geochemical bulk parameters (C/N ratios > 10 and hydrogen index values < 100 mgHC/gOC) as well as high concentrations of long-chain *n*-alkanes (Stein et al., 1994a; Schubert and Stein, 1997).

The minimum contents of both IP_{25} and phytoplankton biomarkers in the Central Arctic indicate the relatively low productivity compared to the adjacent marginal seas, but not zero values (data table see Appendix). Furthermore, the C_{25}-HBI diene also having a common sea-ice source as IP_{25} (Massé et al., 2011; Cabedo-Sanz et al., 2013; Xiao et al., 2013), shows values >0 in the Central Arctic. This is in line with measured modern central Arctic Ocean in-situ algae productivity (see above). Ice algae and phytoplankton probably could benefit from occasional sea-ice melting. Boetius et al. (2013), for example, found ice algal blooms under sea ice and ice-algal deposition on sea floor in the eastern Central Arctic Ocean between 82° to 89°N in summer 2012, when Arctic sea ice declined to a historical record minimum. Although the ice algae reported by Boetius et al. (2013) are probably not the direct source of IP_{25} and brassicasterol, we assume that other ice algae and open-water phytoplankton productivity might have benefited from the enhanced light penetration due to the loss of multiyear ice and an increase of surface melt ponds (Nicolaus et al., 2012; Rösel and Kaleschke, 2012). Similarly, short-chain *n*-alkanes and fatty acids (Schubert and Stein, 1997) and coccoliths (Gard, 1993) interpreted as marine productivity signal and determined in surface sediments from the Central Arctic point to some in-situ productivity. In addition, some of the biogenic matter in the Central Arctic Ocean is certainly allochthonous and originates from the Siberian shelf areas. This is indicated by biomarker data (Fahl et al., 2003) and marine and brackish diatoms found in Central Arctic Ocean sea ice (Abelmann, 1992).

From the high Central Arctic to the Chukchi Plateau and Basin, the IP_{25} concentrations generally increase along the Mendeleev Ridge while the phytoplankton biomarkers still sustain low values. This may be explained by a thinner sea-ice cover than in the Central Arctic Ocean, which allows some sunlight penetration but still restricts the growth of open-water phytoplankton, resulting in the high PIP_{25} values (0.7–0.9) (Figures 4.3 and 4.5).

Concentrations of both IP_{25} and phytoplankton biomarkers increase in the northern Chukchi Sea (south of 75°N) and the IP_{25} contents are also slightly higher in samples along the Lomonosov Ridge than those from the same latitude in the high Arctic (>85°N). This is consistent with the study of Gosselin et al., (1997) who studied the distribution of phytoplankton and ice algae (July, 1994) along a transect from the Chukchi Sea to the Nansen Basin across the North Pole. Based on this study, phytoplankton production was maximum in the Chukchi Sea and decreased from the Chukchi Sea to the Central Arctic while ice algae dominated at both 75°N and 88°N (Chukchi Sea and Lomonosov Ridge, respectively), attributed to the presence of first-year ice in the Chukchi Sea (70–75°N) and at the Lomonosov Ridge station. Furthermore, the nutrient-rich Pacific waters imported to the Chukchi continental shelf through Bering Strait may lead to increasing production of both ice algae and phytoplankton (Torres-Valdés et al., 2013). Arrigo et al. (2012) reported that nutrient-upwelling might trigger the phytoplankton bloom under first-year ice on the Chukchi Sea continental shelf (about 73-74°N), with sufficient light penetration through the first-year ice (0.5 to 1.8 m) and melt ponds, indicating that the influence of environmental factors on biomarker production should be considered.

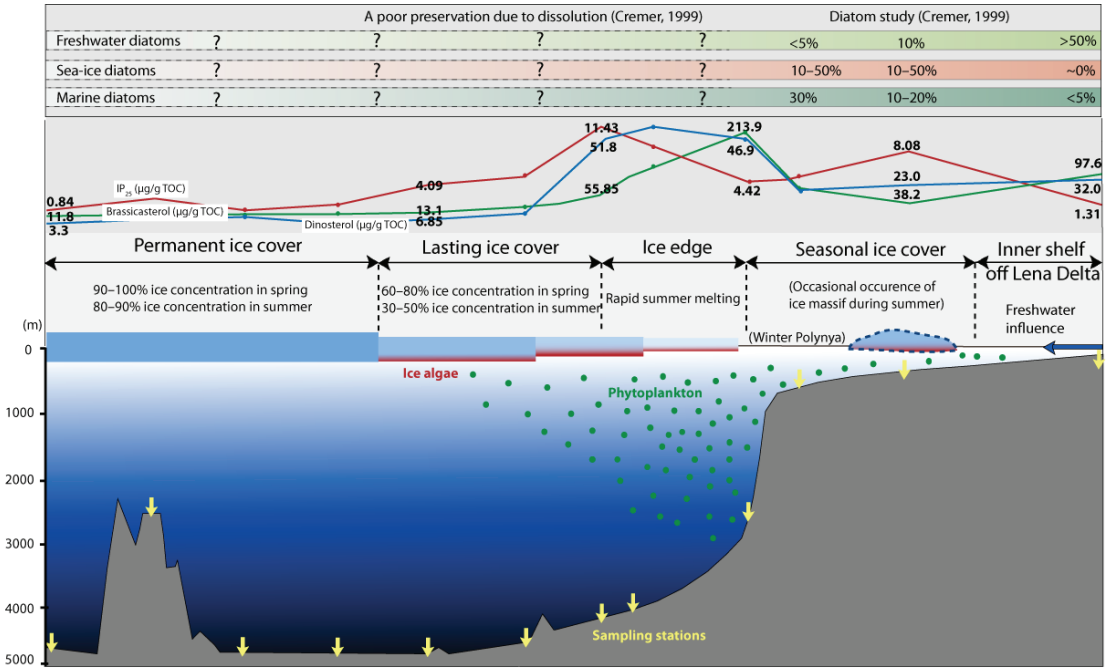

Figure 4.9 Schematic illustration showing the primary production (ice algae and open-water phytoplankton) and summer sea-ice conditions along North Pole to the Laptev Sea transect, and diatom abundances in surface sediments on Laptev Sea shelf. For locations of transects see Figure 4.1. Diatom assamblages in Laptev Sea surface sediments: freshwater diatom: freshwater diatom group and *Aulacoseria spp*., sea-ice diatom: *Fossula arctica* and *Fragilariopsis*-group, marine diatom: *Thalassiosira nordenskioeldii*, (Cremer, 1999). ?: no data.

From the Central Arctic to the area east of Greenland, cold polar water and sea ice carried by the East Greenland Current southwards along East Greenland promote an extended ice cover during summer (Sutherland and Pickart, 2008), which probably causes high IP_{25} concentrations and hampers the growth of phytoplankton along the inner continental shelf of East Greenland (Figure 4.3a). IP_{25} and C_{25}-HBI diene show significant similar distributions along East Greenland. In addition, the C_{25}-HBI diene values also co-vary with the sea-ice variability gradually decreasing eastwards, which further supports the sea-ice source of C_{25}-HBI diene (cf., Massé et al., 2011). Furthermore, sea ice that carries terrestrial matter from the Kara and Laptev seas is exported via the Transpolar Drift through the Arctic Ocean (Meese et al., 1997; Mironov et al., 2007) towards Fram Strait and thus to the East Greenland shelf and into the North Atlantic where it finally melts. However, high concentrations of terrigenous biomarkers in sediments from the continental shelf of East Greenland may also result from the terrestrial input from the East Greenland fjords (Figure 4.8). As a consequence of gradual sea-ice variations in this area, both biomarkers and PIP_{25} show a distinctly gradual decrease from the East Greenland continental shelf to the open water (details see Müller et al., 2011).

4.4.3 Correlation of biomarker and satellite sea-ice data

In order to compare the biomarker-based sea-ice estimate to the real sea-ice concentration in more detail, IP_{25} and PIP_{25} values were correlated with spring and summer sea-ice concentrations, respectively (Figure 4.10). The satellite sea-ice data were derived from SMMR-SSM/I from the National Snow and Ice Data Centre (NSIDC, http://nsidc.org/) between 1988 and 2007. When comparing modern sea-ice data and proxy data from surface sediments one always should have in mind that both data sets represent very different time spans. The surface sediment in our study may represent much longer time intervals than satellite sea-ice data (decades, centuries to millennia), depending on sedimentation rates. These sedimentation rates vary significantly across the Arctic Ocean, i.e., the sedimentation rates range between 0.4 and >2.0 cm/kyr (Stage 1) in the Central Arctic Ocean (Stein et al., 1994b), while they are much higher and more variable in the marginal seas, ranging between about 15–800 cm/kyr (e.g., Stein and Fahl, 2000; Darby and Bischof, 2004; Stein, 2008; Zaborska et al., 2008 and further references therein). Therefore, the surface sediments used within this study may represent time spans from several years to millennia.

In general, IP_{25} values show no clear correlation with sea-ice concentrations as low IP_{25} concentrations are located in both low and high sea-ice concentration areas (Figure 4.10a). Compared to IP_{25}, on the other hand, P_BIP_{25} values correlate well with both spring and summer sea ice within our large dataset (R^2=0.80 and 0.60, respectively), with low values in less ice-covered areas and high values in highly ice-covered areas (Figure 4.10b). P_DIP_{25}

values also correlate with both spring and summer sea-ice concentrations but not as well as P_BIP_{25} does (Figure 4.10c). Based on the similar distribution pattern of P_BIP_{25} and P_DIP_{25}. Partly, this may be caused by the smaller data set of P_DIP_{25} data.

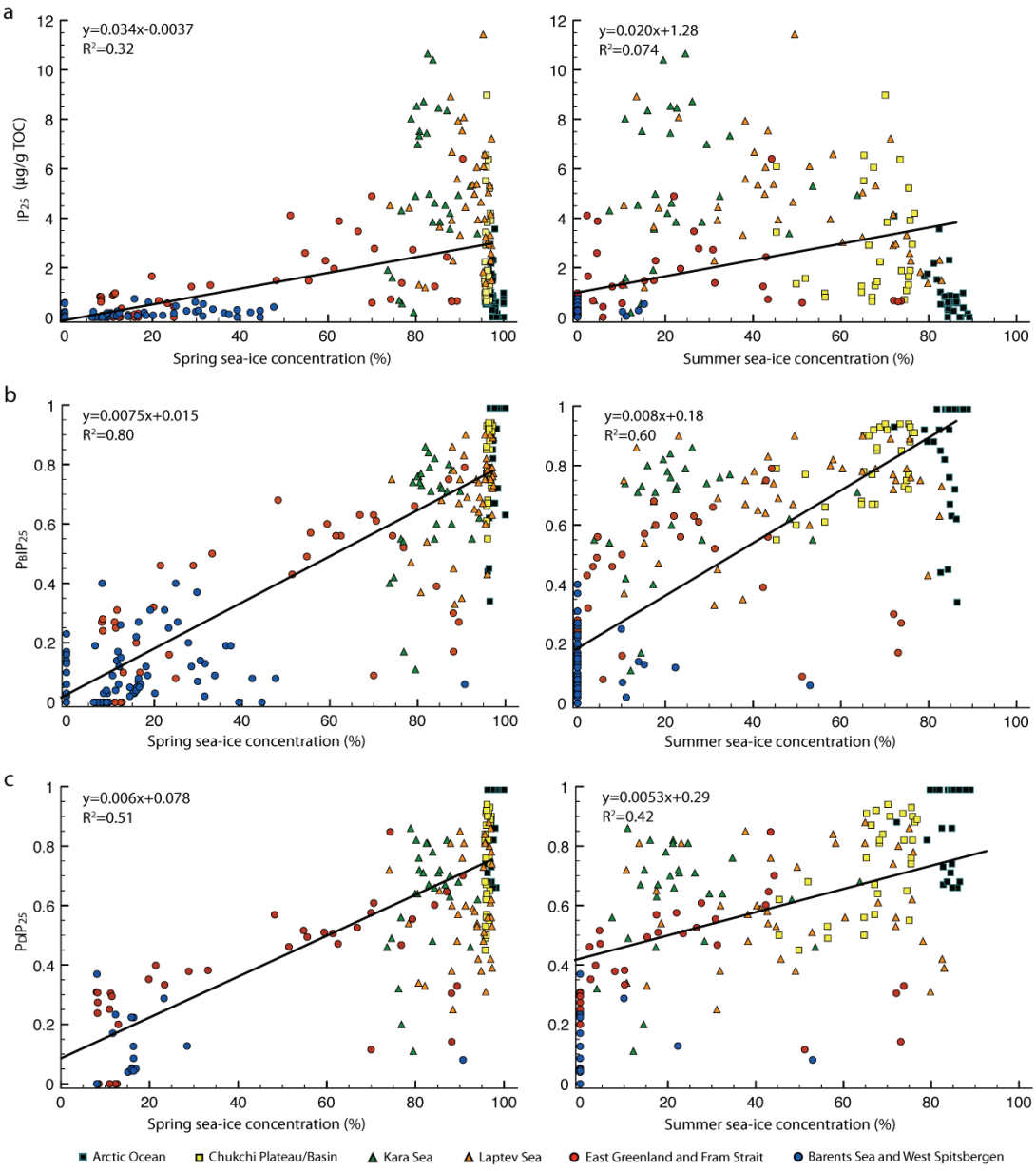

Figure 4.10 Correlations of spring/summer sea ice concentrations derived from satellite data (1988–2007) with IP_{25} concentrations (a), P_BIP_{25} values (b) and P_DIP_{25} values (c), respectively.

Samples from the Kara and Laptev Seas are located in areas with 80–100% spring sea-ice concentration, which decreases to 10–80% during summer due to the strong seasonal variability. Comparing the P_BIP_{25} values with the sea-ice concentrations, we realized that similar P_BIP_{25} values could refer to different sea-ice situations. For instance, high P_BIP_{25}

values result from a permanent multi-year ice coverage as is observed in the Central Arctic Ocean but they can also relate to the occasional occurrence of ice massifs at the continental shelf of the Laptev Sea. Furthermore, zero P_BIP_{25} values in the river sediments (Figure 4.5a) are caused by the absence of IP_{25} due to the unfavourable riverine (freshwater) environment limiting the growth of marine sea-ice algae rather than open-water conditions as observed in the Barents Sea. On the other hand, similar summer sea-ice scenarios can lead to different P_BIP_{25} values as a consequence of the variable melting process (i.e. timing, speed) of the sea ice between different regions.

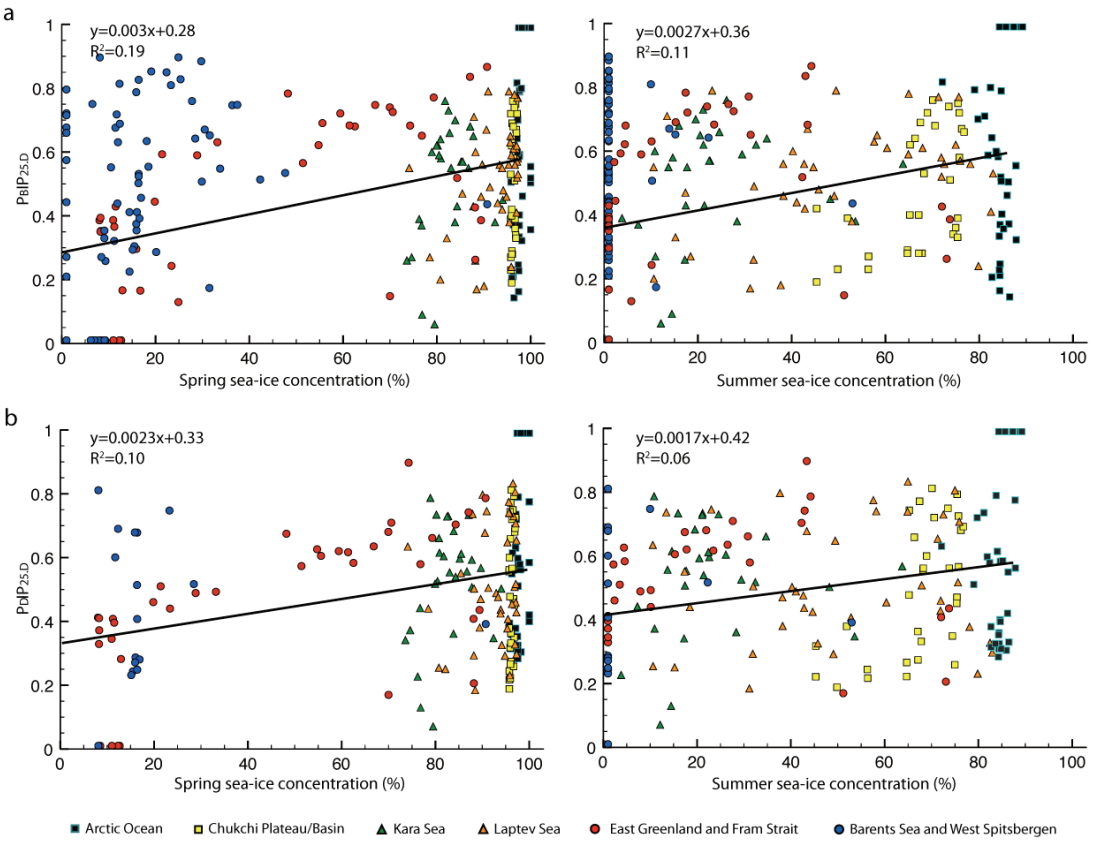

Figure 4.11 Correlations of spring/summer sea ice concentrations derived from satellite data (1988–2007) with $P_BIP_{25.D}$ values (a) and $P_DIP_{25.D}$ (b) calculated with different regional c factors (Table 4.1), respectively.

4.5 Conclusions

Within this study, for the first time numerous surface sediment samples from the permanently ice-covered Central Arctic Ocean (>80°N) have been used to determine the distribution of the sea-ice proxy IP_{25} and phytoplankton biomarkers 24S-brassicasterol and dinosterol. The new biomarker data obtained from fresh and deep-frozen surface sediments

are combined with published data determined in surface sediments from the marginal seas to generate pan-Arctic overview distribution maps of biomarkers.

Based on our data, the permanent sea-ice cover of the Central Arctic Ocean is reflected in the absence/low contents of IP_{25} and phytoplankton biomarkers 24S-brassicasterol and dinosterol. On the other hand, the sea-ice conditions vary significantly between different marginal seas. The PIP_{25} index, a combination of IP_{25} and phytoplankton biomarkers, has been used successfully to estimate sea-ice conditions more quantitatively, showing positive correlations with both spring and summer sea-ice concentrations obtained from satellite observation. When using PIP_{25} values for the reconstruction of sea-ice cover, however, several aspects should be considered: (1) Different correction factors (calculated from mean IP_{25} and phytoplankton biomarker concentrations) may give different PIP_{25} values, a fact to be considered if data sets from different areas/studies are compared. This study shows that PIP_{25} values calculated with one uniform C factor correlate well with satellite sea-ice data when using a large dataset. (2) The marine origin of 24S-brassicasterol has to be approved before using it as phytoplankton marker in the PIP_{25} approach. In this context, the similar distribution patterns of 24S-brassicasterol and dinosterol may be used as indications for a marine origin of brassicasterol. (3) Marine phytoplankton biomarkers as well as IP_{25} may have been incorporated into the sea-ice at the ice edge in the marginal seas and then transported within the sea ice towards the Central Arctic Ocean. (4) In addition to the calculated PIP_{25} values, the single concentrations of IP_{25} and phytoplankton biomarkers should always be considered when reconstructing (past) sea-ice conditions.

Acknowledgements

The materials used for this study were collected during several expeditions. We thank the chief scientists and captains of the research vessels, as well as the crew members and the scientists on board for their contributions during all the cruises. We are grateful to W. Luttmer for technical support in the laboratory. We thank S. Belt for discussion of an earlier version of the manuscript. Finical support by Alfred Wegener Institute (Bremerhaven) and China Scholarship Council is gratefully acknowledged.

5. Last Glacial Maximum sea-ice cover in the Central Arctic Ocean: Reconstruction from biomarkers

Xiaotong Xiao, Ruediger Stein, Kirsten Fahl

Alfred Wegener Institute, Helmholtz Center for Polar and Marine Research, Am Alten Hafen 26, 27568 Bremerhaven, Germany

In preparation.

Abstract

Paleo-sea-ice conditions of the Arctic Ocean were reconstructed for the Marine Isotope Stage (MIS) 3–1 by means of the sea ice proxy IP_{25} and phytoplankton-derived biomarkers (brassicasterol and dinosterol) data obtained from 7 sediment cores. Our results suggest more extensive sea-ice cover than present-day during MIS 3, increasing sea-ice growth during MIS 2 and warmer less ice-covered period during the last deglacial. The summer ice edge sustained north of the Barents Sea even during either extremely cold (i.e., Last Glacial Maximum (LGM)) or warm period (i.e., Bølling-Allerød). Based on the analysis of biomarker variability in 19 sediment cores across the Arctic Ocean, the sea-ice conditions of the LGM were reconstructed for the Central Arctic Ocean and adjacent areas. The West Spitsbergen margin and northern Barents Sea margin areas were characterized by high concentrations of both IP_{25} and phytoplankton biomarkers, considered as a productive ice-edge situations. The open-water conditions occurred in the eastern Fram Strait as well as between the Svalbard-Barents Sea Ice Sheet and the permanent Arctic sea-ice cover during the LGM summer, due to warm Atlantic Water flowing into the Arctic along West Spitsbergen and continuing eastwards along northern continental slope of the Barents Sea. In contrast, the LGM high Arctic proper (north of 84°N) was covered by thick permanent sea ice throughout the year with rare break up, indicated by zero or near-zero biomarker concentrations. The spring/summer sea-ice margin significantly extended southwards to the southern Lomonosov Ridge and Mendeleev Ridge during the LGM. Although the LGM interval was characterized by maximum extension and perennial sea-ice cover, the biomarkers were found in the sediments from the marginal seas, which might be transported by sea-ice drift across the high Arctic proper.

5.1 Introduction

The sea-ice extent, playing an essential role in polar regions (Arctic and South Ocean), is not only one of the most variable components in Earth's climate system, but also influences a number of processes in the oceans (Thomas and Dieckmann, 2010). The present day Arctic sea-ice cover is characterized by distinct seasonal and interannual variability, especially in the marginal seas. Large zones of fast ice occur on the shallow shelf during wintertime, connecting with the islands of the Arctic seas, along the boundary of which, there are polynyas and leads. Both fast ice and polynyas influence the dynamics and thermo-dynamics in the ocean circulation as well as the climate system (Ólason and Harms, 2010; Polyakov et al., 2003). Compared to the present day, the Last Glacial Maximum (LGM) Arctic environmental conditions were significantly different. A much drier and colder LGM climate limited the evaporation and precipitation. The Svalbard-Barents Sea Ice Sheet was centred over the Barents Sea inhibiting the Atlantic water inflow to the Arctic Ocean and the Barents-Kara Ice Sheet extended eastwards as far as Taymyr blocking the drainage of Ob and Yenisei rivers to the Kara shelf (Svendsen et al., 2004; Polyak et al., 2008; Ingólfsson and Landvik, 2013 and references therein). The Innuitian Ice Sheet over Ellesmere Island coalesced with the Laurentide Ice Sheet and Greenland Ice Sheet, blocking the Nares Strait connection to the Baffin Bay (Dyke et al., 2002 and references therein). As a consequence of the extension of LGM ice sheets, the sea level was lowered, and the shallow Bering Strait and Siberian shelves were exposed and occupied by dry grassland (Sher, 1995; Elias and Brigham-Grette, 2013). However, detailed reconstruction of past sea-ice conditions and glacial/interglacial changes are still rare (for review see Polyak et al., 2010; Stein et al., 2012).

Here we focus on the reconstruction of LGM sea-ice conditions in the Arctic Ocean and Fram Strait. The LGM Arctic sea-ice situation, i.e., the relation between the extent of sea-ice cover and ice sheets is still debated. The CLIMAP project (CLIMAP, 1976, 1981) supposed a perennial ice cover in the Arctic Ocean and Nordic Seas blocking the Atlantic water advection and summer polar front in the North Atlantic reaching as far as 50°N, a hypothesis that has to be rejected based on more recent studies. Since Hebbeln et al. (1994) reported that the Atlantic water reached the northern Norwegian Sea and advected through Fram Strait up to northern margin of Svalbard during the LGM, subsequent studies were carried out to support seasonally ice-free conditions in the Nordic seas and eastern Fram Strait. Knies et al (1999) suggested that the Atlantic surface water could penetrate into the Arctic Ocean along the margin of the Svalbard-Barents Sea Ice Sheet causing seasonally open-water conditions along the northern Barents Sea margin. Open-water conditions may also result from coastal polynya formation due to offshore katabatic winds during the LGM (Knies et al., 1999). Furthermore, the GLAMAP Group (Pflaumann et al., 2003; Sarnthein et al., 2003a, 2003b)

reconstructed the LGM polar front in north Atlantic by using planktonic foraminifer data and SST estimates, showing a seasonal ice cover and warmer summer condition in the Nordic Seas, and a summer front retreating to about 73°N with ice-free condition in the eastern Fram Strait during the LGM. Recently, Brandly and England (2008) also pointed out that seasonally open-water conditions occurred at the end of MIS 2 along the northern Barents Sea margin eastwards to the Laptev Sea shelf caused by Atlantic water advection and katabatic winds. In contrast to the continuous sedimentation at the continental margin, however, low sedimentation rates occurred in the Central Arctic during LGM due to the thick ice cover limiting detailed sea-ice reconstruction (Cronin et al., 2012). The sedimentary LGM records from Mendeleev Ridge and Northwind Ridge also point to a permanent sea-ice cover or shelf ice cover, prevailing in the western Arctic Ocean (Polyak et al., 2004, 2007).

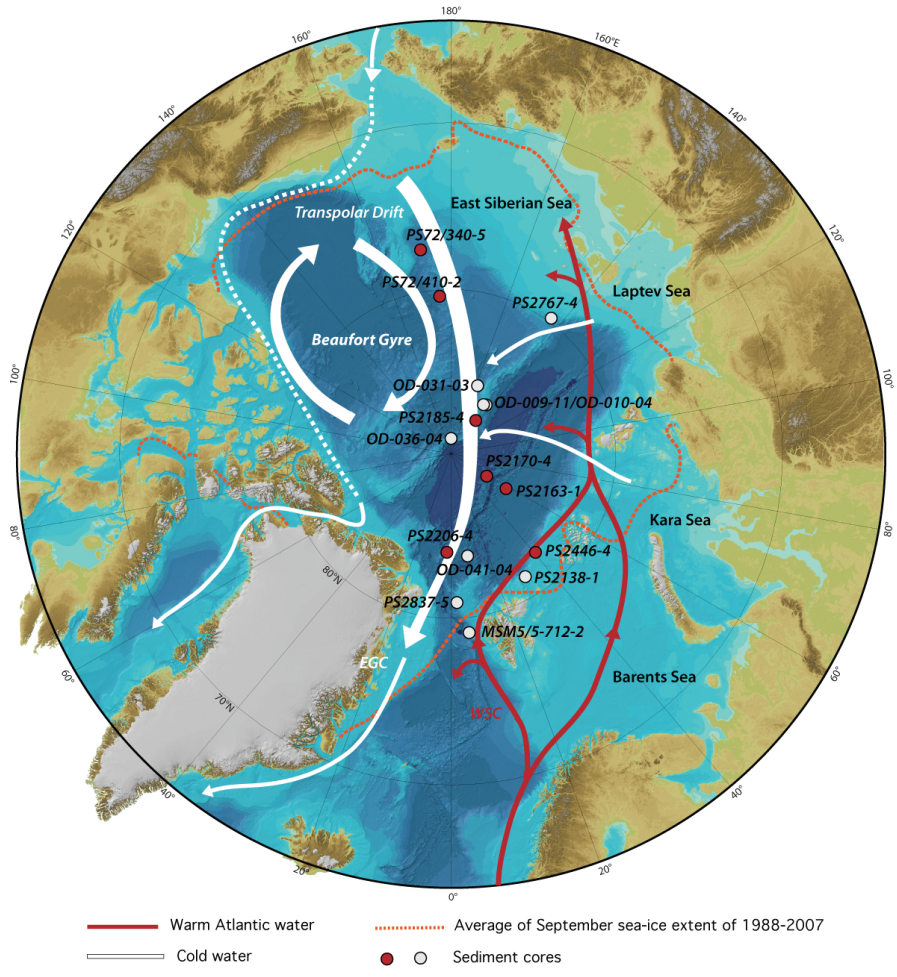

Figure 5.1 Locations of sediment cores used for IP_{25} study in the Arctic Ocean. Red dots represent sediment cores with continuous sedimentary records. White dots represent sediment cores of LGM time-slice. Red arrows show the surface circulation of warm Atlantic Water entering the Arctic Ocean, while white arrows show the process of the cold and less salty water (modified from Stein and Macdonald, 2004). International Bathymetric Chart of the Arctic Ocean (Jakobsson et al., 2008).

Palaeo sea-ice reconstructions are mainly based on microfossil assemblages, and sedimentological and geochemical parameters, including ice-rafted debris (IRD), stable isotopes, dinoflagellate cysts and further more (details see Stein, 2008; Polyak et al., 2010; Stein et al., 2012 and references therein). Here, we use the quite novel molecular sea-ice proxy - so called IP_{25} - to reconstruct past sea-ice conditions in the Arctic Ocean. This compound is a mono-unsaturated highly branched isoprenoid (HBI) alkene biosynthesized by Arctic sea-ice diatoms, which was first determined in Canadian Arctic sediments and sea ice by Belt et al. (2007). Meanwhile, IP_{25} has been universally used in marine sediments for sea-ice reconstruction (for reviews see Stein et al., 2012 and Belt and Müller, 2013 and reference herein). The extraction, identification and quantification of IP_{25} have been well established and intercalibrated between different laboratories (Belt et al., 2012; 2014). IP_{25} studies using surface sediments from different areas of the Arctic strengthen the applicability of the IP_{25} as an indicator for paleo sea-ice reconstruction (Müller et al., 2011; Navarro-Rodriguez et al., 2013; Stoynova et al., 2013; Xiao et al., 2013, 2014). In a pilot study carried out on a sediment core from southern Yermak Plateau, Stein and Fahl (2013) could show that IP_{25} is even preserved in marine sediments as old as 2.2 M. Against this background, we present new IP_{25} records going back in time to MIS 3, with special emphasis on the biomarker distributions of the LGM time slice in the Arctic Ocean.

5.2 Materials and methods

5.2.1 Sediment cores and age model

The depth interval of the LGM time slice in 16 sediment cores used for this study is based on age models published in Nørgaard-Pedersen et al. (2003) for 10 of these cores (Table 5.1). The LGM time slices in cores PS2767-4, PS2837 and MSM5/5-712-5 were identified by Müller and Stein (2000), Müller et al. (2009) and Müller et al. (2014). The other cores (PS2185-4, PS72/340-5 and PS72/410-2) were correlated to the published dated cores as described below. Concerning the age of the LGM time interval we follow GLAMAP (15–18 ^{14}C ka or 18.0–21.5 cal. kyr BP; Sarnthein et al., 2003a). The MARGO group adopted the definition suggested by EPILOG (16.0–19.5 ^{14}C ka or 19.0–23.0 cal. kyr BP; Chronozone Level 2 in Mix et al., 2001), which is slightly different from the GLAMAP LGM time slice (Nørgaard-Pedersen et al., 2003)

During the expedition ARK-VIII/3 of RV *Polarstern* in 1991 (Fütterer, 1992), the cores PS2163-1, PS2170-4, PS2185-4 and PS2206-4 were obtained from the Gakkel Ridge, the Amundsen Basin, the Lomonosov Ridge and the southwestern part of the Gakkel Ridge, respectively (Figure 5.1). All cores were taken by means of multicorer. The chronology of the

sediment cores PS2163-1, PS2170-4 and PS2206-4 is based on AMS ^{14}C datings performed on *Neogloboquadrina pachyderma* (sin.) (Stein et al., 1994a), whereas the age model of multicorer Core PS2185-4 is obtained from correlation with the AMS ^{14}C-dated Core PS2185-3 (boxcorer) (Nørgaard-Pedersen et al., 1998).

Sediment Core PS2446-4 (kastenlot) was recovered from the northern Barents Sea continental margin during the expedition ARK-IX/4 of RV *Polarstern* in 1993 (Fütterer, 1994). This core mainly consists of bioturbated mud and an uppermost brownish unit, with occasional thin pinkish and sandy layers, and several grayish diamictons representing debris flows (Figure 5.2; Fütterer, 1994; Knies, 1999). The chronology is based on AMS ^{14}C datings performed on *Neogloboquadrina pachyderma* and mixed foraminifera, the final age model of PS2446-4 was established by radiocarbon datings and paleomagnetic data (Knies, 1999).

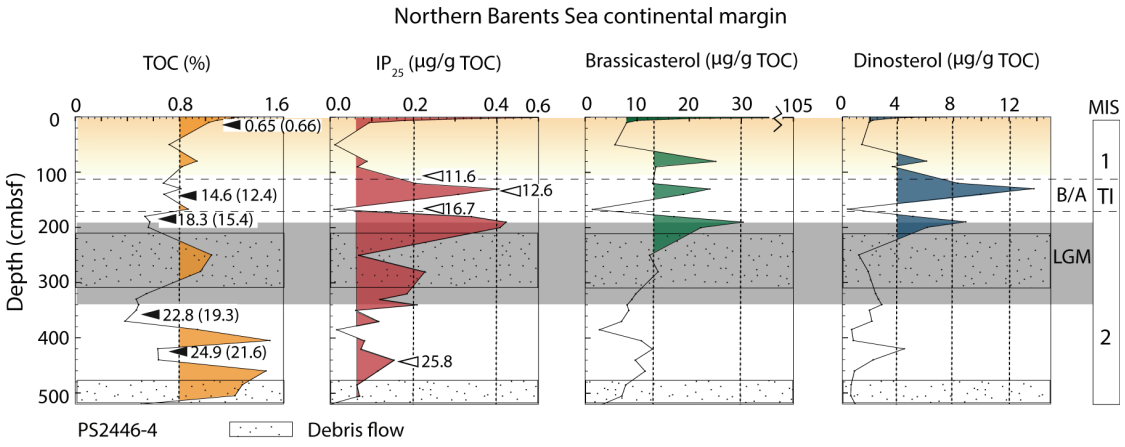

Figure 5.2 Records of total organic carbon (%) and concentrations (µg/g TOC) of IP_{25}, brassicasterol and dinosterol in Core PS2446-4 from Northern Barents Sea continental margin. ^{14}C ages are shown by black arrows in the brackets and numbers outside of the brackets are calendar years (Knies, 1999). Open arrows show the (boundary of) events.

The kastenlot Core PS72/340-5 and multicorer Core PS72/410-2 were taken from the western Arctic Ocean (southern Mendeleev Ridge) during ARK-XXIII/3 in 2008 (Jokat, 2009; Figure 5.1). Core PS72/340-5 consists of an 8.3 m long sedimentary sequence with clear brownish and pinkish layers (Stein et al., 2010). We only focus on the uppermost part (6–92 cm). The age model of Core PS72/340-5 is based on AMS ^{14}C ages and the identification of marine isotope stages (Stein et al., 2010; Bazhenova, 2012). The age model of Core PS72/410-2 is obtained from correlation with the neighbouring Core PS72/410-1 (Kang et al., 2013).

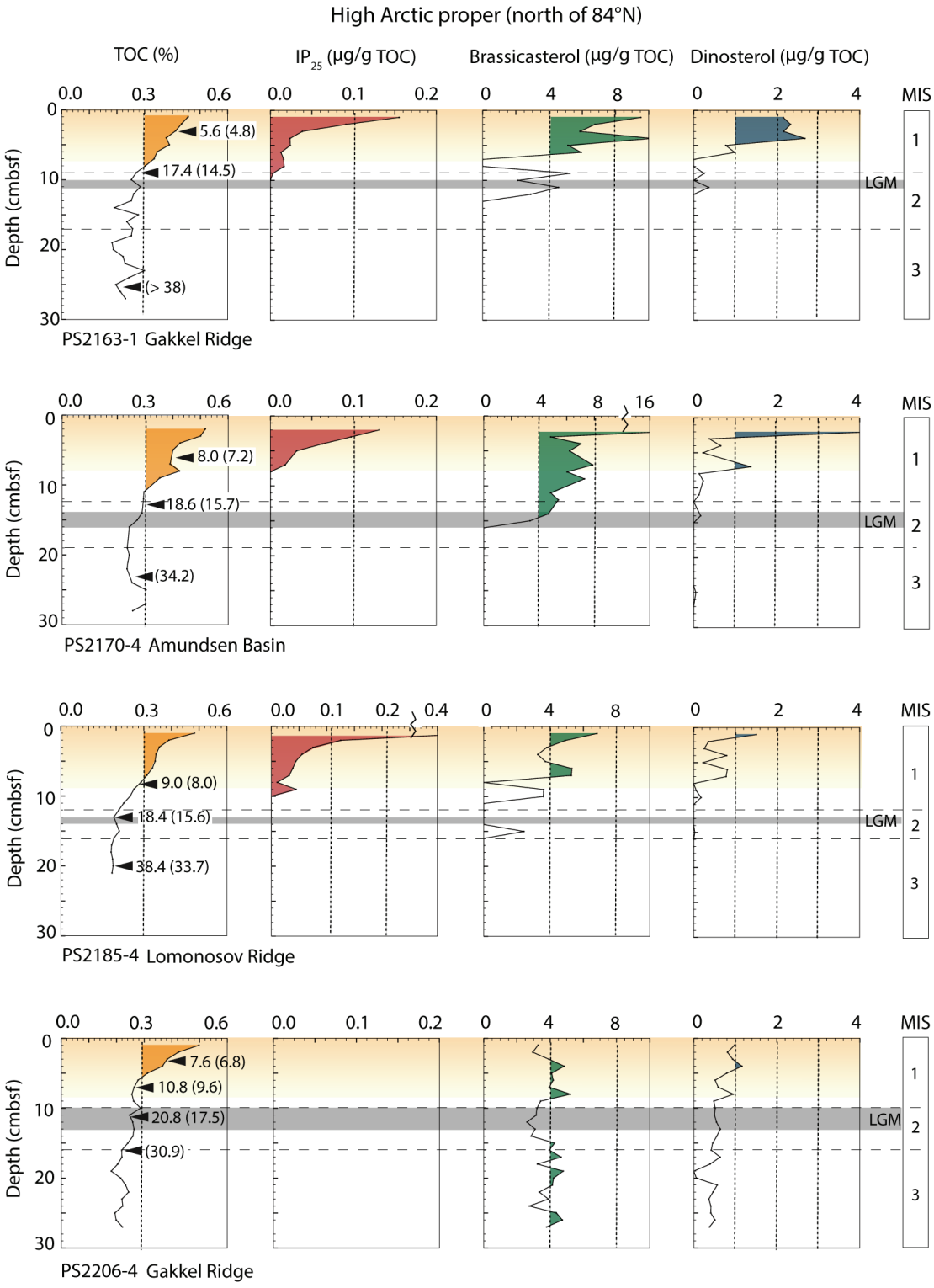

Figure 5.3 Records of total organic carbon (%) and concentrations (µg/g TOC) of IP_{25}, brassicasterol and dinosterol in sediment cores from the Central Arctic and the Mendeleev Ridge. ^{14}C ages are shown by black arrows in the brackets and numbers outside of the brackets are calendar years (Stein et al., 1994a, 1994b; Nørgaard-Pedersen et al., 1998).

Table 5.1 List of sediment cores with depth of LGM intervals for this study. '*' denotes the LGM time slices based on age models published in Nørgaard-Pedersen et al. (2003).

Station	Latitude	Longitude	Depth (cm)	TOC (%)	IP_{25} (µg/g TOC)	Brassicasterol (µg/g TOC)	Dinosterol (µg/g TOC)	References
PS2138-1	81.54	30.88	130-215*	0.41	0.27	10.53	3.32	own data
PS2446-4	82.40	40.91	180-210, 300-340*	0.53	0.28	16.07	4.64	own data
PS2837-5	81.23	2.38	387-392	0.32	0.096	0.00	0.00	Müller et al., 2009
MSM5/5-712-5	78.92	6.77	664-753	0.65	0.19	8.99	6.13	Müller et al., 2014
OD_009_11_1	86.38	144.34	17-18*	0.19	0	5.08	0.26	own data
OD_010_04_1	86.40	142.95	20-21*	0.17	0	3.11	0.21	own data
OD_031_03_1	85.66	160.625	15-16*	0.18	0	3.71	0.02	own data
OD_036_04_1	89	179.95	8-9*	0.26	0	4.07	0.32	own data
OD_041_04_1	84.03	11.24	13-17*	0.27	0	2.52	0.40	own data
PS2163-1	86.24	59.22	10-11*	0.25	0	2.14	0.00	own data
PS2170-4	87.59	60.76	14-16*	0.28	0	4.01	0.08	own data
PS2185-4	87.53	144.17	13-14	0.19	0	0.00	0.00	own data
PS2206-4	84.26	-2.56	10-13*	0.26	0	2.99	0.52	own data
PS2767-4	79.74	144.01	324-354	0.37	0.036	2.42	-	Stein and Fahl., 2012
PS72/340-5	77.60	-171.497	Approximate 65-80	0.36	0.043	5.22	2.69	own data
PS72/410-2	80.52	-175.737	Approximate 8-10	0.16	0	1.32	0.23	own data

5.2.2 Biomarker analyses

All cores were stored at -30°C until further treatment with the exception of PS2206-4 stored at 4°C. The sediments were freeze-dried and homogenised before any further treatment. Prior to the biomarker analyses, the internal standards 7-hexylnonadecane (0.076 µg/sample), squalane (2.4 µg/sample) and cholesterol-d_6 (cholest-5-en-3β-ol-D_6; 20.2 µg/sample) were added to the sediments for quantification. Afterwards the sediments were extracted by an Accelerated Solvent Extractor (DIONEX, ASE 200; 100°C, 5 min, 1000 psi) using dichloromethane:methanol (2:1 v/v) as solvent. Further separation of hydrocarbons and sterols was carried out via open-column chromatography using SiO_2 as stationary phase using 5 ml *n*-hexane and 6 ml ethylacetate:*n*-hexane (20:80 v/v), respectively. Sterols were silylated with 500 µl BSTFA (bis-trimethylsilyl-trifluoroacetamide; 60 °C, 2 h) after elution. Both IP_{25} and and sterols were analysed by gas chromatography (Agilent 6850 GC; 30 m HP-5MS column, 0.25 mm i.d., 0.25 µm film thickness) coupled to an Agilent 5975 C VL mass selective detector (MSD, 70 eV constant ionization potential, ion source temperature 230 °C). For further details concerning the instrumental method see Müller et al. (2011) and Fahl and Stein (2012). Individual compound identification was based on comparisons of their retention times with that of reference compounds (for brassicasterol) and on comparisons of their mass spectra with published data (Boon et al., 1979; Volkman, 1986; Johns et al., 1999; Belt et al., 2007). The biomarker concentrations were calculated on the basis of their individual GC-MS ion responses compared with those of respective internal standards. For the quantification of IP_{25} its molecular ion (m/z 350) in relation to the iron of internal standard 7-hexylnonadecane (m/z 266) was used. For further details concerning the IP_{25} quantification, the reader is referred to Müller et al. (2011) and Fahl and Stein (2012). The sterols were quantified using the molecular ions m/z 470 for brassicasterol (24-methylcholesta-5,22E-dien-3β-ol) and m/z 500 for dinosterol (4α,23,24R-trimethyl-5α-cholest-22E-en-3β-ol), compared with the response of the molecular ion m/z 464 of the internal standard cholesterol-d_6. The detailed identification and quantification of brassicasterol and dinosterol were described in Fahl and Stein (1999). The biomarker concentrations were corrected to the amount of extracted sediment. The absolute biomarker concentrations have been normalised to the TOC content to compensate the different sedimentation rates in our study area, which might cause an overestimation or underestimation of the biomarker concentrations.

5.3 Results

The TOC contents vary from 0.4 to 1.5 % in Core PS2446-4 from the northern Barents Sea continental margin (Figure 5.2). In previous studies carried out on sediment cores along

Eurasian continental margin (including PS2446-4), TOC contents are higher than in the open-ocean marine sediments of the central North Atlantic, related to significant terrigenous organic matter input from sea ice and iceberg (Stein et al., 1994a, 2001; Knies et al., 2000). Furthermore, these authors pointed out that maximum TOC values in these cores occur in debris flows and in laminated and IRD-enriched layers, representing glacial and deglacial periods. In contrast, TOC contents show low values within the range of 0 to 0.6 % in the rest of the sediment cores along a transect from north of Fram Strait across the Central Arctic to the Mendeleev Ridge and Chukchi Plateau (Figures 5.3 and 5.4).

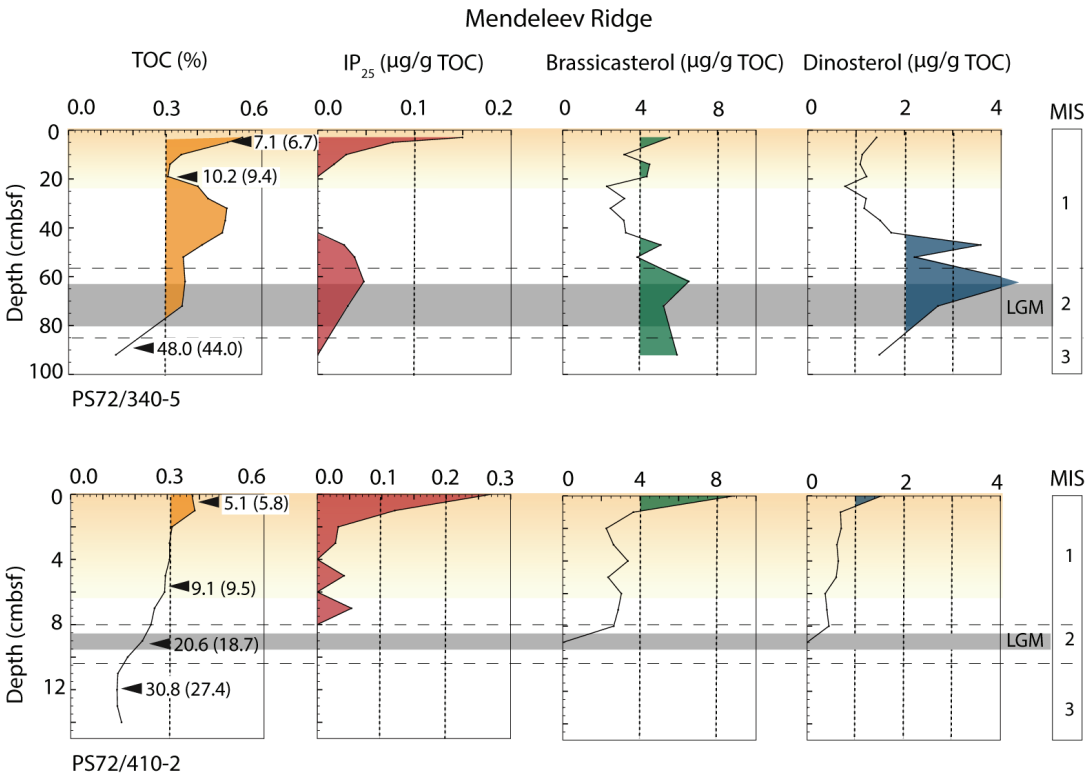

Figure 5.4 Records of total organic carbon (%) and concentrations (µg/g TOC) of IP_{25}, brassicasterol and dinosterol in sediment cores from the Mendeleev Ridge. ^{14}C ages are shown by black arrows in the brackets and numbers outside of the brackets are calendar years (Bazhenova, 2012; Jang et al., 2013).

IP_{25} values are in the range of 0 to 0.63 µg/g TOC in Core PS2446-4, increasing at the end of LGM and during Termination I, and reaching the maxima in the surface layer. Brassicaterol and dinosterol concentrations display a similar variability pattern in this core, showing low values in MIS 2 and increasing at the end of LGM and during Termination I (Figure 5.2). In all the four cores from high Arctic proper, north of 84°N, biomarkers display low concentrations (Figure 5.3). IP_{25} is only determined in the Holocene time interval varying from 0 to 0.4 µg/g TOC in cores PS2163-1, PS2170-4 and PS2185-4, and completely absent in Core PS2206-4 (Figure 5.3). Low brassicasterol values of 0 and 16 µg/g TOC were found

in these cores, and dinosterol shows even lower values from 0 to 4 µg/g TOC. Concentrations of both IP_{25} and phytoplankton biomarkers were low or zero during MIS 2 whereas increasing values could be detected during MIS 1 (Figure 5.3). Biomarker values in cores PS72/340-5 and PS72/410-2 from the Mendeleev Ridge are within the range of that in the high Arctic (Figure 5.4). In general, the biomarkers show increasing concentrations during the Holocene in Core PS72/410-2, while in the neighbouring Core PS72/340-5, IP_{25} occurs not only in the upper layers, but also between 50 and 90 cm, and both brassicasterol and dinosterol show maximum values at around 60 cm (Figure 5.4).

5.4 Discussion

5.4.1 Temporal biomarker variability and sea-ice conditions

The biomarker records in the sediment cores go back in time to MIS 3 except in Core PS2446-4 (Figures 5.2, 5.3 and 5.4). The completely absence of IP_{25} in sediment cores PS2163-1, PS2170-4, PS2185-4, PS2206-4 and PS72/410-2 during MIS 3, accompanied with low or zero concentrations of phytoplankton biomarkers, indicate perennial and dense ice cover from north of Fram Strait across the Central Arctic to Mendeleev Ridge and Chukchi Plateau throughout the year (Figure 5.6a). The sea-ice cover was more extensive during MIS 3 than during the Holocene with a lower sea level and smaller continental shelf (Cronin et al., 2012).

Generally low concentrations of IP_{25} and phytoplankton biomarker in Core PS2446-4 during MIS 2 point to a reduced primary productivity attributed to an increasing sea-ice growth, however, slightly variability of both biomarkers indicate occasional ice margin/break along the north continental slope of the Barents Sea (Figures 5.2 and 5.6a). In this sediment core, elevated IP_{25} contents were found in the LGM interval. Another peak concentration of IP_{25} as well as phytoplankton biomarkers occurred at about cal. 25 kyr BP. These two time intervals of increased IP_{25} are consistent with two short-term events (31.4-26.5 cal. kyr BP and 23-17.4 cal. kyr BP) of warm Atlantic Water advection into the Nordic Sea determined on sediment cores from the Fram Strait (Hebbeln et al., 1994). The abundance of benthic foraminifer during MIS 2 reflected the sub-surface Atlantic water could reach the northern Barents Sea margin (Mackensen et al., 1985). Furthermore, the high accumulation rates of biogenic calcite on northern Barents Sea margin have been related to a coastal polynya caused by upwelling warm water (Knies and Stein, 1998; Knies et al., 1999). During that pre-LGM interval, an extensive coastal polynya existed along northern Barents Sea continental margin westwards at least to 2.4°E (core site PS2837, see Müller et al., 2009) and eastwards at least to Franz Victoria Through (core site PS2446-4, this study), triggered by katabatic wind (Figure 5.7a).

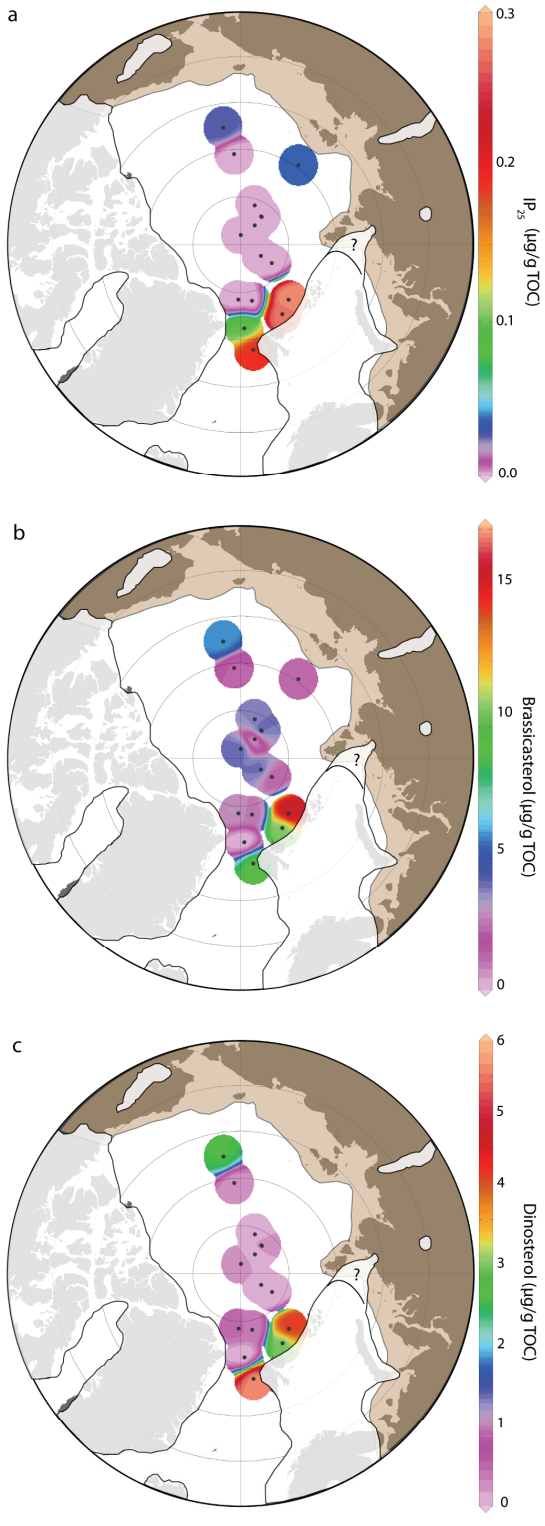

From the northern Barents Sea margin to the interior Arctic Ocean, the absence of IP_{25} and near-zero concentrations of phytoplankton biomarkers in cores PS2163-1, PS2170-4 and PS2185-4 reflect that the perennial ice cover during MIS 2 was significantly thicker than during modern time (Figures 5.3 and 5.6a). In addition, the carbonate contents (associated mainly with planktonic foraminifers) also show low flux during this period (Stein et al., 1994a, 1994b). In the vicinity of the southern Mendeleev Ridge, the low values of IP_{25} in PS72/340-5 and the absence of IP_{25} in PS72/410-2 during MIS 2 indicate the spring/summer sea-ice cover extended southwards over these core sites, inhibiting the light penetration (Figures 5.4 and 5.6a).

Both IP_{25} and phytoplankton biomarkers increased extremely in PS2446-4 in the post-LGM stage between 16 and 11 kyrs BP (MIS 1), and especially dinosterol reached its maximum values, indicating a more productive period with a quite stable ice margin/seasonal ice cover north of the Barents Sea (Figures 5.2 and 5.6a). The major IRD input on the northern Barents Sea continental margin and eastern Greenland margin occurred between 14 and 13 kyr (Nam et al., 1995; Knies et al., 1999), consistent with the continuous inflow of Atlantic Water being present at western and northern

Figure 5.5 Concentrations (µg/g TOC) of IP25 (a), phytoplankton biomarkers brassicasterol (b) and dinosterol (c) in LGM time-slice from the Arctic Ocean. White shields indicate the ice sheets during the LGM. Question marks propose an uncertain ice sheet in the easternmost Kara Sea. The exposed continental shelves were indicated by brown shield (after Mangerud et al., 2002).

Svalbard shelf since > 14.5 kyr BP (Ślubowska-Woldengen et al., 2007, 2008) and reflecting the decay of ice sheets after LGM (Figure 5.7c). In the high Arctic, the near-zero concentrations of IP_{25} and brassicasterol in cores PS2163-1, PS2170-4 and PS2185-4 during the last deglacial (Figure 5.3), however, are consistent with the occurrence of minimum $\delta^{18}O$ and $\delta^{13}C$ at these cores (Stein et al., 1994a, 1994b), interpreted as strong meltwater causing an extended stratification and a decrease in the ventilation, which precludes the nutrient availability. Although the time resolution of the biomarker records are low and the ^{14}C age is uncertain in PS72/340-5, the maximum phytoplankton biomarker concentrations are observed during the glacial-interglacial transition (Figure 5.4), consistent with seasonally ice-free conditions during last deglacial based on a new ostracode sea-ice proxy study in sediment cores from the Central Arctic and Mendeleev Ridge (Cronin et al., 2010). Taken together, we postulate the Arctic sea-ice cover was less than the modern sea-ice cover with open-ocean conditions in the marginal seas year round, supporting the minimum sea-ice extent during the last deglacial (16–11kyr BP) as reported by Cronin et al. (2010).

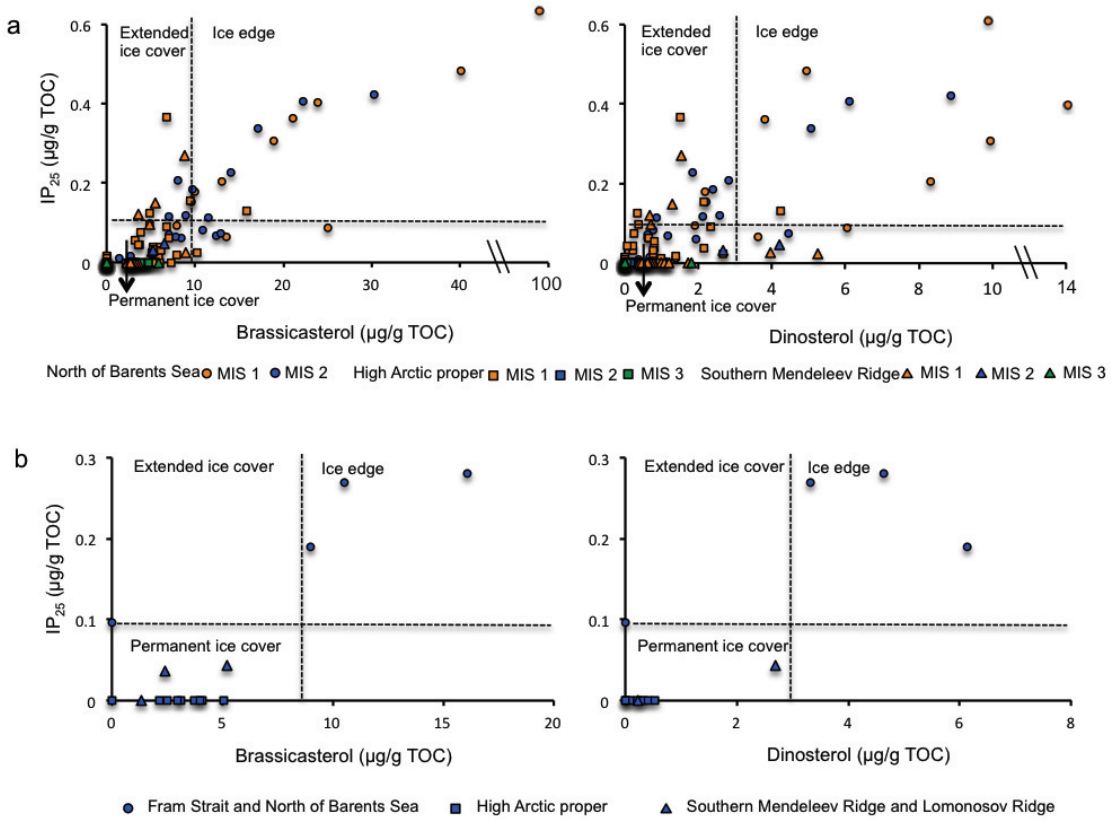

Figure 5.6 Correlations between the concentrations of IP_{25} and phytoplankton biomarkers in the sediments of the different time intervals (MIS3-1) (a) and in the sediments of the LGM time slices (b) from different regions of the Arctic Ocean.

5.4.2 LGM biomarker distribution and sea-ice conditions

In order to reconstruct the LGM sea-ice conditions in the Central Arctic and adjacent areas, the spatial biomarker distributions in LGM sediments from the Fram Strait across the high Arctic to the southern Lomonosov Ridge and southern Mendeleev Ridge have been studied (Figure 5.5; Table 1). Similar to the modern biomarker distributions, both IP_{25} and phytoplankton biomarkers show low values in the Central Arctic and comparatively high values along the continental margin during the LGM. That means, the West Spitsbergen margin and northern Barents Sea margin area were characterized by high concentrations of both IP_{25} and brassicasterol. Furthermore, the high sedimentation rates and relatively high fluxes of planktonic foraminifers and IRD during the LGM were found at these sites, typical for a productive ice-edge region (Nørgaard-Pedersen et al., 2003). In contrast, the interior Arctic Ocean (>84°N) was described as an area of low sedimentation rates and low fluxes of planktonic foraminifers and IRD owing to an extensive sea-ice cover (Stein et al., 1994b; Nørgaard-Pedersen et al., 2003; Cronin et al., 2012), as also reflected in the zero or near-zero biomarker concentrations in this study. In the sediments from southern Lomonosov Ridge and southern Mendeleev Ridge, the biomarkers also showed minor values during the LGM.

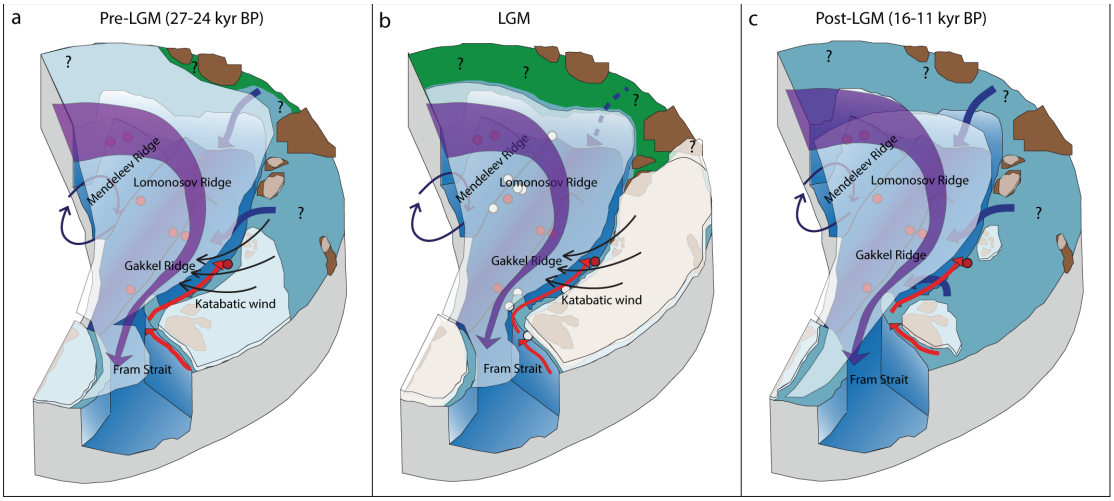

Figure 5.7 Schematic illustration showing the general sea-ice conditions for the study areas during pre-LGM (a), LGM (b) and post-LGM (c). Red arrows refer to the Atlantic Water advection and dark blue arrows from the continental shelves show the freshwater input. Semi-transparent purple arrows indicate Transpolar Drift. The circle arrows represent Beaufort Gyre. The exposed continental shelves occupied by grassland due to lower sea level are indicated by green shield (Sher, 1995). Question marks show the uncertain sea-ice conditions. For explanation of the dots, see Figure 5.1.

The LGM IP_{25} values from the northern Barents Sea continental margin were only slightly lower than in the surface layer. Thus, we postulate a stable ice edge between the Svalbard-

Barents Sea Ice Sheet and the permanent Arctic ice cover during LGM summer (Figures 5.5 and 5.6b). Coincidently, Knies et al. (1999) reported the high fluxes of $CaCO_3$ were found north of the Barents Sea resulted from the calving of ice margin, indicating the open-ocean area occurred along the northern Barents Sea margin blew off the Svalbard-Barents Sea Ice Sheet by katabatic winds and influenced by warm Atlantic Water advection. The relatively high concentrations of IP_{25} at the northern Barents Sea continental margin and the West Spitsbergen margin reflect that the warm Atlantic water flowed into the Arctic along West Spitsbergen and continued eastwards along northern Barents Sea continental slope, which deduced some growth of ice algal and phytoplankton during spring and summer (Figure 5.7b). There were ice-free conditions in eastern Fram Strait during the LGM summer, supporting the reconstruction of LGM sea-ice extent based on foraminifer paleo-temperature estimates (Sarnthein et al., 2003). This advance of Atlantic water has resulted in seasonally open-water conditions in Nordic Sea, which would have triggered the increasing evaporation and precipitation for the extension of ice sheets (Hebbeln et al., 1994; Siegert et al., 2002; Ingólfsso and Landvik, 2013). Responding to these factors as well as lower summer insolation, the ice sheets have grown to maximum size by around 21 kyr BP (Figure 5.7b). Furthermore, a distant moisture source originating from the evaporation in the subtropics could also possibly contribute to LGM evolution (Hebbeln et al., 1994). Low IP_{25} concentration and zero-values of phytoplankton biomarkers in the north Fram Strait indicated that the summer sea-ice margin during LGM must have been located south of 81°N (Müller et al., 2009), however, the sea ice only covered the western Fram Strait (Sarthein et al., 2003). This is also supported by dinoflagellate cyst assemblages data indicating that dense sea-ice cover was restricted to the East Greenland continental margins (de Vernal et al., 2005). On the other hand, brassicasterol values here are much lower than those in the surface sediments due to the weakening Atlantic Water advection as the extent of Svalbard-Barents Sea Ice Sheet inhibited the Barents Sea branch of Atlantic water advection, and the Fram Strait branch was also restricted by the ice sheet, and permanent Arctic ice cover could not reach as far as it does today.

IP_{25} was completely absent in LGM sediments from the high Arctic (>84°N) alongside with the near-zero brassicasterol, caused by coherent permanent ice cover, which was sufficiently thick to limit the light penetrating the sea-ice cover (Figs. 5 and 6b). Thus, minor primary productivity happened during LGM. This is supported by previous studies reporting the thick sea ice in the Central Arctic only rarely broke up and significantly limited the planktonic productivity and sedimentation rates (Darby et al., 1997; Nørgaard-Pedersen et al., 1998, 2003; Cronin et al., 2012).

Low concentrations of both IP_{25} and brassicasterol were found in sediments from north of the continental shelf of the Laptev Sea (southern Lomonosov Ridge), suggesting the spring/summer sea-ice margin significantly extended southwards during the LGM (Figures 5.5 and 5.6b). Sediment cores from the southern Mendeleev Ridge and Chukchi Plateau also contained less biomarker in the LGM interval, consistent with the absence of foraminifers at these sites as a consequence of an extensive and thick ice cover year round (Darby et al., 1997; Phillips and Grantz, 1997). Additionally, the low abundances of the ostracode *A. arcticum* in sediment cores from the Central Arctic and the Mendeleev Ridge during the LGM also indicate the occurrence of thick sea ice or ice shelves not suitable for pelagic amphipods (Poirier et al., 2012). We assume that the dense and thick perennial Arctic sea-ice cover extended southwards, probably reaching or approaching the present coast of the Laptev Sea and Chukchi Sea. The sea-ice conditions in the marginal seas during the LGM were much severer than in the modern Central Arctic, with only rarely break-up from which neither ice algae nor phytoplankton could benefit. Furthermore, the Atlantic water could barely reach the continental margin of the Laptev Sea inhibited by the ice sheet and Arctic ice cover (Figure 5.7b).

5.4.3 Biomarker-related versus modeled sea-ice conditions

In order to compensate the proxy uncertainties in reconstruction of glacial Arctic sea ice due to the low sedimentation rates, Stärz et al. (2012) recently used a regional sea-ice model, North Atlantic/Arctic Ocean Sea Ice Model (NAOSIM) coupled to a dynamics-thermodynamics sea ice model to examine the Arctic sea-ice conditions during the LGM. The modeled results suggest a closed perennial sea-ice cover in the Central Arctic, consistent with the zero values of IP_{25} and minimum concentrations of sterols (Figures 5.5 and 5.8a). The sea-ice drift follows the Beaufort Gyre and Transpolar Drift exiting the Arctic Ocean through the Fram Strait (Figure 5.8b). Therefore, some marine phytoplankton biomarkers as well as IP_{25} may have been incorporated into the sea-ice at the ice edge in the marginal seas and then transported within the sea ice by the Transpolar Drift system towards the Central Arctic Ocean. This interpretation may be supported by the partly positive correlation between IP_{25} and the phytoplankton biomarkers (Fig. 6b). This may also explain low but more than zero brassicasterol and dinosterol contents in the Central Arctic, however, IP_{25} could not be determined in the sediments of the LGM intervals from the Central Arctic due to the minor magnitude of the concentrations (Figure 5.5). Similarly, planktic foraminifers were found in the LGM sediment slice of Core OD-041-04 from the Central Arctic (84.03°N) (Nørgaard-Pedersen et al., 2003). These authors, however, believed the foraminifers in the Central Arctic presented local productions as the ^{18}O values of these foraminifers are different than those

from high productive zones in southwestern Eurasian Basin and Fram Strait. From our study, we have no evidence to deny the possible presence of allochthonous from the Chukchi Sea and/or East Siberian Sea continental slope following the sea-ice drift presented in Stärz et al (2012).

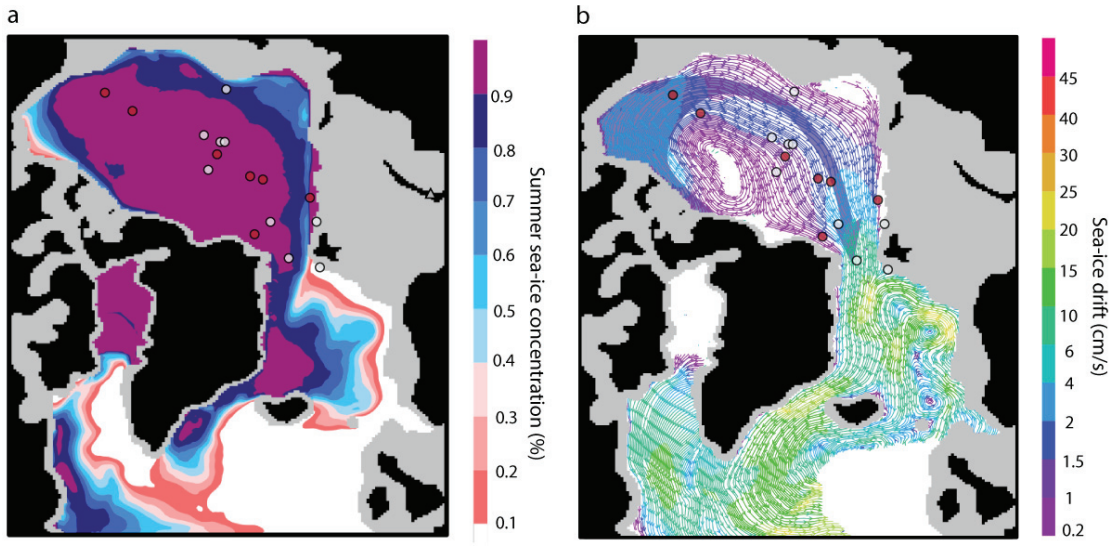

Figure 5.8 Modelled mean sea-ice concentration for summer (a) and 30-yr mean sea-ice drift (b) during the LGM (Stärz et al., 2012 supplemented). For explanation of the dots, see Figure 1.

Seasonally open water conditions occurred along Atlantic Water advection in the Nordic Seas up to north of Svalbard, supporting the high concentrations of IP_{25} and phytoplankton biomarkers at west continental margin of Svalbard and north continental margin of the Barents Sea (Figures 5.5 and 5.8a). Even though the LGM sea-ice cover was thick and approached to the continental shelf, the modelled sea-ice concentrations show 50-80% along the continental margin of the Kara Sea, the Laptev Sea and East Siberian Sea (Figure 5.8a), which was less severer than in the modern Central Arctic Ocean and probably provide opportunity for the primary productivity (Figure 5.5).

5.5 Conclusions

Within our study, biomarker records going back in time to MIS 3, are presented from the north of Barents Sea across the Central Arctic to the southern Mendeleev Ridge. These data indicated that the sea-ice cover was more extensive during MIS 3 and MIS 2 than during the Holocene according to our biomarker data. During the last deglacial, the Arctic sea-ice cover was less than the modern sea-ice cover with open-ocean conditions in the marginal seas year around. IP_{25} was only present during Holocene in the high Arctic (>84°N).

For the LGM, our biomarker data suggest that the warm Atlantic water flowed into the Arctic along West Svalbard and continued eastwards along northern Barents Sea continental slope causing ice-free conditions. In contrast, the LGM Central Arctic and western Arctic was covered by thick permanent sea ice. The occurrence of warm Atlantic water advection events prior to or during the LGM provide the moisture to build up the ice sheets. Furthermore, our results also supported modeled LGM Arctic sea-ice conditions, which suggested the existence of the Transpolar Drift and summer open-water conditions in eastern Fram Strait.

Acknowledgements

The materials used for this study were collected during several expeditions. We thank the chief scientists and captains of the research vessels, as well as the crew members and the scientists on board for their contributions during all the cruises. We are grateful to W. Luttmer for technical support in the laboratory and to M. Stärz for providing original figures of modelled LGM Arctic sea-ice concentrations and sea-ice drift. Finical support by Alfred Wegener Institute (Bremerhaven) and China Scholarship Council is gratefully acknowledged.

6. Conclusion and outlook

6.1 Conclusion

Within this thesis, the novel ice proxy IP_{25} was used to reconstruct the spatial and temporal sea-ice variability in the Arctic Ocean and its marginal seas.

The application of IP_{25} in the surface sediments from the Kara and Laptev Sea was presented in Chapter 3. Based on the concentration of IP_{25} and open-water phytoplankton biomarkers, the complex sea-ice conditions in this area were indicated. The occasional occurrence of summer ice massif on the Laptev Sea continental shelf, for example, was reflected by high concentrations of IP_{25} and relatively low concentrations of phytoplankton biomarkers. The complete absence of IP_{25} in the river confirms an unfavourable riverine environment for IP_{25} production, although seasonal ice also occurs in the river. In this area, both IP_{25} and PIP_{25} do not show any clear correlations with satellite sea-ice data due to the complex environmental situation.

Surface sediment samples from the Central Arctic Ocean proper (>80°N latitude) and from the Chukchi Plateau/Basin were used for IP_{25} determination in Chapter 4. In addition, published data from other Arctic and sub-Arctic regions with new data included to these areas were added to generate an overview distribution map of IP_{25} across the major part of the Arctic Ocean. For the first time numerous surface sediment samples from the permanently ice-covered Central Arctic Ocean (>80°N) have been used to determine the distribution of IP_{25} and phytoplankton biomarkers. The sea-ice conditions vary significantly between different marginal seas, as reflected in the biomarker distribution maps. The PIP_{25} values obtained from this large data set show positive correlations with both spring and summer sea-ice concentrations obtained from satellite observation. When using PIP_{25} values for the reconstruction of sea-ice cover, the marine origin of brassicasterol has to be approved before using it as phytoplankton marker in the PIP_{25} approach as this sterol can be produced by the majority of diatoms. The similar distribution patterns of brassicasterol and dinosterol confirmed the marine origin of brassicasterol.

IP_{25} determination was performed on the sediment cores representing MIS3 to MIS1 and sediments of LGM time-slices across the Arctic Ocean to reconstruct the temporal sea-ice variability and the spatial sea-ice variability (LGM interval) in Chapter 5. The sea-ice cover was more extensive during MIS 3 and MIS 2 than during the Holocene according to the biomarker data. During the last deglacial, the Arctic sea-ice cover was less than the modern sea-ice cover with open-ocean conditions in the marginal seas year round. In the high Arctic (>85°N), IP_{25} was only present during the Holocene. The spatial biomarker distributions for the LGM interval suggest that warm Atlantic water flowed into the Arctic along West

Svalbard and continued eastwards along the northern continental slope of the Barents Sea between the Svalbard-Barents Sea Ice Sheet and the permanent Arctic ice cover during LGM summer. In contrast, the LGM high Arctic (>85°N) and western Arctic was covered by thick permanent sea ice.

6.2 Future perspectives

The biomarker data presented within this thesis provide information about the distribution of IP_{25} in surface sediments as well as in the sediments covering the LGM time-slice in the high Arctic proper. These data set extend the ground truth data of IP_{25} and confirm the feasibility of IP_{25} application for Arctic sea-ice reconstructions. As IP_{25} still is a new proxy, further work is required to solve the uncertainties discovered during this thesis.

Figure 6.1 Locations where IP_{25} has been studied in Arctic sediments. Core sites of palaeo (downcore) studies are indicated with red dots. White dots indicate sediment samples of LGM time-slice. Coloured boxes refer to regions where analyses of surface sediments have been carried out (modified from Belt and Müller, 2013).

First, the specific source of IP_{25} is still uncertain, although *Haslea* spp. is considered as the origin of IP_{25}. However, the laboratory culturing of individual *Haslea* spp. at low temperature has failed (Belt et al., 2007, 2013). To date, only a few studies of sea ice samples from the Arctic Canadian Archipelago and the Beaufort Sea provided information about the sea ice source of IP_{25} (Belt et al., 2007, 2013; Brown et al., 2011). Therefore, further field collection of sea ice cores is required for IP_{25} analysis and IP_{25} origin studies.

Furthermore, though the study of IP_{25} in Arctic surface sediments has spanned a large region including the high Arctic proper, there is still a major gap of information from the Canadian Basin and north of Greenland, where also the availability of downcore sediments is restricted (Figure 6.1). Further studies of sediment cores from the Bering Strait, the East Siberian Sea and the Laptev Sea can extend the knowledge about IP_{25} and its potential as sea ice proxy.

The quantitative application of IP_{25} in terms of the PIP_{25} index, however, still has some limitations. Thus, the further testing of PIP_{25} and the development of this hitherto only semiquantitative approach is needed to obtain a reliable proxy for the quantitative assessment of a palaeo sea ice cover.

6.3 Comparison of biomarker and modelled data

The modelled sea ice parameters and the biomarker-based estimate of sea ice coverage show a good correlation in surface sediments from the East Greenland and West Spitsbergen (Müller et al., 2011). Within this thesis, the biomarker data, both IP_{25} and phytoplankton biomarkers distributions in the surface sediments, are in agreement with modelled pan-Arctic primary production in sea ice and the upper 100 m of the ocean, respectively (Jin et al., 2012). These simulated mean open-ocean production and sea-ice algal production data are reliable because they are in the ranges of remote sensing-derived data and multi-observational estimates by in-situ measurements (Jin et al., 2012). Generally, modelled open-ocean and sea-ice production show low contents in the Central Arctic Ocean, while increase towards the marginal seas with an exception of the Barents Sea where no data are available for modelled ice algal production due to ice free condition (Figures 6.2).

In the future study, further modelled sea-ice parameters are required to compare with biomarker-based indices, which can provide comprehensive estimate of both spatial and temporal sea-ice variability. Combined with the numerical modeling parameters, the biomarker proxy can be developed as quantitative approach for sea-ice reconstruction.

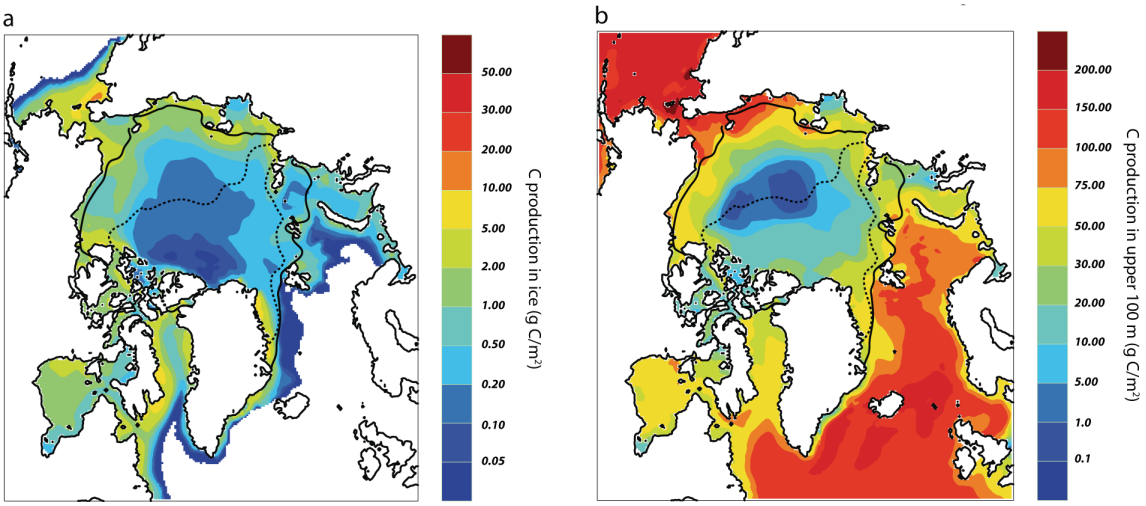

Figure 6.2 Modelled pan-Arctic annual primary production averaged over 1998–2007 in sea ice (a) and ocean upper 100 m (b) (Jin et al., 2011 supplemented). For explanation of black and dotted lines, see Figure 4.3.

References

Aagaard, K., Carmack, E.C., 1989. The role of sea ice and other fresh water in the Arctic circulation. Journal of Geophysical Research 94, 14485–14498.

Armand, L.K., Leventer, A., 2010. Palaeo sea ice distribution and reconstruction derived from the geological record. In: Thomas, D.N., Dieckmann, G.S. (Eds.), Sea Ice. Blackwell Publishing, Oxford, pp. 469–529.

Backman, J., Jakobsson, M., Løvlie, R., Polyak, L., Febo, L.A., 2004. Is the central Arctic Ocean a sediment starved basin? Quaternary Science Reviews 23, 1435–1454.

Barbara, L., Crosta, X., Massé, G., Ther, O., 2010. Deglacial environments in eastern Prydz Bay, East Antarctica. Quaternary Science Reviews 29, 2731–2740.

Bareiss, J., Görgen, K., 2005. Spatial and temporal variability of sea ice in the Laptev Sea: Analyses and review of satellite passive-microwave data and model results, 1979 to 2002. Global and Planetary Change 48, 28–54.

Barrick, R.C., Hedges, J.I., Peterson, M.L., 1980. Hydrocarbon geochemistry of the Puget Sound region—I. Sedimentary acyclic hydrocarbons. Geochimica et Cosmochimica Acta 44**,** 1349–1362.

Bauch, H.A., Erlenkeuser, H., Bauch, D., Mueller-Lupp, T., Taldenkova, E., 2004. Stable oxygen and carbon isotopes in modern benthic foraminifera from the Laptev Sea shelf: implications for reconstructing proglacial and profluvial environments in the Arctic. Marine Micropaleontology 51, 285–300.

Bazhenova, E., 2012. Reconstruction of late Quaternary sedimentary environments at the southern Mendeleev Ridge (Arctic Ocean). PhD thesis.

Belt, S.T., Allard, W.G., Massé, G., Robert, J.-M., Rowland, S.J., 2000. Highly branched isoprenoids (HBIs): identification of the most common and abundant sedimentary isomers. Geochimica et Cosmochimica Acta 64, 3839–3851.

Belt, S.T., Massé, G., Allard, W.G., Robert, J.-M., Rowland, S.J., 2001a. Identification of a C_{25} highly branched isoprenoid triene in the freshwater diatom *Navicula* sclesvicensis. Organic Geochemistry 32, 1169–1172.

Belt, S.T., Massé, G., Allard, W.G., Robert, J.-M., Rowland, S.J., 2001b. C_{25} highly branched isoprenoid alkenes in planktonic diatoms of the *Pleurosigma* genus. Organic Geochemistry 32, 1271-1275.

Belt, S.T., Massé, G., Rowland, S.J., Poulin, M., Michel, C., LeBlanc, B., 2007. A novel chemical fossil of palaeo sea ice: IP25, Organic Geochemistry 38, 16–27.

Belt, S.T., Massé, G.,Vare, L.L., Rowland, S.J., Poulin, M., Sicre, M.-A., Sampei, M., Fortier, L., 2008. Distinctive ^{13}C isotopic signature distinguishes a novel sea ice biomarker in Arctic sediments and sediment traps. Marine Chemistry 112(3–4), 158–167.

Belt, S.T., Vare, L.L., Massé, G., Manners, H.R., Price, J.C., MacLachlan, S.E., Andrews, J.T., Schmidt, S., 2010. Striking similarities in temporal changes to spring sea ice occurrence across the central Canadian Arctic Archipelago over the last 7000 years, Quaternary Science Reviews 29, 3489–3504.

Belt, S.T., Brown, T.A., Navarro Rodriguez, A., Cabedo Sanz, P., Tonkin, A., Ingle, R., 2012. A reproducible method for the extraction, identification and quantification of the Arctic sea ice proxy IP_{25} from marine sediments. Analytical Methods 4, 705–713.

Belt, S.T., Brown, T.A., Ringrose, A.E., Cabedo-Sanz, P., Mundy, C.J., Gosselin, M., Poulin, M., 2013. Quantitative measurement of the sea ice diatom biomarker IP_{25} and sterols in Arctic sea ice and underlying sediments: Further considerations for palaeo sea ice reconstruction. Organic Geochemistry 62, 33–45.

Belt, S.T., Müller, J., 2013. The Arctic sea ice biomarker IP_{25}: a review of current understanding, recommendations for future research and applications in palaeo sea ice reconstructions. Quaternary Science Reviews 79, 9–25.

Belt, S.T., Brown T.A., Ampel, L., Cabedo-Sanz, P., Fahl, K., Kocis, J. J., Massé, G., Navarro-Rodriguez, A., Ruan, J., Xu, Y., 2014. An inter-laboratory investigation of the Arctic sea ice biomarker proxy IP_{25} in marine sediments: key outcomes and recommendations. Climate of the Past 10, 155–166.

Birgel D., Stein R. and Hefter J., 2004. Aliphatic lipids in recent sediments of the Fram Strait/Yermak Plateau (Arctic Ocean): composition, sources and transport processes. Marine Chemistry 88 (3–4), 127–160.

Boetius, A., Albrecht, S., Bakker, K., Bienhold, C., Felden, J., Fernández-Méndez, M., Hendricks, S., Katlein, C., Lalande, C., Krumpen, T., Nicolaus, M., Peeken, I., Rabe, B., Rogacheva, A., Rybakova, E., Somavilla, R., Wenzhöfer, F., RV Polarstern ARK 27-3-S.S. Party, 2013. Export of Algal Biomass from the Melting Arctic Sea Ice, Science 339, 1430–1432.

Boon, J.J., Rijpstra, W.I.C., Lange, F.De., Leeuw, J.W.De., Yoshioka, M., Shimizu, Y., 1979. Black Sea sterol - a molecular fossil for dinoflagellate blooms, Nature 277, 125–127.

Bradley, R. S., England, J. H., 2008. The Younger Dryas and the sea of ancient ice. Quaternary Research 70, 1–10.

Brown, T., Belt, S.T., Philippe, B., Mundy, C., Massé, G., Poulin, M., Gosselin M., 2011. Temporal and vertical variations of lipid biomarkers during a bottom ice diatom bloom in the Canadian Beaufort Sea: further evidence for the use of the IP_{25} biomarker as a proxy for spring Arctic sea ice. Polar Biology 34, 1857–1868.

Cabedo-Sanz, P., Belt, S.T., Knies, J.K., 2013. Identification of contrasting seasonal sea ice conditions during the Younger Dryas. Quaternary Science Reviews 79, 74–86.

Cavalieri, D., Parkinson C., Gloersen P., and Zwally H. J., 1996. Sea ice concentrations from Nimbus-7 SMMR and DMSP SSM/I-SSMIS passive microwave data. National Snow and Ice Data Center (Digital media, updated yearly).

CLIMAP Project Members, 1976. The surface of the Ice-Age Earth. Science 191, 1131–1137.

CLIMAP, 1981. Seasonal Reconstruction of the Earth's Surface at the Last Glacial Maximum. Geological Society of America Map and Chart Series MC-36.

Comiso, J.C., Parkinson, C.L., 2004. Satellite-Observed Changes in the Arctic. Physics Today 57, 38–44.

Comiso, J.C., 2010. Variability and trends of the global sea ice cover. In: Thomas, D.N., Dieckmann, G.S. (Eds.), Sea Ice. Blackwell Publishing, Oxford, pp. 205–246.

Cremer, H., 1999. Distribution patterns of diatom surface sediment assemblages in the Laptev Sea (Arctic Ocean). Marine Micropaleontology 38, 39–67.

Cronin, T.M., Whatley, R., Wood, A., Tsukagoshi, A., Ikeya, N., Brouwers, E.M., Briggs Jr., W.M., 1993. Microfaunal evidence for elevated Pliocene temperatures in the Arctic Ocean. Paleoceanography 8, 161–173.

Cronin, T.M., Gemery, L., Briggs Jr., W.M., Jakobsson, M., Polyak, L., Brouwers, E.M., 2010. Quaternary sea-ice history in the Arctic Ocean based on a new Ostracode sea-ice proxy. Quaternary Science Reviews 29 (25–26), 3415–3429.

Cronin, T.M., Dwyer, G.S., Farmer, J., Bauch, H.A., Spielhagen, R.F., Jakobsson, M., Nilsson, J., Briggs, W.M., Stepanova, A., 2012. Deep Arctic Ocean warming during the last glacial cycle. Nature Geosci 5, 631–634.

Darby, D. A., Bischof, J. F., Jones, G. A., 1997. Radiocarbon chronology of depositional regimes in the western Arctic Ocean, Deep Sea Res., Part II, 44 (8), 1745–1757.

Darby, D.A., Bischof, J.F., 2004. A Holocene record of changing Arctic Ocean ice drift, analogous to the effects of the Arctic Oscillation. Paleoceanography 19 (PA1027). doi:10.1029/2003PA000961 9 pp.

Darby, D.A., 2008. Arctic perennial ice cover over the last 14 million years. Palaeoceanography 23, PA1S07.

Denis, D., Crosta, X., Barbara, L., Massé, G., Renssen, H., Ther, O., Giraudeau, J., 2010. Sea ice and wind variability during the Holocene in East Antarctica: insight on middle-high latitude coupling. Quaternary Science Reviews 29, 3709–3719.

Dethleff, D., Loewe, P., Kleine, E., 1998. The Laptev Sea flaw lead-detailed investigation on ice formation and export during 1991/1992 winter season. Cold Regions Science and Technology 27, 225–243.

de Vernal, A., Eynaud, F., Henry, M., Hillaire-Marcel, C., Londeix, L., Mangin, S., Matthiessen, J., Marret, F., Radi, T., Rochon, A., Solignac, S., Turon, J.L., 2005. Reconstruction of sea-surface conditions at middle to high latitudes of the Northern Hemisphere during the Last Glacial Maximum (LGM) based on dinoflagellate cyst assemblages. Quaternary Science Reviews 24, 897–924.

Dieckmann, G.S., Hellmer, H.H., 2010. The importance of sea ice: an overview. In: Thomas, D.N., Dieckmann, G.S. (Eds.), Sea Ice. Blackwell Publishing, Oxford, pp. 1–22.

Divine, D.V., Korsnes, R., Makshtas, A.P., 2004. Temporal and spatial variation of shore-fast ice in the Kara Sea. Continental Shelf Research 24, 1717–1736.

Dyke, A.S., Andrews, J.T., Clark, P.U., England, J.H., Miller, G.H., Shaw, J., Veillette, J.J., 2002. The Laurentide and Innuitian ice sheets during the Last Glacial Maximum. Quaternary Science Reviews 21, 9–31.

Eicken, H., Reimnitz, E., Alexandrov, V., Martin, T., Kassens, H., Viehoff, T., 1997. Sea-ice processes in the Laptev Sea and their importance for sediment export. Continental Shelf Research 17, 205–233.

Eldrett, J.S., Harding, I.C., Wilson, P.A., Butler, E., Roberts, A.P., 2007. Continental ice in Greenland during the Eocene and Oligocene. Nature 446, 176–179.

Elias, S.A., Brigham-Grette, J., 2013. GLACIATIONS | Late Pleistocene Glacial Events in Beringia. Encyclopedia of Quaternary Science (Second Edition). Elsevier, Amsterdam. pp. 191–201.

Fahl, K., Stein, R., 1997. Modern organic-carbon-deposition in the Laptev Sea and the adjacent continental slope: Surface-water productivity vs. terrigenous supply. Org. Geochem. 26 (5/6), 379–390.

Fahl, K., Stein, R., 1999. Biomarkers as organic-carbon-source and environmental indicators in the Late Quaternary Arctic Ocean: problems and perspectives. Marine Chemistry 63, 293–309.

Fahl, K., Cremer, H., Erlenkeuser, H., Hansserr, H., Hölemann, J., Kassens, H., Knickmeier, K., Kosobokova, K., Pirrung, M.K., Lindemann, F., Markhaseva, E., Lischka, S., Petryashov, V., Piepenburg, D., Schmid, M., Spindler, M., Stein, R., Tuschling, K., 2001. Sources and pathways of organic carbon in the modern Laptev Sea (Arctic

Ocean): implications from Biological, Geochemical and Geological Data. Polarforschung 69 (1999), 193–205.

Fahl, K., Stein, R., Gaye-Haake, B., Gebhardt, C., Kodina, L.A., Unger, D., Ittekkot, V., 2003. Biomarkers in surface sediments from Ob and Yenisei estuaries and southern Kara Sea: Evidence for particulate organic carbon sources, pathways, and degradation. In: Stein, R., Fahl, K., Fütterer, D.K., Galimov, E.M., Stepanets, O.V. (Eds), Siberian River run-off in the Kara Sea: Characterisation, Quantification, variability, and environmental significance, Proceeding of Marine Science 6. Elsevier, Amsterdam, 329–348.

Fahl, K., Stein, R., 2007. Biomarker records, organic carbon accumulation, and river discharge in the Holocene southern Kara Sea (Arctic Ocean). Geo-Marine Letters 27, 13–25.

Fahl, K., Stein, R., 2012. Modern seasonal variability and deglacial/Holocene change of central Arctic Ocean sea-ice cover: New insights from biomarker proxy records. Earth and Planetary Science Letter 351–352, 123–133.

Fahrbach, E., Meincke, J., Østerhus, S., Rohardt, G., Schauer, U., Tverberg, V., Verduin, J., 2001. Direct measurements of volume transports through Fram Strait. Polar Research 20, 217–224.

Fernandes, M.B., Sicre, M.A., 2000. The importance of terrestrial organic carbon inputs on Kara Sea shelves as revealed by n-alkanes, OC and $\delta^{13}C$ values. Organic Geochemistry 31, 363–374.

Francis, J.A., Hunter, E., Key, J.R., Wang, X.J., 2005. Clues to variability in Arctic minimum sea ice extent. Geophysical Research Letters, L21501.

Fütterer, D.K., 1992. ARCTIC '91: the expedition ARK-VIII/3 of RV "Polarstern" in 1991, Reports on Polar Research. Alfred Wegener Institute for Polar and Marine Research, Bremerhaven.

Fütterer, D.K., 1994. The Expedition ARCTIC 93 Leg ARK-IX/4 of RV Polarstern 1993. Reports on Polar Research 149, 244 pp.

Gaye, B., Fahl, K., Kodina, L.A., Lahajnar, N., Nagel, B., Unger, D., Gebhardt, A.C., 2007. Particulate matter fluxes in the southern and central Kara Sea compared to sediments: Bulk fluxes, amino acids, stable carbon and nitrogen isotopes, sterols and fatty acids. Continental Shelf Research 27, 2570–2594.

Gearing, P., Gearing, J.N., Lytle, T.F., and Lytle, J.S., 1976. Hydrocarbons in 60 northeast Gulf of Mexico shelf sediments: A preliminary survey. Geochimica et Cosmochimica Acta 40**,** 1005–1017.

Gosselin, M., Levasseur, M., Wheeler, P.A., Horner, R.A., Booth, B.C., 1997. New measurements of phytoplankton and ice algal production in the Arctic Ocean. Deep Sea Research II 44, 1623–1644.

Gradinger, R., 2009. Sea-ice algae: Major contributors to primary production and algal biomass in the Chukchi and Beaufort Seas during May/June 2002. Deep Sea Research Part II: Topical Studies in Oceanography 56 (17), 1201–1212.

Grosswald, M., Hughes, T., 2002. The Russian component of an Arctic ice sheet during the last glacial maximum. Quaternary Science Reviews 21,121–146.

Grosswald, M., Hughes, T., 2008. The case for an ice shelf in the pleistocene Arctic Ocean. Polar Geography 1, 69–98.

Haas, C., 2010. Dynamics versus thermodynamics: the sea ice thickness distribution. In: Thomas, D.N., Dieckmann, G.S. (Eds.), Sea Ice. Blackwell Publishing, Oxford, pp. 113–152.

Hebbeln, D., Berner, H., 1993. Surface sediment distribution in the Fram Strait. Deep Sea Research I: Oceanographic Research Paper 40 (9), 1731–1745.

Hebbeln, D., Dokken, T., Andersen, E.S., Hald, M., Elverhøi, A., 1994. Moisture supply for northern ice-sheet growth during the Last Glacial Maximum. Nature 370, 357–359.

Holland, M.M., Finnis, J., Serreze, M.C., 2006. Simulated Arctic Ocean freshwater budgets in the 20th and 21st centuries. Journal of Climate 19, 6221–6242.

Holland, M.M., Serreze, M.C., Stroeve, J., 2009. The sea ice mass budget of the Arctic and its future change as simulated by coupled climate models. Climate Dynamics 34, 185–200.

Huang, W.Y., Meinschein, W. G., 1976. Sterols as source indicators of organic material in sediments. Geochimica et Cosmochimica Acta 40, 323–330.

Hughes, T.J., Denton, G.H., Grosswald, M.G., 1977. Was there a late-Würm Arctic ice sheet? Nature 266, 596–602.

Ingólfsson, Ó., Landvik, J.Y., 2013. The Svalbard-Barents Sea ice-sheet-Historical, current and future perspectives. Quaternary Science Reviews 64, 33–60.

Jakobsson, M., 2002. Hypsometry and volume of the Arctic Ocean and its constituent seas. Geochemistry, Geophysics, Geosystems 3, 1-18.

Jakobsson, M., Backman, J., Rudels, B., Nycander, J., Frank, M., Mayer, L., Jokat, W., Sangiorgi, F., O'Regan, M., Brinkhuis, H., King, J., Moran, K., 2007. The Early Miocene onset of a ventilated circulation regime in the Arctic Ocean. Nature 447, 986–990.

Jakobsson, M., Andreassen, K., Bjarnadottir, L.R., Dove, D., Dowdeswell, J.A., England, J.H., Funder, S., Hogan, K., Ingolfsson, O., Jennings, A., Krog Larsen, N., Kirchner, N., Landvik, J.Y., Mayer, L., Mikkelsen, N., Möller, P., Niessen, F., Nilsson, J., O'Regan, M., Polyak, L., Norgaard-Pedersen, N., Stein, R., Arctic Ocean glacial history. Quaternary Science Reviews 92, 40–67.

Jakobsson, M., Macnab, R., Mayer, M., Anderson, R., Edwards, M., Hatzky, J., Schenke, H.-W., Johnson, P., 2008. An improved bathymetric portrayal of the Arctic Ocean: implications for ocean modeling and geological, geophysical and oceanographic analyses. Geophysical Research Letters 35, L07602.

Jang, K., Han, Y., Huh, Y., Nam, S.-II., Stein, R., Mackensen, A., Matthiessen, J., 2013. Glacial freshwater discharge events recorded by authigenic neodymium isotopes in sediments from the Mendeleev Ridge, western Arctic Ocean. Earth and Planetary Science Letters 369, 148-157.

Jansen, E., Fronval, T., Rack, F. and Channell, J.E.T., 2000. Pliocene-Pleistocene Ice Rafting History and Cyclicity in the Nordic Seas During the Last 3.5 Myr. Paleoceanography, 15(6): 709–721.

Jin, M., Deal, C., Lee, S.H., Elliott, S., Hunke, E., Maltrud, M., Jeffery, N., 2012. Investigation of Arctic sea ice and ocean primary production for the period 1992–2007 using a 3-D global ice–ocean ecosystem model. Deep Sea Research Part II: Topical Studies in Oceanography 81, 28–35.

Johannessen, O.M., Miles, M., Bjorgo, E., 1995. The Arctic's shrinking sea ice. Nature 376, 126–127.

Johannessen, O.M., Shalina, E.V., Miles, M.W., 1999. Satellite Evidence for an Arctic Sea Ice Cover in Transformation. Science 286, 1937–1939.

Johns, L., Wraige, E.J., Belt, S.T., Lewis, C.A., Masse, G., Robert, J.M., Rowland, S.J., 1999. Identification of a C-25 highly branched isoprenoid (HBI) diene in Antarctic sediments, Antarctic sea-ice diatoms and cultured diatoms. Organic Geochemistry 30(11), 1471–1475.

Jokat, W., 2009. The expedition of the research vessel "Polarstern" to the Arctic in 2008 (ARK-XXIII/3). Reports on Polar and Marine Research 597, 266 pp.

Jones, E.P., 2001. Circulation in the Arctic Ocean. Polar Research 20, 139–146.

Jones, E.P., Swift, J.H., Anderson, L.G., Lipizer, M., Civitarese, G., Falkner, K.K., Kattner, G., McLaughlin, F., 2003. Tracing Pacific water in the North Atlantic Ocean. Journal of Geophysical Research 108, 3116.

Karklin, V.P., Kalerin, I.D., Gorbunov, Y.A., Losev, S.M., 2007. Eastern Part of the Northern Sea Route. In: Johannessen, O.M., Alexandrov, V.Yu., Frolov, I.Ye., Sandven, S., Pettersson, L.H., Bobylev, L.P., Kloster, K., Smirnov, V.G., Mironov, Ye.U., Babich, N.G. (Eds), Remote sensing of Sea Ice in the Northern Sea Route: studies and applications. Springer, Berlin and Praxis Publishing, Chichester.

Kassens, H., Karpiy, V.Y., 1994. Russian-German Cooperation: The Transdrift I Expedition to the Laptev Sea. Rep. Pol. Res, 151-168.

Kaufman, D.S., Schneider, D.P., McKay, N.P., Ammann, C.M., Bradley, R.S., Briffa, K.R., Miller, G.H., Otto-Bliesner, B.L., Overpeck, J.T., Vinther, B.M., Arctic Lakes 2k Project Members, 2009. Recent warming reverses long-term Arctic cooling. Science 325, 1236–1239.

Kern, S., 2008. Polynya Area in the Kara Sea, Arctic, Obtained With Microwave Radiometry for 1979-2003. Geoscience and Remote Sensing Letters, IEEE 5, 171–175.

Kerr, R.A., 2007. Is battered Arctic sea ice down for the count? . Science 318: 33-34.

Killops, S. and Killops, V., 2005. Introduction to Organic Geochemistry, 2nd edition. Blackwell Publishing, Malden, Oxford, Carlton.

Knies, J., Stein, R., 1998. New aspects of organic carbon deposition and its paleoceanographic implications along the northern Barents Sea margin during the last 30,000 years. Paleoceanography 13, 384–394.

Knies, J., C. Vogt, and R. Stein, 1999. Late Quaternary growth and decay of the Svalbard/Barents Sea ice sheet and paleoceanographic evolution in the adjacent Arctic Ocean. Geo Mar. Lett. 18 (3), 195– 202.

Knies, J., 1999. Late Quaternary paleoenvironment along the northern Barents and Kara seas continental margin. A multi parameter analysis. Reports on Polar Research 304, 159 pp.

Knies, J., Nowaczyk, N., Müller, C., Vogt, C., Stein, R., 2000. A multiproxy approach to reconstruct the environmental changes along the Eurasian continental margin over the last 150,000 years. Mar. Geol. 163, 317–344.

Knies, J., Kleiber, H.-P., Matthiessen, J., Müller, C., Nowaczyk, N., 2001. Marine ice-rafted debris records constrain maximum extent of Saalian and Weichselian ice-sheets along the northern Eurasian margin. Glob. Planet. Change 31, 45–64.

Knies, J., Gaina, C., 2008. Middle Miocene ice sheet expansion in the Arctic – views from the Barents Sea. Geochemistry, Geophysics, Geosystems 9, Q02015.

Knies, J., Matthiessen, J., Vogt, C., Laberg, J.S., Hjelstuen, B.O., Smelror, M., Larsen, E., Andreassen, K., Eidvin, T., Vorren, T.O., 2009. The Plio–Pleistocene glaciation of

the Barents Sea–Svalbard region: a new model based on revised chronostratigraphy. Quatern. Sci. Rev. 28, 812–829.

Krishnamurthy, R.V., Machavaram, M., Baskaran, M., Brooks, J.M., Champs, M. A., 2001. Organic carbon flow in the Ob, Yenisei rivers and Kara Sea of the Arctic region. Marine Pollution Bulletin 42, 726–732.

Krylov, A.A., Andreeva, I.A., Vogt, C., Backman, J., Krupskaya, V.V., Grikurov, G.E., Moran, K., Shoji, H., 2008. A shift in heavy and clay mineral provenance indicates a middle Miocene onset of a perennial sea-ice cover in the Arctic Ocean. Paleoceanography 23, PA1S06.

Legendre, L., Ackley, S., Dieckmann, G., Gulliksen, B., Horner, R., Hoshiai, T., Melnikov, I., Reeburgh, W., Spindler, M., Sullivan, C., 1992. Ecology of sea ice biota. Polar Biology 12, 429–444.

Lisitsyn, A.P., Vinogradov, M.E., 1995. International high-latitude expedition in the Kara Sea (the 49th cruise of the R/V Dmitriy Mendeleev). Oceanology of the Russian Academy of Sciences 34, 583–590.

Lisitzin, A.P., 1995. The marginal filter of the ocean. Oceanology 34(5), 671–682.

Liu, J., Song, M., Horton, R.M., Hu, Y., 2013. Reducing spread in climate model projections of a September ice-free Arctic. Proceedings of the National Academy of Sciences 110, 12571-12576.

Mackensen, A., Sejrup, H.P., Jansen, E., 1985. The distribution of living benthic foraminifera on the continental slope and rise off southwest Norway. Marine Micropaleontology 9, 275–306.

Mangerud, J., Astakhov, V., Svendsen, J.-I., 2002. The extent of the Barents-Kara ice sheet during the Last Glacial Maximum. Quaternary Science Reviews 21, 111–119.

Massé, G., Belt, S.T., Rowland, S.J., Rohmer, M., 2004. Isoprenoid biosynthesis in the diatoms Rhizosolenia setigera (Brightwell) and Haslea ostrearia (Simonsen). Proceedings of the National Academy of Sciences of the United States of America 101, 4413–4418.

Massé, G., Rowland, S.J., Sicre, M.A., Jacob, J., Jansen, E., Belt, S.T., 2008. Abrupt climate changes for Iceland during the last millennium: evidence from high resolution sea ice reconstructions. Earth and Planetary Science Letters 269, 565–569.

Massé, G., Belt, S.T., Crosta, X., Schmidt, S., Snape, I., Thomas, D.N., Rowland, S.J., 2011. Highly branched isoprenoids as proxies for variable sea ice conditions in the Southern Ocean. Antarctic Science 23(5), 487–498.

Martin, S., Cavalieri, D.J., 1989. Contributions of the Siberian Shelf Polynyas to the Arctic Ocean Intermediate and Deep Water. J. Geophys. Res. 94, 12725–12738.

Matthiessen, J., Knies, J., Vogt, C., Stein, R., 2009. Pliocene paleoceanography of the Arctic Ocean and subarctic seas. Phil. Trans. R. Soc. 367, 21–48.

Meese, D.A., Reimnitz, E., Tucker III, W.B., Gow, A.J., Bischof, J., Darby, D., 1997. Evidence for radionuclide transport by sea ice. Science of the Total Environment 202, 267–278.

Mercer, J.H., 1970. A former ice sheet in the Arctic Ocean? Palaeogeogr. Palaeoclimatol. Palaeoecol. 8, 19–27.

Mironov, Ye.U., Gudkovich, Z.M., Karklin, V.P., 2007a. The Arctic Eurasian shelf seas. In: Johannessen, O.M., Alexandrov, V.Yu., Frolov, I.Ye., Sandven, S., Pettersson, L.H., Bobylev, L.P., Kloster, K., Smirnov, V.G., Mironov, Ye.U., Babich, N.G. (Eds),

Remote sensing of Sea Ice in the Northern Sea Route: studies and applications. Springer, Berlin and Praxis Publishing, Chichester.

Mironov, Ye.U., Frolov, I.Ye., Spichkin, V.A., Karklin, V.P., Kalerin, I.D., Gorbunov, Y.A., Losev, S.M., 2007b. Western Part of the Northern Sea Route. In: Johannessen, O.M., Alexandrov, V.Yu., Frolov, I.Ye., Sandven, S., Pettersson, L.H., Bobylev, L.P., Kloster, K., Smirnov, V.G., Mironov, Ye.U., Babich, N.G. (Eds), Remote sensing of Sea Ice in the Northern Sea Route: studies and applications. Springer, Berlin and Praxis Publishing, Chichester.

Moran, K., Backman, J., Brinkhuis, H., Clemens, S.C., Cronin, T., Dickens, G.R., Eynaud, F., Gattacceca, J., Jakobsson, M., Jordan, R.W., Kaminski, M., King, J., Koç, N., Krylov, A., Martinez, N., Matthiessen, J., McInroy, D., Moore, T.C., Onodera, J., O'Regan, A.M., Pa¨ like, H., Rea, B., Rio, D., Sakamoto, T., Smith, D.C., Stein, R., St. John, K., Suto, I., Suzuki, N., Takahashi, K., Watanabe, M., Yamamoto, M., Farrell, J., Frank, M., Kubik, P., Jokat, W., Kristoffersen, Y., 2006. The Cenozoic palaeoenvironment of the Arctic Ocean. Nature 441, 601–605.

Müller, C., Stein, R., 2000. Variability of fluvial sediment supply to the Laptev Sea continental margin during Late Weichselian to Holocene times: Implications from clay-mineral records. In: Stein, R (ed.), International Journal of Earth Sciences Special Issue: Circum Arctic River Discharge and its Geological Record, Springer.

Müller, J., Massé, G., Stein, R., Belt, S.T., 2009. Variability of sea-ice conditions in the Fram Strait over the past 30,000 years. Nature Geoscience 2, 772–776.

Müller, J., Wagner, A., Fahl, K., Stein, R., Prange, M., Lohmann, G., 2011. Towards quantitative sea ice reconstructions in the northern North Atlantic: A combined biomarker and numerical modelling approach. Earth and Planetary Science Letters 306, 137–148.

Müller, J.,Werner, K., Stein, R., Fahl, K., Moros, M., Jansen, E., 2012. Holocene cooling culminates in sea ice oscillations in Fram Strait. Quaternary Science Reviews 47, 1–14.

Nam S-I, Stein, R., Grobe, H., Hubberten, H., 1995. Late Quarternary glacial–interglacial changes in sediment composition at the East Greenland continental margin and their paleoceanographic implications. Marine Geology 122, 243–262.

Navarro-Rodriguez, A., Belt, S.T., Knies, J., Brown, T.A., 2013. Mapping recent sea ice conditions in the Barents Sea using the proxy biomarker IP_{25}: implications for palaeo sea ice reconstructions. Quaternary Science Reviews 79, 26–39.

Nichols, P.D., Volkman, J.K., Palmisano, A.C., Smith, G.A., White, D.C., 1988. Occurrence of an isoprenoid C25 diunsaturated alkene and high neutral lipid content in Antarctic seaice diatom communities. Journal of Phycology 24, 90–96.

Nicolaus, M., Katlein, C., Maslanik, J. A., Hendricks, S., 2012. Changes in Arctic sea ice result in increasing light transmittance and absorption. Geophys. Res. Lett. 39, L24501.

Niemi, A., Michel, C., Hille, K., Poulin, M., 2011. Protist assemblages in winter sea ice: setting the stage for the spring ice algal bloom. Pol. Bio. 34, 1803–1817.

Nørgaard-Pedersen, N., Spielhagen, R.F., Thiede, J., Kassens, H., 1998. Central Arctic surface ocean environment during the past 80,000 years. Paleoceanography 13, 193–204.

Nørgaard-Pedersen, N., Spielhagen, R.F., Erlenkeuser, H., Grootes, P.M., Heinemeier, J., Knies, J., 2003. The Arctic Ocean during the Last Glacial Maximum: Atlantic and

Polar domains of surface water mass distribution and ice cover. Paleoceanography 18 (3), 1063–1063.

Nørgaard-Pedersen, N., Mikkelsen, N., Lassen, S.J., Kristoffersen, Y., Sheldon, E., 2007. Arctic Ocean sediment cores off northern Greenland reveal reduced sea ice concentrations during the last interglacial period. Paleoceanography 22, PA1218.

Nürnberg, D., Wollenburg, I., Dethleff, D., Eicken, H., Kassens, H., Letzig, T., Reimnitz, E., Thiede, J., 1994. Sediments in Arctic sea ice: Implications for entrainment transport and release. Marine Geology 119, 185–214.

Ólason, E.Ö., Harms, I., 2010. Polynyas in a dynamic-thermodynamic sea-ice model. The Cryosphere 4, 147–160.

Parkinson, C.L., Cavalieri, D.J., Gloersen, P., Zwally, H.J., Comiso, J.C., 1999. Arctic sea ice extents, areas, and trends, 1978–1996. Journal of Geophysical Research 104, 20837–20856.

Perovich, D.K., Richter-Menge, J.A., Jones, K.F., Light, B., 2008. Sunlight, water, and ice: Extreme Arctic sea ice melt during the summer of 2007. Geophysical Research Letters 35, L11501.

Pesant, S., Legendre, L., Gosselin, M., Smith, R. E. H., Kattner, G., Ramseier, R., 1996. Size-differential regimes of phytoplankton production in the Northeast Water Polynya (77°–81° N). Marine Ecology Progress Series 142, 75–86.

Peterson, B.J., Holmes, R.M., McClelland, J.W., Vörösmarty, C.J., Lammers, R.B., Shiklomanov, A.I., Shiklomanov, I.A., Rahmstorf, S., 2002. Increasing River Discharge to the Arctic Ocean. Science 298, 2171–2173.

Peterson, B.J., McClelland, J., Curry, R., Holmes, R.M., Walsh, J.E., Aagaard, K., 2006. Trajectory Shifts in the Arctic and Subarctic Freshwater Cycle. Science 313, 1061–1066.

Petrich , C., Eicken, H., 2010. Growth, Structure and properties of sea ice. In: Thomas, D.N., Dieckmann, G.S. (Eds.), Sea Ice. Blackwell Publishing, Oxford, pp. 23–78.

Pfirman, S.L., Kogeler, J., Anselme, B., 1995. Coastal environments of the western Kara and eastern Barents Seas. Deep Sea Research Part II: Topical Studies in Oceanography 42, 1391–1412.

Pfirman, S.L., Kögeler, J.W., Rigor, I., 1997. Potential for rapid transport of contaminants from the Kara Sea. Science of The Total Environment 202, 111–122.

Pflaumann, U., Sarnthein, M., Chapman, M., d'Abreu, L., Funnell, B., Huels, M., Kiefer, T., Maslin, M., Schulz, H., Swallow, J., van Kreveld, S., Vautravers, M., Vogelsang, E., Weinelt, M., 2003. Glacial North Atlantic: sea-surface conditions reconstructed by GLAMAP 2000. Paleoceanography 3, 1065.

Poirier, A., Hillaire-Marcel, C., 2011. Improved Os-isotope stratigraphy of the Arctic Ocean. Geophysical Research Letters 38, L14607.

Poirier, R.K., Cronin, T.M., Briggs Jr., W.M., Lockwood, R., 2012. Central Arctic paleoceanography for the last 50 kyr based on ostracode faunal assemblages. Marine Micropaleontology 88–89, 65–76.

Polyak, L., Curry, W.B., Darby, D.A., Bischof, J., Cronin, T.M., 2004. Contrasting glacial/interglacial regimes in the western Arctic Ocean as exemplified by a sedimentary record from the Mendeleev Ridge. Palaeogeogr., Palaeoclimatol., Palaeoecol. 1–2, 73–93.

Polyak, L., Darby, D.A., Bischof, J.F., Jakobsson, M., 2007. Stratigraphic constraints on late Pleistocene glacial erosion and deglaciation of the Chukchi margin, Arctic Ocean. Quat. Res. 2, 234–245.

Polyak, L., Niessen, F., Gataullin, V., Gainanov, V., 2008. The eastern extent of the Barents–Kara ice sheet during the Last Glacial Maximum based on seismic-reflection data from the eastern Kara Sea. Polar Research 27, 162–174.

Polyak, L., Alley, R.B., Andrews, J.T., Brigham-Grette, J., Cronin, T.M., Darby, D.A., Dyke, A.S., Fitzpatrick, J.J., Funder, S., Holland, M., Jennings, A.E., Miller, G.H., O'Regan, M., Savelle, J., Serreze, M., St. John, K., White, J.W.C., Wolff, E., 2010. History of sea ice in the Arctic. Quatern. Sci. Rev. 29, 1757–1778.

Polyakov, I.V., Alekseev, G.V., Bekryaev, R.V., Bhatt, U.S., Colony, R., Johnson, M.A., Karklin, V.P., Walsh, D., Yulin, A.V., 2003. Long-Term Ice Variability in Arctic Marginal Seas. Journal of Climate 16, 2078–2085.

Polyakova, Ye.I., 2003. Diatom assemblages in surface sediments of the Kara Sea (Siberian Arctic) and their relationship to oceanological conditions. In: Stein, R., Fahl, K., Fütterer, D.K., Galimov, E.M., Stepanets, O.V. (Eds), Siberian River run-off in the Kara Sea: Characterisation, Quantification, variability, and environmental significance. Proceeding of Marine Science 6. Elsevier, Amsterdam, pp. 401–432.

Polyakova, Ye.I., Stein, R., 2004. Holocene paleoenvironmental implications of diatom and organic carbon records from the southeastern Kara Sea (Siberian Margin). Quaternary Research 62, 256–266.

Rachold, V., Hubberten, H.-W., 1999. Carbon isotope composition of particulate organic material in East Siberian rivers. In: Kassens, H., Bauch, H., Dmitrenko, I., Eicken, H., Hubberten, H.W., Melles, M., Thiede, J., Timokhov, L. (Eds), Land-ocean systems in the Siberian: Dynamics and history. Springer, Berlin, pp. 223–238.

Rachor, E., 1997. Scientific Cruise Report of the Arctic Expedition ARK-XI/1 of the RV Polarstern in 1995 (German-Russian Project LADI: Laptev Sea - Arctic Deep Basin Interrelations), Reports on Polar Research. Alfred Wegener Institute, Helmholtz Center for Polar and Marine Research, Bremerhaven. 226, 330 pp.

Rayner, N.A., Parker, D.E., Horton, E.B., Folland, C.K., Alexander, L.V., Rowell, D.P., Kent, E.C., Kaplan, A., 2003. Global analyses of sea surface temperature, sea ice, and night marine air temperature since the late nineteenth century. J. Geophys. Res. 108, 4407.

Rivera, J., Karabanov, E.B., Williams, D.F., Buchinskyi, V., Kuzmin, M., 2006. Lena River discharge events in sediments of Laptev Sea, Russian Arctic. Estuarine, Coastal and Shelf Science 66, 185–196.

Romankevich, E.A., 1984. Geochemistry of Organic Matter in the Ocean. Springer, Berlin.

Round, F.E., Crawford, R.M. and Mann, D.G., 1990. The Diatoms: Biology and Morphology of the Genera. Cambridge University Press, Cambridge, pp. 576–577.

Rowland, S.J., Belt, S.T., Wraige, E.J., Massé, G., Roussakis, C., Robert, J.M., 2000. Effects of temperature on polyunsaturation in cytostatic lipids of *Haslea ostrearia*. Phytochemistry 56, 597–602.

Rowland, S.J., Allard, W.G., Belt, S.T., Massé, G., Robert, J.M., Blackburn, S., Frampton, D., Revill, A.T., Volkman, J.K., 2001. Factors influencing the distributions of polyunsaturated terpenoids in the diatom, *Rhizosolenia setigera*. Phytochemistry 58, 717–728.

Rudels, B., Friedrich, H., 2000. The transformations of Atlantic water in the Arctic Ocean and their significance for the freshwater budget. In: Lewis, L.L., Jones, E.P., Lemke, P.,

Prowse, T. D., Wadhams, P. (Eds), The Freshwater Budget of the Arctic Ocean, Kluwer Academic Publishers, Netherlands, 503–532.

Sarnthein, M., R. Gersonde, S. Niebler, U. Pflaumann, R. Spielhagen, J. Thiede, G. Wefer, and W. Weinelt, 2003a. Overview of Glacial Atlantic Ocean Mapping (GLAMAP 2000). Paleoceanography, 18(2), 1030.

Sarnthein, M., U. Pflaumann, M. Weinelt, 2003b. Past extent of sea ice in the northern North Atlantic inferred from foraminiferal paleotemperature estimates. Paleoceanography, 18(2), 1047.

Schauer, U., Muench, R.D., Rudels, B., Timokhov, L., 1997. Impact of Eastern Arctic shelf waters on the Nansen Basin intermediate layers. J. Geophys. Res. 102, 3371–3382.

Schauer, U., 2012. The expedition of the research vessel "Polarstern" to the Arctic in 2011 (ARK-XXVI/3-TransArc), Reports on polar and marine research. Alfred Wegener Institute, Helmholtz Center for Polar and Marine Research, Bremerhaven. 649, 205 pp.

Schlitzer, R., 2012. Ocean Data View. http://odv.awi.de/

Schoster, F., Levitan, M., 2003. Scientific Cruise Report of the joint Russian-German Kara Sea Expedition in 2002 with RV "Akademik Boris Petrov". Ber. Polarforsch. Meeresforsch. 450. ISSN 1618–3193.

Schulz, H. D. and Zabel M., 2000. Marine geochemistry. Springer-Verlag, Heidelberg.

Serreze, M.C., Maslanik, J.A., Scambos, T.A., Fetterer, F., Stroeve, J., Knowles, K., Fowler, C., Drobot, S., Barry, R.G., Haran, T.M., 2003. A record minimum arctic sea ice extent, area in 2002. Geophys Res Lett 30, 1110.

Serreze M.C., Holland M.M., Stroeve J., 2007. Perspectives on the Arctic's shrinking sea-ice cover. Science 315, 1533–1536.

Siegel, V., Holm-Hansen, O., Hewitt, R., Fraser, W., Trivelpiece, W., Trivelpiece, S., 1997. Effects of sea-ice extent and krill or salp dominance on the Antarctic food web. Nature 387, 897–900.

Siegert, M.J., Dowdeswell, J.A., Svendsen, J.I., Elverhøi, A., 2002. The Eurasian Arctic during the last Ice Age. American Scientist 90, 32–39.

Sher, A., 1995. Is there any real evidence for a huge shelf ice sheet in East Siberia? Quaternary International 28, 39–40.

Stärz, M., Gong, X., Stein, R., Darby, D.A., Kauker, F. and Lohmann, G., 2012. Glacial shortcut of Arctic sea-ice transport. Earth and Planetary Science Letters, 257–267.

Stein, R., Grobe, H., Wahsner, M., 1994a. Organic carbon, carbonate, and clay mineral distributions in eastern central Arctic Ocean surface sediments. Mar. Geol. 119, 269–285.

Stein, R., Nam, S.I., Schubert, C., Vogt, C., Fütterer, D., Heinemeier, J., 1994b. The Last Deglaciation Event in the Eastern Central Arctic Ocean, Science 264, 692–696.

Stein, R., Fahl, K., 2000. Holocene accumulation of organic carbon at the Laptev Sea continental margin (Arctic Ocean): sources, pathways, and sinks. Geo-Mar. Lett. 20 (1), 27–36.

Stein, R., Boucsein, B., Fahl, K., Garcia de Oteyza, T., Knies, J., Niessen, F., 2001. Accumulation of particulate organic carbon at the Eurasian continental margin during late Quaternary times: controlling mechanisms and paleoenvironmental significance. Global and Planetary Change 31, 87–104.

Stein, R., Stepanets, O., 2001. The German-Russian Project On Siberian River Run-off (SIRRO): Scientific Cruise Report of the Kara-Sea Expedition "SIRRO 2000" of RV

"Akademik Boris Petrov" and first results. Ber. Polarforsch. Meeresforsch. 393. ISSN 0176–5027.

Stein, R., Stepanets, O., 2002. Scientific Cruise Report of the Kara Sea Expedition 2001 of RV "Akademik Boris Petrov": The German-Russian Project on Siberian River Run-off (SIRRO) 2nd the EU-Project "ESTABLISH ". Ber. Polarforsch. Meeresforsch. 419. ISSN 1618–3193.

Stein, R., Fahl, K., Fütterer, D.K., Galimov, E.M., Stepanets, O.V., 2003. Siberian River run-off in the Kara Sea: characterisation, quantification, variability, and environmental significance. In: Proceeding of Marine Science, vol. 6. Elsevier, Amsterdam, 487 pp.

Stein, R., Dittmers, K., Fahl, K., Kraus, M., Matthiessen, J., Niessen, F., Pirrung, M., Polyakova, Y., Schoster, F., Steinke, T., Fütterer, D.K., 2004. Arctic (palaeo) river discharge and environmental change: evidence from the Holocene Kara Sea sedimentary record. Quaternary Science Reviews 23, pp. 1485–1511.

Stein, R., Fahl, K., 2004a. The Kara Sea: Distribution, sources, variability and burial of organic carbon. In: Stein, R., Macdonald, R.W. (Eds.), The organic carbon cycle in the Arctic Ocean. Springer, Berlin, pp. 237–266.

Stein, R., Fahl, K., 2004b. The Laptev Sea: Distribution, sources, variability and burial of organic carbon. In: Stein, R., Macdonald, R.W. (Eds.), The organic carbon cycle in the Arctic Ocean. Springer, Berlin, pp. 213–237.

Stein, R., and Macdonald, R. (Eds.), 2004. The Organic Carbon Cycle in the Arctic Ocean. Springer, Heidelberg, 363 pp.

Stein, R., 2008. Proxies used for palaeoenvironmental reconstructions in the Arctic Ocean. In: Arctic Ocean sediments: processes, proxies, and paleoenvironment. Developments in Marine Geology, vol. 2. Elsevier, Amsterdam, 133–246.

Stein, R., Matthiessen, J., Niessen, F., Krylov, A., Nam, S., Bazhenova, E., 2010. Towards a better (litho-) stratigraphy and reconstruction of Quaternary paleoenvironment in the Amerasian Basin (Arctic Ocean). Polarforschung 79, 97–121.

Stein, R., Fahl, K., 2012. A first southern Lomonosov Ridge (Arctic Ocean) 60 ka IP25 sea-ice record. Polarforschung 82, 83–86.

Stein, R., Fahl, K., Müller, J., 2012. Proxy reconstruction of Arctic Ocean sea ice history: from IRD to IP25. Polarforschung 82, 37–71.

Stein, R., Fahl, K., 2013. Biomarker proxy shows potential for studying the entire Quaternary Arctic sea ice history, Organic Geochemistry 55, 98–102.

Stickley, C.E., John, K.S., Koc, N., Jordan, R.W., Passchier, S., Pearce, R.B., Kearns, L.E., 2009. Evidence for middle Eocene Arctic sea ice from diatoms and ice-rafted debris. Nature 460, 376–380.

St.John, K.E., 2008. Cenozoic ice-rafting history of the central Arctic Ocean–terrigenous sands on the Lomonosov Ridge. Paleoceanography 23, PA1S05.

Stoynova, V., Shanahan, T.M., Hughen, K.A., de Vernal, A., 2013. Insights into Circum-Arctic sea ice variability from molecular geochemistry. Quaternary Science Reviews 79, 63–73.

Stroeve, J.C., Serreze,M.C., Fetterer, F., Arbetter, T., Meier, W.,Maslanik, J., Knowles, K., 2005. Tracking the Arctic's shrinking ice cover: Another extreme September minimu in 2004. Geophysical Research Letters 32, L04501.

Stroeve, J., Holland, M.M., Meier, W., Scambos, T., Serreze, M., 2007. Arctic sea ice decline: faster than forecast. Geophysical Research Letters 34, L09501.

Stroeve, J., Frei, A., McCreight, J., Ghatak, D., 2008. Arctic sea-ice variability revisited. Annals of Glaciology 48, 71–81.

Stroeve, J., Serreze, M., Holland, M., Kay, J., Malanik, J., Barrett, A., 2012. The Arctic's rapidly shrinking sea ice cover: a research synthesis. Climatic Change 110, 1005–1027.

Sutherland, D.A., Pickart, R.S., 2008. The East Greenland Coastal Current: Structure, variability, and forcing. Progress In Oceanography 78, 58–77.

Svendsen, J.I., Gataullin, V., Mangerud, J., Polyak, L., Ehlers, J., Gibbard, P.L., 2004. The glacial History of the Barents and Kara Sea Region. Developments in Quaternary Sciences, Elsevier, pp. 369–378.

Ślubowska-Woldengen, M., Rasmussen, T.L., Koç, N., Klitgaard-Kristensen, D., Nilsen, F., Solheim, A., 2007. Advection of Atlantic water to the western and northern Svalbard shelf since 17,500 cal yr B.P. Quaternary Science Reviews 26, 463–478.

Ślubowska-Woldengen, M., Koç, N., Rasmussen, T.L., Klitgaard-Kristensen, D., Hald, M., Jennings, A.E., 2008. Time-slice reconstructions of ocean circulation changes on the continental shelf in the Nordic and Barents Seas during the last 16,000 cal yr B.P. Quaternary Science Reviews 27, 1476–1492.

Thomas, D.N., Dieckmann, G.S., 2010. Sea Ice. Blackwell Publishing, Oxford, 640 pp.

Tissot, B.P. and Welte, D.H., 1984. Petroleum Formation and Occurrence. Springer-Verlag, Heidelberg.

Torres-Valdés, S., Tsubouchi, T., Bacon, S., Naveira-Garabato, A. C., Sanders, R., McLaughlin, F. A., Petrie, B., Kattner, G., Azetsu-Scott, K., Whitledge, T. E., 2013. Export of nutrients from the Arctic Ocean. J. Geophys. Res. Oceans 118, 1625–1644.

Vare, L.L., Massé, G., Gregory, T.R., Smart, C.W., Belt, S.T., 2009. Sea ice variations in the central Canadian Arctic Archipelago during the Holocene. Quat. Sci. Rev. 28 (13–14), 1354–1366.

Vare, L.L., Massé, G., Belt, S.T., 2011. A biomarker-based reconstruction of sea ice conditions for the Barents Sea in recent centuries. The Holocene 20, 637–643.

Volkman, J.K., Farrington, J.W., Gagosian, R.B., Wakeham, S.G., 1983. Lipid composition of coastal marine sediments from the Peru upwelling region. In: Bjoroy, M. (Eds.), Advances in Organic Geochemistry 1981. Wiley, Chichester, UK, pp.228–240.

Volkman, J.K., 1986. A review of sterol markers for marine and terrigenous organic matter, Organic Geochemistry 9, 83–99.

Volkman, J.K., Barrett, S.M., Dunstan, G.A., 1994. C25 and C30 highly branched alkenes in laboratory cultures of two marine diatoms. Organic Geochemistry 21, 407–413.

Volkman, J.K., 2006. Lipid markers for marine organic matter. In. J. K. Volkman. Handbook of Environmental Chemistry. Berlin, Heidelberg, Springer-Verlag. 2nd volume: 27–70.

von Quillfeldt, C.H., 2000. *Pleurosigma tenuiforme* spec. nov.; a marine *Pleurosigma* species with long, slender apices, occurring in Arctic. Diatom Research 15, 221–236.

Walsh, J.J., 1989. Arctic carbon sinks: present and future. Global Biogeochem Cycles 3, 393–411.

Walsh, J. E., and W. L. Chapman, 2001. Twentieth-century sea ice variations from observational data. Ann. Glaciol. 33, 444–448.

Wang, M., Overland, J.E., 2009. A sea ice free summer Arctic within 30 years? . Geophysical Research Letters 36, L07502.

Wassmann, P., Reigstad, M., 2011. Future Arctic Ocean seasonal ice zones and implications for pelagic-benthic coupling. Oceanography 24(3): 220–231.

Witkowski, A., Lange-Bertalot, H., Metzeltin, D., 2000. Diatom flora of marine coasts I. In: Lange-Bertalot, H. (Eds.), Iconographia Diatomologica 7, 223–225.

Wollenburg, J., Kuhnt, W., Mackensen, A., 2001. Changes in Arctic Ocean paleoproductivity and hydrography during the last 145kyr: the benthic foraminiferal record. Paleoceanography 16 (1), 65–77.

Wollenburg, J., Knies, J., Mackensen, A., 2004. High-resolution palaeoproductivity fluctuations during the past 24 kyr as indicated by benthic foraminifera in the marginal Arctic Ocean. Palaeogeography palaeoclimatology palaeoecology 204, 209–238.

Wraige, E.J., Belt, S.T., Lewis, C.A., Cooke, D.A., Robert, J.-M., Massé, G., Rowland, S.J., 1997. Variations in structures and distributions of C_{25} highly branched isoprenoid (HBI) alkenes in cultures of the diatom, Haslea ostrearia (Simonsen). Organic Geochemistry 27, 497–505.

Wraige, E.J., Belt, S.T., Massé, G., Robert, J.M., Rowland, S.J., 1998. Variations in distributions of C25 highly branched isoprenoid (HBI) alkenes in the diatom, Haslea ostrearia: influence of salinity. Organic Geochemistry 28, 855–859.

Xiao, X., Fahl, K., Stein, R., 2013. Biomarker distributions in surface sediments from the Kara and Laptev seas (Arctic Ocean): indicators for organic-carbon sources and sea-ice coverage. Quaternary Sci. Rev. 79, 40–52.

Xiao, X., Stein, R., Fahl, K., Müller, J., in review. Biomarker records from Arctic Ocean surface sediments: New aspects for Arctic sea-ice reconstruction. Geochimica et Cosmochimica Acta.

Yunker, M.B., Macdonald, R.W., Veltkamp, D.J., Cretney, W.J., 1995. Terrestrial and marine biomarkers in a seasonally ice-covered Arctic estuary – integration of multivariate and biomarker approaches. Marine Chemistry 49, 1–50.

Zaborska, A., Carroll, J., Papucci, C., Torricelli, L., Carroll, M.L., Walkusz-Miotk, J., Pempkowiak, J., 2008. Recent sediment accumulation rates for the Western margin of the Barents Sea. Deep Sea Research Part II: Topical Studies in Oceanography 55, 2352–2360.

Zhang, J., Lindsay, R., Schweiger, A., Steele, M., 2013. The impact of an intense summer cyclone on 2012 Arctic sea ice retreat. Geophysical Research Letters 40, 720–726.

Appendix

Data in Appendix 1: http://doi.pangaea.de/10.1594/PANGAEA.803232

Data in Appendix 2: http://doi.pangaea.de/10.1594/PANGAEA.803232

Data in Appendix 3: http://doi.pangaea.de/10.1594/PANGAEA.819526